THE UNIVERSITY OF TULSA

THE GRADUATE SCHOOL

FRACTAL AND ANOMALOUS DIFFUSION MODELS FOR ANALYZING WELL TEST DATA FROM LIQUID DOMINATED AND VAPOR DOMINATED GEOTHERMAL RESERVOIRS

by
Yasin Ozkan

A thesis submitted in partial fulfillment of

the requirements for the degree of Master of Science

in the Discipline of Petroleum Engineering

The Graduate School

The University of Tulsa

2020

T H E   U N I V E R S I T Y   O F   T U L S A

THE GRADUATE SCHOOL

FRACTAL AND ANOMALOUS DIFFUSION MODELS FOR ANALYZING WELL TEST DATA FROM LIQUID DOMINATED AND VAPOR DOMINATED GEOTHERMAL RESERVOIRS

by

Yasin Ozkan

A THESIS

APPROVED FOR THE DISCIPLINE OF

PETROLEUM ENGINEERING

By Thesis Committee

Mustafa Onur, Chair
Ovadia Shoham
Christian Constanda

ABSTRACT

Yasin Ozkan (Master of Science in Petroleum Engineering)

Fractal and Anomalous Diffusion Models for Analyzing Well Test Data from Liquid Dominated and Vapor Dominated Geothermal Reservoirs

Directed by Mustafa Onur

166 pp., Chapter 5: Summary and Conclusions

(467 words)

The importance of geothermal reservoirs is rising day by day because of the world's enormous energy demand. Now, governments give special emphasis to renewable energy sources like geothermal energy more than fossil fuels since these renewable energy sources are considered environmentally friendly and sustainable. On the other hand, one of the most challenging tasks of geothermal reservoirs is to model these reservoirs for resource evaluation and performance analysis because geothermal reservoirs are quite heterogeneous and include complex network of fractures and faults.

Appropriate modeling of geothermal reservoirs is crucial for determining appropriate production strategies. For instance, the effects of production and/or injection wells, and the locations of those wells on reservoir performance are assessed by the reservoir model. In addition to these, enhanced recovery production, injection wells operations, production rate prediction, and feasibility analysis of given field are determined by considering reservoir models. Hence, reservoir models are extremely important for companies. Well testing is applied to reservoirs to investigate

the efficiency of the wells by companies. They characterize well performance and reservoirs by utilizing well-test data.

The objective of this study is to apply fractal and anomalous diffusion models to geothermal reservoirs to analyze the well-test pressure data acquired from such reservoirs. These models are applied to well-test data to find reservoir parameters governing the resource potential and production rate performance, such as porosity and permeability.

In this study, the diffusivity equations based on the fractal and anomalous diffusion concepts were solved by considering three different production boundary conditions; specified constant rate production, specified constant bottomhole pressure production, and variable rate/variable bottomhole pressure conditions. For all cases, the reservoir is assumed to be infinite acting. For each production boundary condition, the initial value problem (IBVP) was solved by using the Laplace transformation method and the Laplace space solutions were converted to the real time domain by numerical inversion using Stehfest's inversion algorithm. Both dimensional and dimensionless solutions were presented for each condition and model. These solutions are compared, and the differences were determined and presented for each condition. Then, the solutions based on the fractal and anomalous diffusion models were applied to analyze well-test data from the Kizildere geothermal field in Turkey and the Kamojang geothermal field from Indonesia. Each geothermal field is examined to estimate the reservoir parameters by applying automated history matching based on the ensemble smoother with multiple data assimilation (ES-MDA) method. The main conclusion is that fractal parameters have a remarkable effect on the reservoir characteristics. Changing fractal parameters results in different reservoir characteristics. Fractal parameters cannot be interpreted from well test data, so the box-counting method is extremely important. Furthermore, fractal model achieves very good results for both the liquid-dominated and vapor-dominated reservoirs. On the other side of the coin, the Raghavan anomalous model’s performance should not be ignored for vapor-dominated reservoirs.

ACKNOWLEDGEMENTS

To begin with, I would like to express gratitude for my research advisor, Prof. Dr. Mustafa Onur, who has always patiently led the way and made this study perfect. Prof. Onur, besides mentoring me, became not only a role model but also a friend. I am grateful to him for giving me academic working principles and ethics. He has expanded my horizon and taught me ‘Never say *enough* and give up’.

Besides my advisor, I would like to thank the great leader Mustafa Kemal ATATURK who started this scholarship in 1929. I am grateful and thankful to him for providing me this opportunity.

I am also grateful to my committee members, Dr. Ovadia Shoham and Dr. Christian Constanda, for sharing their valuable time and experience. I am thankful for their invaluable contributions to my knowledge.

I would like to express my special thanks to my father, Caner; my mother, Dilek, and my sister Ozge for their unflagging support, faith, and love. I could not have completed without their unconditional support.

I would like to thank my grandfathers, Ahmet Ozkan and Hasan Yildiz, and my grandmothers, Husne Ozkan and Hediye Yildiz. They always supported and believed in me.

I am grateful to our family friend, Muharrem Atik, and his wife, Sibel Atik, who vouched for me and gave me this opportunity. In addition, I owe this priceless life and scientific experience to my cousin, Selcuk Subasi, and his wife, Duygu Subasi, who vouched for me and gave me this chance.

I am also grateful to my friends Arif Eser and Kaan Inanc Ozdemir. They always supported my family and me both materially and spiritually throughout my study in the USA.

Lastly, I would like to thank the Republic of Turkey Ministry of Education and the General Directorate of Mineral Research and Exploration for providing me a scholarship and their support throughout my study. I am grateful to the Turkish people for providing me this priceless opportunity.

TABLE OF CONTENTS

LIST OF TABLES

LIST OF FIGURES

CHAPTER 1

INTRODUCTION

Global energy demand has risen significantly in the 20th century especially due to the two world wars. Inevitably, energy demand continues to increase dramatically in the 21st century due to uncontrolled population growth, advanced technology, and industrialization. Because of that, each country that has geothermal sources pays attention to geothermal energy.

Geothermal is a type of thermal energy. The geothermal energy originated from the Greek words: geo (earth) and thermal (thermos). In other words, it is thermal energy that produced and stored by the earth. Geothermal energy is the internal heat of the earth and this heat diffuses from the magma which is the hot zone in the center towards the earth's surface. This heat sometimes reaches the earth surface by following cracks under the earth's crust, for example, volcanic eruption. Geothermal energy comes to the surface by the radiation, convection, and conduction heat transfer mechanisms. However, this heat is sometimes kept under a cover rock. Thanks to this holding mechanism, the heat warms up the water. After the drilling operation, that energy comes to the surface as hot water or steam. Most importantly, the energy provided in the geothermal system is not produced from water. On the contrary, it is the energy obtained as a result of converting underground heat energy into electrical energy. Water and steam that serve as heat carrier carry the energy to the ground (Duffield and Sass, 2003).

Geothermal energy is not a new resource on the contrary to what many people think. It is one of the oldest types of energy used by humans. Archaeological evidence shows that Paleo – Indians used hot springs directly for cleaning, bathing, and cooking 10,000 years ago (History of geothermal energy, 2020). On the other side of the continent, the peoples of ancient Greece and Rome used hot water for healing in Europe and Anatolia (Geothermal Energy throughout the Ages, 2020). But now, geothermal energy is mostly used to produce electricity. Geothermal power generation in the world yielded 92.7 TWH in 2018 (IEA,2020). The first geothermal electric power plant is located in Larderello. In 1904, Italian scientist Piero Ginori Conti used to steam to produce power (History of geothermal energy, 2020). After the Second World War, the United States gave much weight to a geothermal power plant because the Mayacamas Mountains north of San Francisco has a huge potential for geothermal energy thanks to the geysers. The San Andreas Fault runs through California from the Imperial Valley to the San Francisco area, and there is a geothermal activity.

The installed capacity of geothermal energy in the world reached 13.9 gigawatts in 2019. Geothermal power generation went up by 3.7% in 2019. The United States has the highest installed geothermal power capacity (2.6 GW) in the world. It is nearly 18% of the world’s total. Indonesia (2.1 GW), the Philippines (1.9 GW) and the Republic of Turkey (1.5 GW) are the countries that follow the United States in this regard.

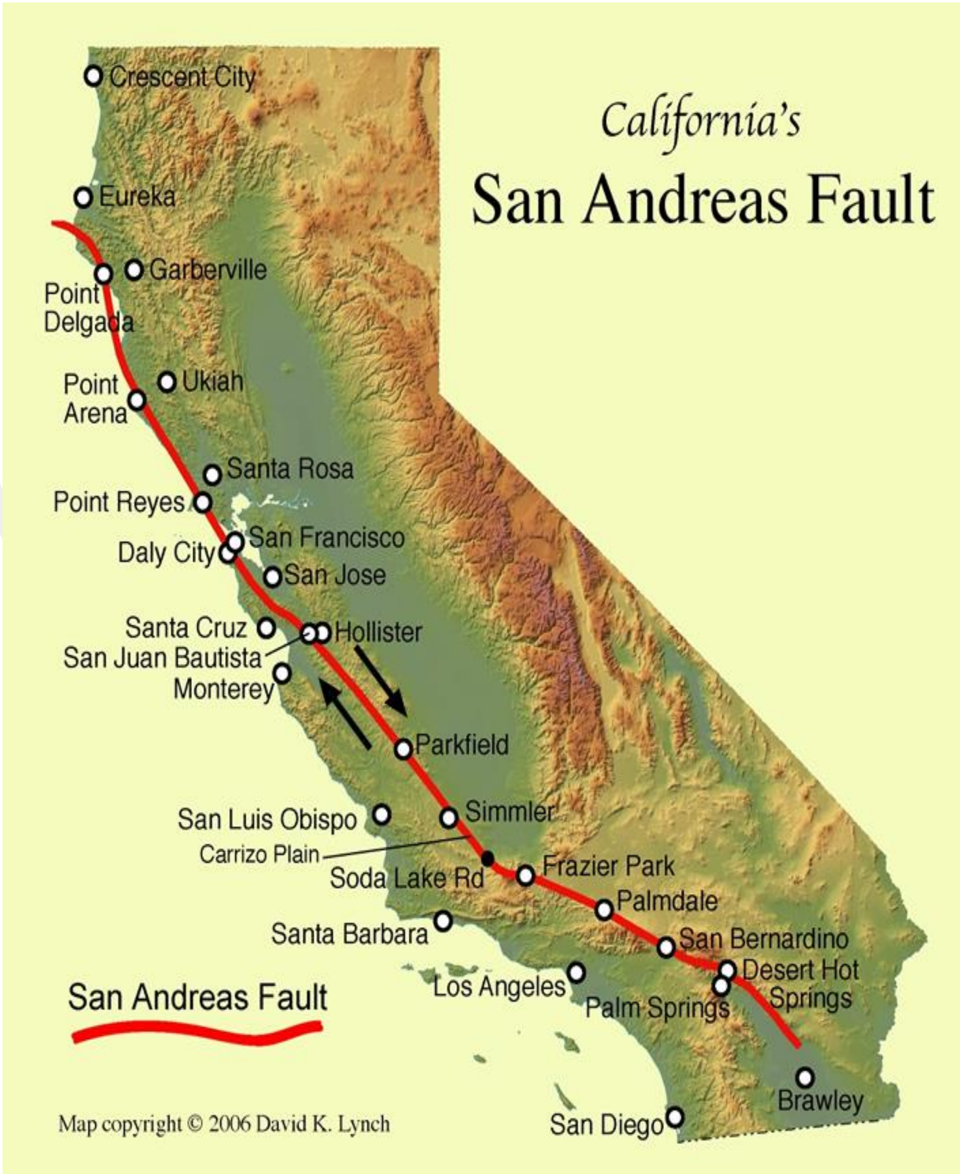

Figure 1.1 San Andreas Fault (Lynch D. K., 2006).

The Republic of Turkey is making a remarkable investment in the geothermal field. The Republic of Turkey installed the most geothermal capacity additions both at 219 megawatts (MW) in 2018 (Sönnichsen, 2020), and 232 MW in 2019. (BP, 2020). Figure 1.2 demonstrates that global geothermal installed capacity goes up substantially.

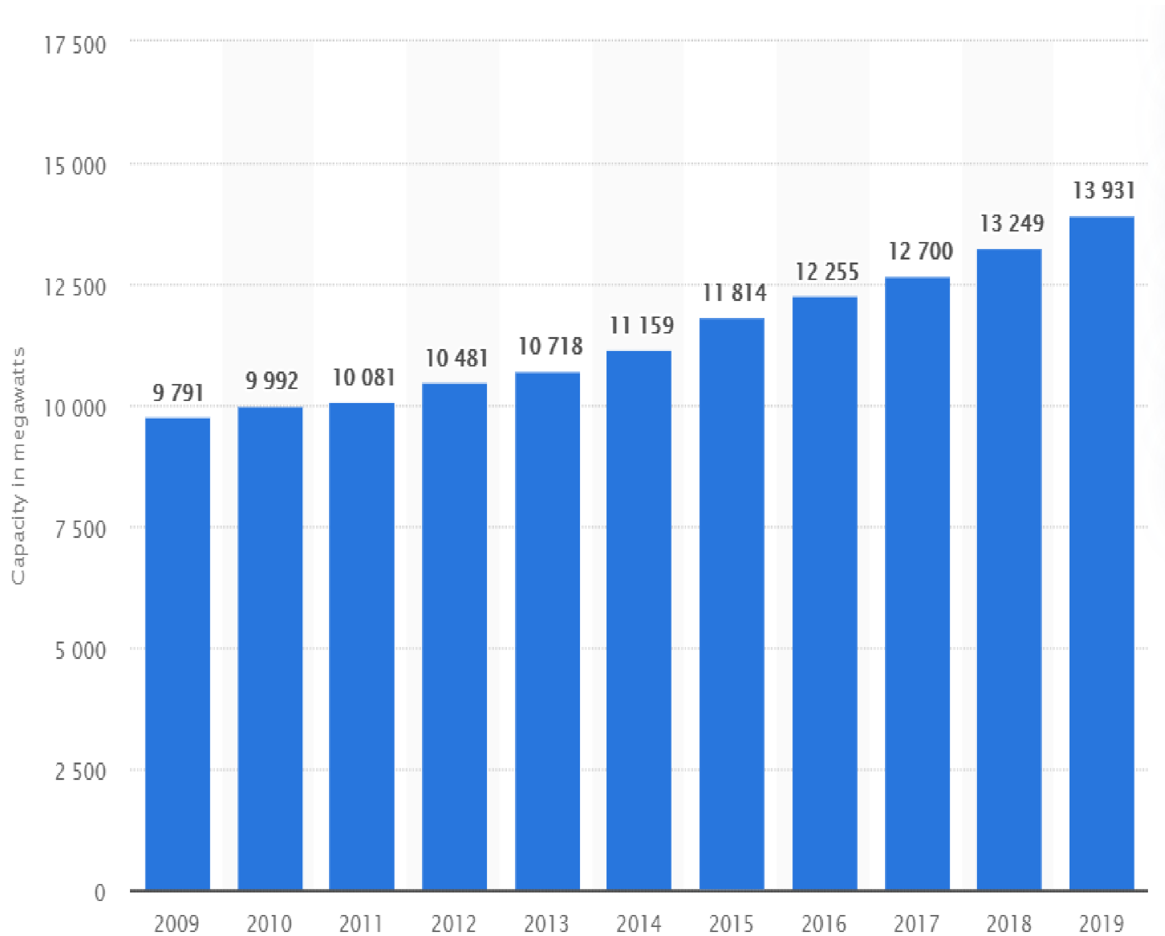

Figure 1.2 Geothermal Energy Capacity in the world between 2019 and 2019 (Sönnichsen, 2020).

The total number of geothermal wells drilled for power projects is 1,159 from 2015 to 2020, and 10,367 million $US was spent on those projects. The world total installed capacity would be 19,361 MWe in 2025 (Huttrer, 2020). In addition, the International Energy Agency (IEA) expects that geothermal power generation will be 162 TWh in 2025 and 282 TWh in 2030.

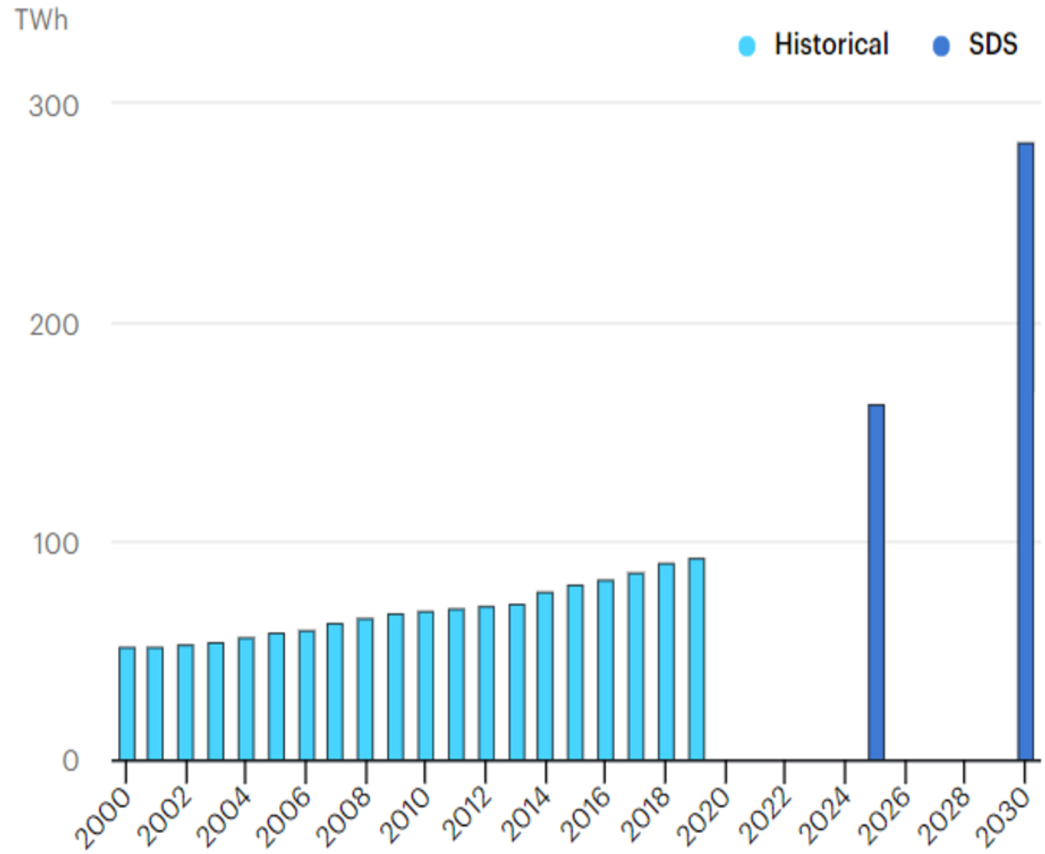

Figure 1.3 Geothermal power generation in the sustainable development scenario (IEA, 2019).

Geothermal energy has a lot of advantages. The first and most important advantage is that it is renewable energy. The produced hot water can be used to generate electricity. Then, the colder water can be pumped through the injection well, so this process provides sustainability. Sustainable geothermal energy systems impact poverty, health, education, demographics, natural hazards, atmosphere, land, freshwater, biodiversity, economic development, etc. (Shortall et al., 2015). Geothermal energy is baseload. That is, geothermal power plants can generate electricity 24 hours per day / 7 days per week. They are not affected by severe weather conditions. Furthermore, geothermal energy has a smaller footprint than other energy types. Geothermal power plants use less land per GWh (404 m^2) than coal (3642 m^2), wind (1335 m^2), or solar PV (3237 m^2). In addition, geothermal is clean energy. Geothermal power plants emit no greenhouse gasses

(Geothermal Basics, 2020). Moreover, geothermal energy has a lot of direct use applications. It is used for swimming, bathing, balneology, space heating, and cooling. Furthermore, there are agriculture applications; for example, greenhouse heating to get maximum production for fruit and vegetable products and fishpond and raceway heating. Thanks to these benefits, people tend to use geothermal energy much more year by year. Figure 1.4 depicts that there is an increasing trend for direct use applications.

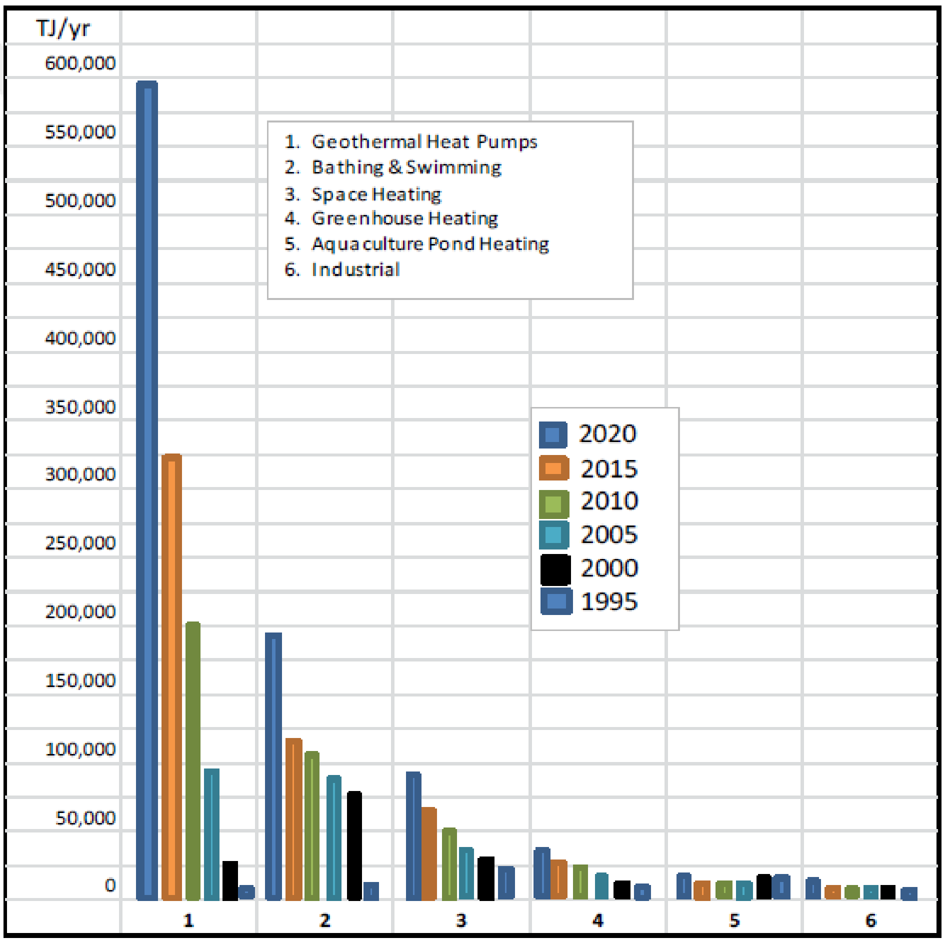

Figure 1.4 Comparison of worldwide direct use of geothermal energy in TJ/yr from 1995, 2000, 2005, 2010, 2015 and 2020 (Lund and Toth, 2020).

After drilling a geothermal well, well testing and reservoir characterization are required. While the main purpose of reservoir characterization is to characterize the lithology, fractures, and stress, well test analysis provides to evaluate well properties such as maximum production or injection flow rate. Gamma – ray logs and spectral gamma – ray help to identify petroleum and geothermal reservoir lithology. On the other side of the coin, well testing supplies the estimation of reservoir hydraulic parameters, for example, well productivity or injectivity index, average reservoir pressure, well skin factor, reservoir permeability, and reservoir boundaries. It is obvious that wells cannot be produced efficiently without modeling the reservoir. Well test analysis is extremely important to evaluate the dynamic data because the derived models may match the observed data. There will be one correct answer and more than a few probable answers. Thanks to this good match, well test analysis provides estimate of permeability and porosity under in – situ flow conditions, estimates of well performance, and estimates of distances to boundaries. As a result, the production lifetime of the well could be extended, and human beings get a chance to benefit more from this energy. Thus, well test analysis is non – negligible to the petroleum and geothermal industry. Well testing and reservoir characterization play a key role to understand how fluid and heat energy are transferred. Applying history matching on pressure data helps to understand well characteristics. For instance, possible barriers and faults/fractures in vertical directions can be interpreted.

1.1 Geothermal Systems and Power Plants

The geothermal reservoirs consist of porous and fractured rocks where are fed with rain, snow, sea, and magmatic waters. When rising hot water or steam is trapped in those rocks under an impermeable rock (cover or cap rock), it can form a geothermal reservoir. Those reservoirs exist in the location where the volcanic activity occurs. Because of tectonic movement, the earth's crust is broken into plates. Magma drives the plates in three different ways: divergent, convergent, and transform. While a divergent boundary means when two plates are moving apart from each other, the convergent boundary is when two plates are pushed into each other. A transform boundary is that two plates slide past one another. Furthermore, the most tectonic activity is seen in the Ring of Fire where most earthquakes and volcanic eruptions occur.

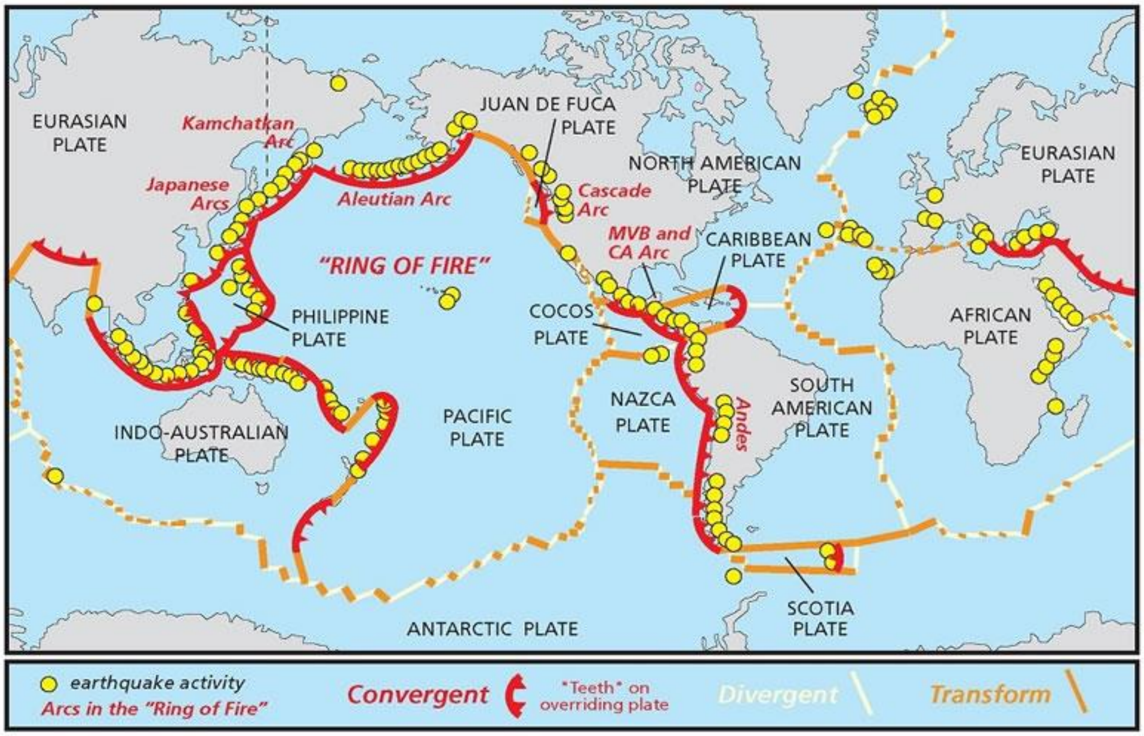

Figure 1.5 World Plate Boundaries: divergent, convergent and transform (Geology.com, 2020).

There are six types of geothermal resources: magma, hydrothermal, geopressured, hot dry rock (HDR), enhanced (or engineered) geothermal systems (EGS), and waste heat systems. Magma is the largest geothermal resource. The heat from magma diffusive through the fracture and heat the cold water. Hydrothermal resources require three components: a heat source, an aquifer, and an impermeable rock. These systems convey heat to the surface as steam or hot water. On the other hand, hot dry rock systems have either dry aquifer or low permeable rock. These systems can be activated both creating artificial fractures and injecting water. Geopressured systems contain hot brine saturated with methane. These systems have deep aquifers under high pressure. Moreover, geothermal systems can be called enhanced geothermal systems when the heat is produced in an economical way from low permeability and/or porosity rock. Therefore, these systems are also called engineered geothermal systems because these type of rocks needs stimulation or enhancement operations. Finally, the waste heat system is different than others. These systems can be seen at the hydrocarbon reservoirs. After many years of production, some hydrocarbon reservoirs exposed to water floating. Hence, hydrocarbon production may be uneconomical. Then, these systems can be used as artificial geothermal systems because the heat can be carried by water circulation (Falcone et al. 2011).

There are three types of geothermal power plants: dry steam, flash steam, and binary cycle. Dry steam power plants pull underground resources of the steam directly to generate electricity. The steam is directed into a turbine or generator unit. The dry steam power plant is suitable in case steam is not mixed with water. These geothermal systems temperatures are between 180 – 350 °C. The first example of the dry steam power plant is located at Larderello, Italy (1904).

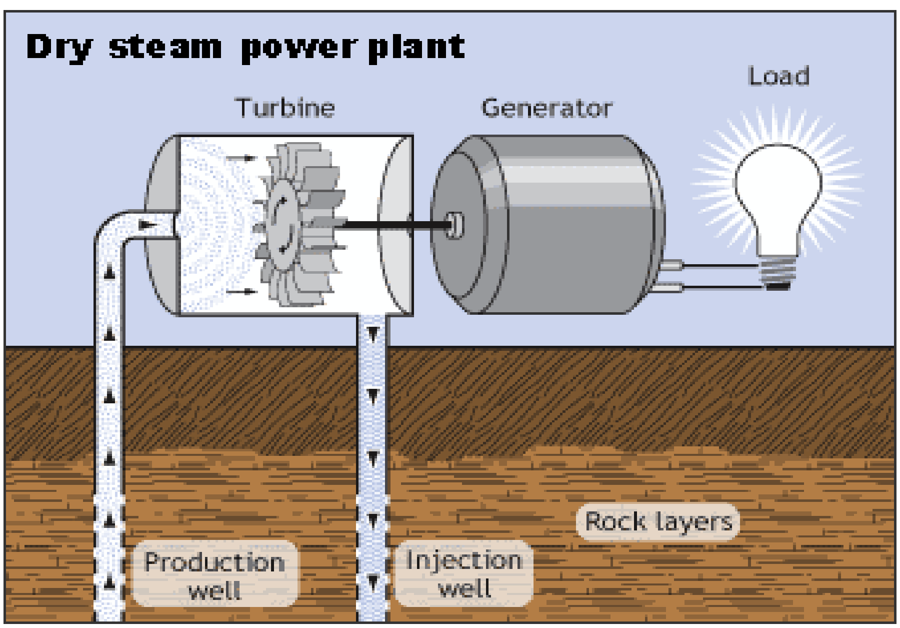

Figure 1.6 Dry steam power plant (EIA, 2019).

Flash steam plants are different than dry steam plants. High pressure hot water flows up through wells with its own pressure. During this process, the pressure decreases and some of the hot water boils into steam. Then, the steam is directed to turbines and electricity is produced. After this process, the steam cools, and it condenses to water. Thus, the water is separated and is injected back into the ground since this water can be used again. Flash steam power plants are used with the temperature greater than 182 °C.

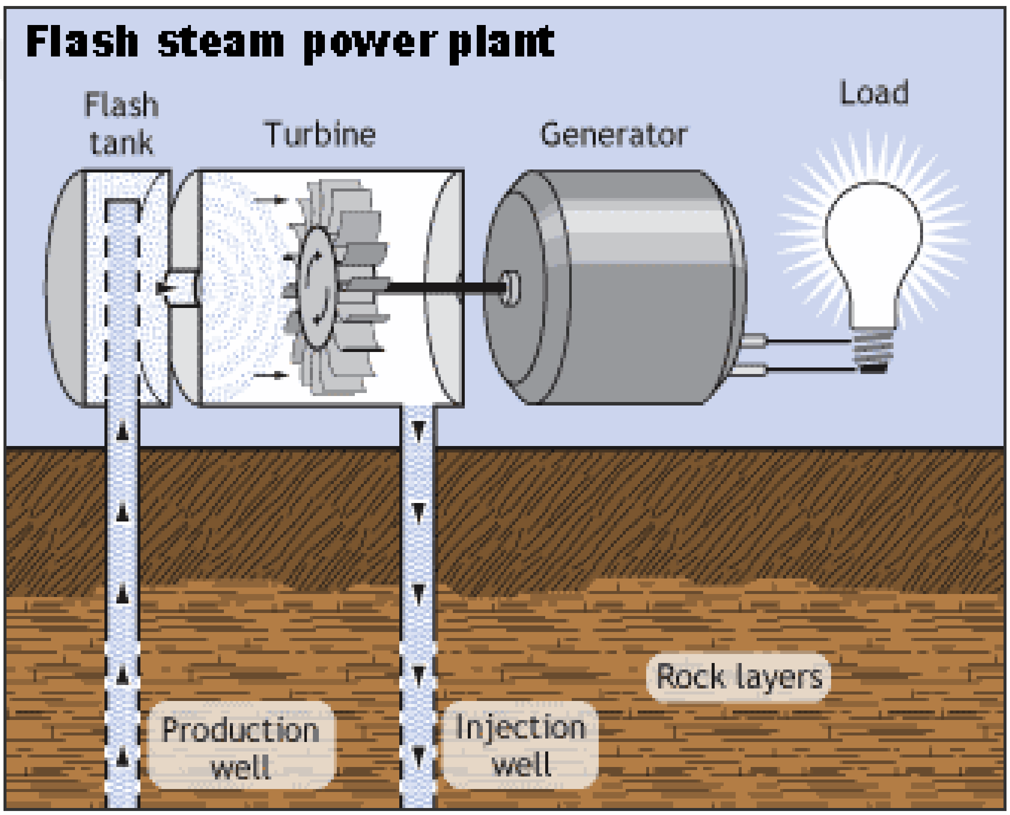

Figure 1.7 Flash steam power plant (EIA, 2019).

Binary cycle power plants are used at lower temperatures of geothermal systems (100 – 182 °C). In these geothermal systems, the steam cannot be used directly due to low temperature. Hence, another liquid is used to generate electricity. To put it another way, the heat is taken from the hot water and is transferred to working fluid by using a heat exchanger. The main goal is to vaporize the working fluid and sent to it the turbine to produce electricity. It is important that the working fluid boiling point should be lower than the water boiling point.

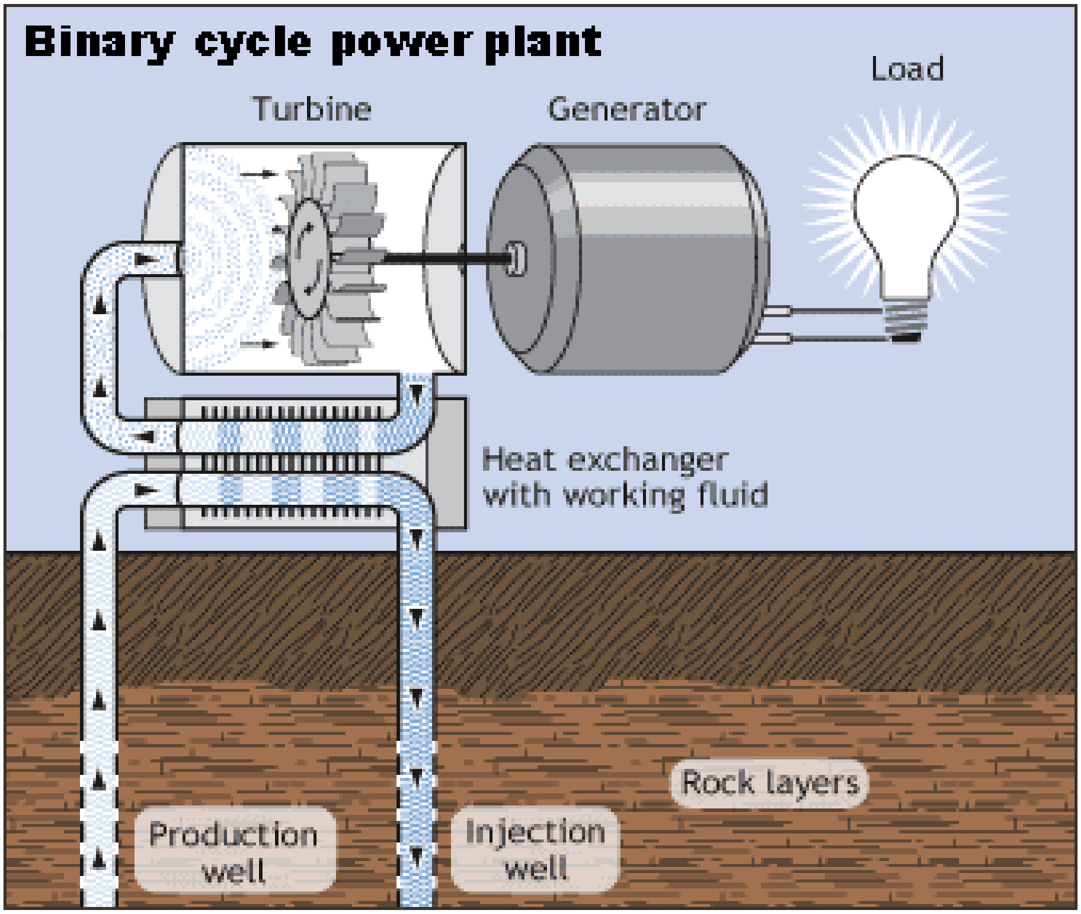

Figure 1.8 Binary cycle power plant (EIA, 2019).

1.2 Literature Review

In this study, the focus is on the analysis and interpretation of well test data from hydrothermal geothermal reservoir by considering fractal and anomalous diffusion models. As mentioned before, geothermal reservoirs are quite heterogeneous with complex networks of fractures and faults. After the 1950s, fractured and unconventional reservoirs have got remarkable attention in the geothermal, oil, and gas field industry because traditional modeling which is applied to homogeneous reservoirs has some drawbacks against fractured reservoirs. In 1963, Warren and Root studied the naturally fractured reservoirs by applying two – scale (fracture – matrix). This study has significantly influenced today's studies and formed the background.

In 1983, Gefen et al. described the mean square displacement as:

$$r^2(t) \sim Zt^{\frac{2}{2+\theta}} \tag{1.1}$$

or

$$r^2(t) \sim Zt^{\frac{2}{d_w}}, \tag{1.2}$$

where Z is a diffusion coefficient, and d_w is called Fickian value, and it is equal to $2 + \theta$. Before Gefen et al. Fickian value is accepted as $d_w = 2$. However, they proved that d_w can be 2 if the reservoir is homogeneous. In other words, when θ = 0, the diffusion is called normal diffusion. On the other hand, if θ>0 or θ<0, then the diffusion process is called anomalous diffusion. Furthermore, Gefen et al. claimed that the mean square displacement should be shown as $t^{\frac{2}{2+\theta}}$ rather than t because of heterogeneous geometry. Although percolating cluster geometry is heterogeneous, there is a self-similarity. In addition to this, Gefen et al., introduced the hydraulic diffusivity η for a fractal network as

$$\eta \sim r^{-\theta}, \tag{1.3}$$

where θ is the topology of the network (conductivity index). This means that the diffusivity goes down with a distance ($\theta > 0$). Actually, this variation explains the anomalous diffusion effect. In other words, when the fractal network consists of a highly tortuous path ($\theta > 0$), the diffusion is slower than normal diffusion, and this process is called subdiffusion. On the other side of the coin, as the fractal network contains a less tortuous path ($\theta < 0$), the diffusion is faster than normal diffusion, so it is called superdiffusion.

In 1984 and 1985, O’Shaughnessy and Procaccia studied analytical solutions for diffusion on fractal objects. Then, they worked for diffusion fractals in 1985. They showed that the generalization of the diffusion equation is proposed for Euclidean lattices which have the case of lattices of noninteger dimension. Diffusion on fractals is presented based on scaling argument for conductivity and supported by a renormalization group analysis and numerical solutions. They proved that anomalous diffusion and scaling of conductivity proceed from Θ. The conservation of probability equation is defined as a change in probability (M) at time t is equal to change in net radial current within the shell.

$$\frac{\partial M(r,t)}{\partial t} = \frac{\partial J(r,t)}{\partial r}. \tag{1.4}$$

By using this relationship, the diffusion equation is proposed for the spherically symmetric shell

$$\frac{\partial p(r,t)}{\partial t} = \frac{1}{r^{D-1}} \frac{\partial}{\partial r}\left(K(r) r^{D-1} \frac{\partial p(r,t)}{\partial r}\right), \tag{1.5}$$

where $K(r) = K r^{-\Theta}$, and K is constant, D is defined as fractal dimension and Θ is the anomalous diffusion coefficient.

In 1990, Chang and Yortsos introduced fractals to petroleum (fractal media) reservoirs successfully. Chang and Yortsos developed the study for O’Shaughnessy and Procaccia’s (1985). O’Shaughnessy and Procaccia defined the permeability using the fractal distribution. On the other hand, Chang and Yortsos (1990) extended their formulation and apply one example. Then, Beier (1994) explained both permeability and porosity using fractal distribution. Chang and Yortsos proposed a diffusivity equation for single phase flow in a system where the fractal object embedded into a Euclidean matrix. The diffusivity equation derived by Chang and Yortsos (1990) is

$$c_t \frac{\partial p(r,t)}{\partial t} = \frac{m}{\mu} \frac{1}{r^{d_f-1}} \frac{\partial}{\partial r}\left(r^{\beta} \frac{\partial p(r,t)}{\partial r}\right). \tag{1.6}$$

They developed a model (fractal model) that has a disconnected matrix, but it might get in contact with the fracture network. This provides that fluid from to and from wells occurs through the connected fracture. In addition, they worked on pressure transient response in two cases: contribution of matrix participation and when both the fracture network and the matrix participate.

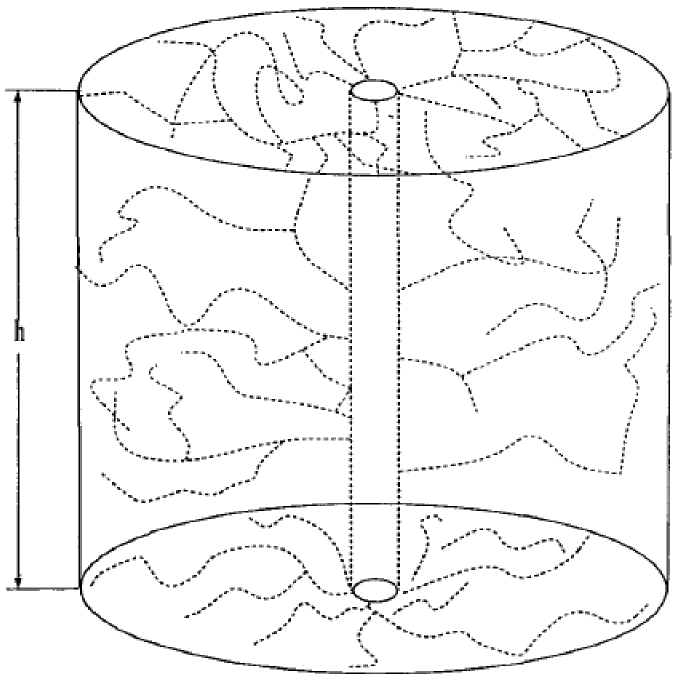

Figure 1.9 Porous media (Chang and Yortsos, 1990).

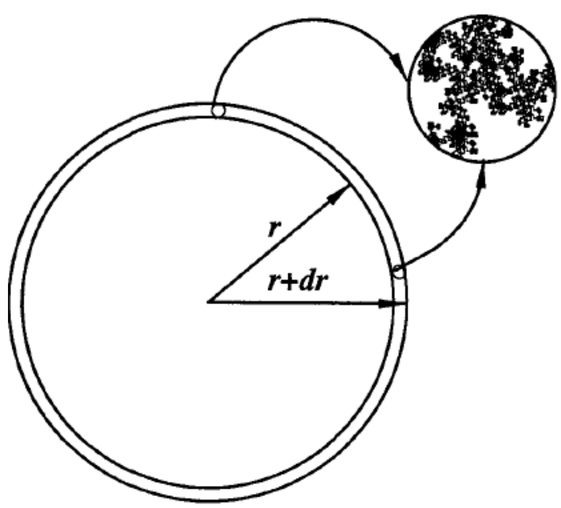

Figure 1.10 Flow across a differential shell (Chang and Yortsos, 1990).

Figure 1.9 depicts the model of porous media. Dash lines represent the fractal fracture network which has a fractal property. The rest of the space is occupied by the Euclidean matrix. In Figure 1.10, radial r refers to the Euclidean distance from the origin. Chang and Yortsos presented the flow in fracture networks and diffusivity equation by using this model. Their mathematical model is based on the flow of slightly compressible fluid in a fractal reservoir and is examined both the matrix and the network participate in the flow. Consequently, they found out that either porosity well logs or another transient test should be used in order to determine the fractal parameters.

In 1990 and 1994, Beier improved the study of Chang and Yortsos. While Chang and Yortsos solved the diffusivity equations by assuming finite wellbore condition, Beier solved the governing equation based upon line source well with radial symmetry. Furthermore, Beier expected that the fractal dimension (d_f) should be 2 or slightly less in oil in place calculations. In addition to that, Beier applied fractal theory to field pressure test examples and got fair enough results for the pressure transient behavior of a fractal reservoir. As a result, he observed that there is a power – law behavior for the linear and radial flow.

In 1994, Metzler et al. introduced the new model which is called the anomalous model. Metzler et al. (1994) claimed that the anomalous model is different than the fractal model. They believed that anomalous diffusion cannot be described by the fractal model because the diffusion process of fractal (fractured) reservoirs is history dependent. They proposed the new diffusivity equation, which is quite similar to the fractal model, but it includes the temporal fractional derivative. The diffusivity equation proposed by Metzler et al. (1994) is

$$\frac{1}{\tilde{\eta}}\frac{\partial p^{\alpha}(r,t)}{\partial t^{\alpha}} = \frac{1}{r^{d_f-1}}\frac{\partial}{\partial r}\left(r^{\beta}\,\frac{\partial p(r,t)}{\partial r}\right), \tag{1.7}$$

where α is the anomalous diffusion exponent.

In 1995, Acuna et al. indicated that porosity and permeability of any region of radial distance are scale dependent as a power law. They obtained pretty good results for pressure transient responses from well in the geothermal field. They found out that wellbore pressure change has a power law relationship according to time. The topology of the network is indicated as archaeological $0 < \theta < 0.5$. They also stated that $0.6 < \frac{d_f}{d_w} < 0.86$ depend on their evaluation of field examples. Moreover, Acuna and Yortsos (1995) mentioned the box-counting method which has been used to characterize the fractal properties of real networks. For instance, Serpen (2000) determined the topology of the network and fractal dimension by using box-counting method.

Flamenco – Lopez and Camacho – Velazquez (2001) states that $0.47 < \frac{d_f}{d_w} < 0.67$ depends on the fractal reservoir in Mexico. Moreover, Flamenco – Lopez and Camacho – Velazquez (2003) showed that the fractal parameters can be found by using a fractal model which is Chang and Yortsos vertical well model when the transient flow and boundary dominated flow exists. Flamenco – Lopez and Camacho – Velazquez found that the determination of the four parameters of a fractal model requires the utilization of boundary dominated flow information because the single well transient test cannot define the fractal parameters. In addition, they showed an analytical solution for matrix blocks and fractal fracture contribution during transient and pseudo steady state flow period.

Camacho – Velazquez et al. (2008) evaluated the naturally fractured reservoirs and compared the fractal model and Metzler anomalous model. While they mentioned O'Shaughnessy and Procaccia (1985) and Chang and Yortsos (1990) study for the fractal model, they paid attention to Metzler work for the anomalous model. The main difference is that Metzler proposed a diffusivity equation involving time fractional fractal diffusion. Moreover, Camacho – Velazquez et al. (2008) referred OP expression for O'Shaughnessy and Procaccia (1985) and Chang and Yortsos (1990) study, and also, called MGN expression for Metzler et al. (1994). They investigated diffusion on a vertical well in a closed reservoir and an infinite reservoir. Both methods are applied with a dimensionless variable in Laplace space based on the constant wellbore pressure condition and the finite wellbore case. The main purpose of this study is to observe the production decline behavior in naturally fractured reservoirs consisting of single and double porosity with fractal networks of fractures. Camacho et al. recognized that when $\alpha = 1$ for suggested by Metzler, it is the same as that proposed by Chang and Yortsos (1990).

In 2011, Camacho et al. applied the Metzler method to analyze interference tests in actual field cases. The analysis of interference tests in single porosity naturally fractured fractal reservoirs are examined by using the Metzler anomalous method since this method includes memory through a fractional temporal derivative.

Raghavan (2011) looked at the anomalous diffusion from another point of view. Raghavan (2011) introduced a new flux definition different than Chang and Yortsos (1990) and Metzler et al. (1994) because Chang and Yortsos and Metzler et al. used the conventional form of Darcy's law and they did not change the continuity equation. Indeed, they used the convolved form of the continuity equation. Hence, Raghavan claimed that here is no way to obtain a differential equation involving fractional derivative by using conventional Darcy law and standard continuity equation. He proposed that either flux law or continuity equation should be changed for a fractional operator to result. Therefore, Raghavan (2011) changed the flux law. Moreover, Raghavan established new dimensionless pressure, flow rate, and time equations. Then, Raghavan (2011) solved the differential equation in radial symmetry both production at a constant rate by assuming a line source well and production at a constant pressure by considering finite wellbore case.

In 2012, Raghavan studied to figure out linear trends over exceedingly long-time frames without considering geometrical configurations. Raghavan considered two different types of fractional operators: Riemann – Liouville and Caputo. He preferred using Caputo fractional operator since Riemann – Liouville fractional operator does not pay regard to the use of physically interpretable initial conditions.

Then, Raghavan and Chen (2013a) applied the time fractional fractal model to the single vertical fracture model. They solved the equation using a Laplace transformation and derived the asymptotic solutions. These solutions are important, especially for numerical computations. Solutions are presented considering the constant terminal rate case and the constant terminal pressure case. In the same year, Raghavan and Chen (2013b) combined the analytical solution for transient linear flow under subdiffusion with a finite conductivity fracture.

In 2015, Raghavan and Chen introduced a new flux equation involving both time fractional derivative and spatial fractional derivative. They worked on the transient behavior in a linear reservoir. While time fractional derivative refers to subdiffusion, spatial fractional derivative refers to superdiffusion. In other words, they mentioned highly conductive paths with superdiffusion (spatial fractional derivative) and impediments to flow with subdiffusion (time fractional derivative).

1.3 Problem Statement

Humankind absolutely needs energy in order to survive on earth. Therefore, maximum efficiency, low-cost investment, and sustainability must be ensured when producing energy. Unfortunately, hydrocarbon reservoirs cannot provide this comfort zone at the same time. Because of unsustainable hydrocarbon reservoirs, governments and companies tend to utilize geothermal energy more these days. However, geothermal reservoirs are different than conventional hydrocarbon reservoirs. Thus, appropriate reservoir models are developed to investigate heterogenous reservoirs. In the literature, some of the reservoir models are used to analyze the heterogeneous reservoirs. Each model provides appropriate matches with real field data. However, these models have not been compared and applied to the same field case. In addition, the effect of each fractal parameter has not been shown for each reservoir model in the same study. Because of the different diffusivity equations, it is expected that solutions of each model and the effect of the fractal parameters should be different.

1.4 Objective and Scope of the Study

The main purpose of this study is to derive analytical solutions to model heterogeneous reservoirs and apply the reservoir models into the real fields by considering fractal and anomalous diffusion models. Another important objective of the study is to compare the responses from these two models for different inner boundary conditions such as constant-rate production and constant bottomhole pressure (BHP) and then to apply each of these model to analyze real pressure data sets by using a history matching method based on the ES-MDA method to characterize and estimate the models parameters for the geothermal reservoir system under consideration. This thesis is organized as follows. In chapter 2, the basic definition of fractal and the theory of fractal model and anomalous models are presented in detail. This part answers the definition of fractal, description of reservoir rock properties using fractal distributions, definition, and type of anomalous diffusion, and proposed anomalous diffusion models. In chapter 3, fractal and anomalous models are solved analytically by considering the constant rate, constant bottomhole pressure and variable rate – variable bottomhole pressure. The details for each solution are given in the appendix. In chapter 4, the analysis of interference pressure data from Kizildere (Liquid – dominated) and Kamojang (Vapor – dominated) geothermal fields are analyzed by using models. Nonlinear regression analysis (ES-MDA) is presented and used for analysis purposes. Finally, we state the main conclusions of this thesis.

CHAPTER 2

BASICS OF FRACTAL AND ANOMALOUS DIFFUSION MODELS

In this chapter, we describe basics of fractal and anomalous diffusion models, and present diffusivity equations for fractal model and anomalous models.

2.1 Fractal Diffusion Model

Firstly, the definition of a fractal is explained. Then, the fractal model which was derived by Chang and Yortsos (1990) is discussed.

2.1.1 Definition of fractal

In the 1970's, Mandelbrot was firstly introduced the term "fractal". Fractals comes from the Latin "fractus". The meaning is an irregular surface like a broken stone. Fractals could be regular or non – regular geometric shape that has a complex pattern. Although fractals are very complex, they consist of similar patterns and looks like self – similar with respect to different scales. To put it another way, while scale decreases or increases, the general overview looks like the same. Therefore, fractals can be thought that fractal is never ending pattern and forms the infinite loop.

Fractals have three fundamental characteristics: self – similarity, power law expression and noninteger dimension. Fern leaves are good examples for the fractals since a fern pattern is repeated across the different scales. As you can see in Figure 2.1, the fern leaf has a repeated pattern. Even though the smallest scale is reached, the shape of leaf has an exact replication of the overall leaf. Thus, the most obvious feature of the fractal is that the object has the similarity at different scales (Hardy and Beier, 1994).

Figure 2.1 Fern leaf (Hardy and Beier, 1994).

One of the most typical characteristic properties of the fractal is to have a positive noninteger dimension. People are familiar with 1D, 2D and 3D, but this is not applicable for the fractals because the dimension of the fractal is not an integer such as 1.8 or 2.4. Sierpinski Carpet is one of the best examples for this issue. Following figures demonstrates the Sierpinski Carpets.

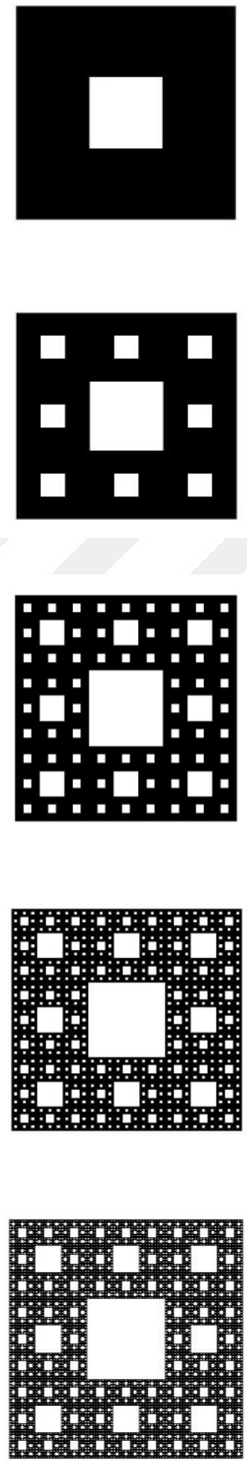

Figure 2.2 5 steps of a Sierpinski Carpet derived by MATLAB.

Figure 2.2 depicts 5 steps of the Sierpinski Carpet. In the first step, it starts one square with a square hole in its center, and then, this pattern is repeated with a smaller scale. If hole sides are 1/3 of the entire square and this condition is repeated in each of the four corners and sides of the large squares, the second step of Figure 2.2 is obtained. After repeating this process, third, fourth and fifth steps are achieved. To conclude, the dimension of the second step of the Sierpinski Carpet in Figure 2.2 is 1.893, if the first step of the Sierpinski Carpet has a length 3. The dimension is calculated by the following area formula:

$$A = cL^b \,, \tag{2.1}$$

where *A* is area, *b* and *c* are constants and *L* is length.

Table 2.1 b and c variables with respect to different shapes.

Shape	**c**	**b (refers dimension)**
Square	1	2
Equilateral triangle	$\sqrt{\frac{3}{4}}$	2
Half circle	$\frac{\pi}{2}$	2
Cube	1	3
Sphere	$\frac{4}{3}$	3
Pyramid	$\frac{1}{6}$	3
Sierpinski Carpet (Figure 2.2)	1	1.893

2.1.2 Fractal model

A pressure transient model based on fractals was developed by Chang and Yortsos in 1990. They extended the study for O'shaughnessy and Procaccia's (1985). The main idea of this model is to express the fracture network ($k\ and\ \phi$) as fractals. This model only can be applied to the subdiffusion condition (see Section 2.2 for definition of subdiffusion). In other words, fractal network is highly tortuous path, so topology of the network (θ) has to be bigger than zero. Although O'shaughnessy and Procaccia define the permeability as a fractal, Chang and Yortsos (1990) and Beier (1994) identified both permeability and porosity as a fractal. The porosity and permeability are presented depending on the position.

$$\phi(r) = \phi_0 \left(\frac{r}{r_0}\right)^{d_f - d} \tag{2.2}$$

and

$$k(r) = k_0 \left(\frac{r}{r_0}\right)^{d_f - d - \theta}, \tag{2.3}$$

where d is the Euclidean dimension, k_0 is reference permeability at r_0, r radius, r_0 is reference radius, and ϕ_0 is reference porosity at r_0. It is note that while Euclidean dimension (d) is an integer number, fractal dimension (d_f) is noninteger. Euclidean dimension $d = 1{,}2{,}3$ for rectilinear, cylindrical, and spherical geometry, respectively. Moreover, porosity and permeability at wellbore radius can be described as

$$\phi(r_w) = \phi_0 \left(\frac{r_w}{r_0}\right)^{d_f - d} \tag{2.4}$$

and

$$k(r_w) = k_0 \left(\frac{r_w}{r_0}\right)^{d_f - d - \theta}. \tag{2.5}$$

As a result, the porosity and permeability at any point r can be written as

$$\phi(r) = \phi(r_w)\left(\frac{r}{r_w}\right)^{d_f-d} \tag{2.6}$$

and

$$k(r) = k(r_w)\left(\frac{r}{r_w}\right)^{d_f-d-\theta}. \tag{2.7}$$

The classical diffusivity equation for a cylindrical system ($d = 2$)

$$\frac{\partial p}{\partial t} = \frac{c_1}{\phi(r)c_t\mu}\frac{1}{r}\frac{\partial}{\partial r}\left(k(r)r\frac{\partial p}{\partial r}\right), \tag{2.8}$$

where $c_1 = 1$ in SI unit, and $c_1 = 2.637x10^{-4}$ in oil field unit. Using Eqs. 2.6 and 2.7, the diffusivity equation for the fractal diffusion model is described as:

$$\frac{\partial p}{\partial t} = \frac{c_1 k(r_w) r_w^{\theta}}{\phi(r_w)c_t\mu}\frac{1}{r^{d_f-1}}\frac{\partial}{\partial r}\left(r^{d_f-\theta-1}\frac{\partial p}{\partial r}\right). \tag{2.9}$$

In addition, the diffusivity equation for the fractal diffusion model can be written as dimensionless by using the following dimensionless radius, time, and pressure,

$$r_D = \frac{r}{r_w}, \tag{2.10}$$

$$t_D = \frac{c_1 k(r_w) t}{\phi(r_w)c_t\mu\, r_w^2}, \tag{2.11}$$

and

$$p_D = \frac{k(r_w)h}{c_2 qB\mu}(p_i - p), \tag{2.12}$$

where $c_2 = 2\pi$ in SI unit and $c_2 = 141.2$ in oil field units. As a result, the dimensionless diffusivity equation for fractal diffusion model is

$$\frac{\partial p_D}{\partial t_D} = \frac{1}{r_D^{d_f-1}}\frac{\partial}{\partial r_D}\left(r_D^{\beta}\frac{\partial p_D}{\partial r_D}\right), \tag{2.13}$$

where $\beta = d_f - \theta - 1$. Furthermore, Raghavan (2011) redisplayed the fractal model in a different notation. He showed that Chang and Yortsos described the diffusivity equation for flow of a slightly compressible fluid in a fractal network in dimensional coordinate system:

$$\frac{1}{\dot{\eta}}\frac{\partial p(r,t)}{\partial t} = \frac{1}{r^{d_f-1}}\frac{\partial}{\partial r}\left(r^{\beta}\frac{\partial p(r,t)}{\partial r}\right), \tag{2.14}$$

where

$$\dot{\eta} = \frac{m}{c_t \mu}, \tag{2.15}$$

where m is fracture network parameter in the fractal system, c_t is compressibility, μ is viscosity.

$$m = \frac{k_f}{\phi_f}, \tag{2.16}$$

where k_f and ϕ_f are permeability and porosity in the fracture, respectively.

2.2 Anomalous Diffusion Models

Firstly, we explain the definition of anomalous diffusion. Then, the anomalous diffusion model which is derived by Metzler is presented. Finally, another anomalous diffusion model which is introduced by Raghavan is shown.

2.2.1 Definition of anomalous diffusion

In statistic, the position of the particles which depends on time have a relationship between mean – square displacement (MSD) of the particle and time. The MSD in fractal (heterogenous) media can be shown as

$$r^2 \sim t^{\gamma}. \tag{2.17}$$

When the exponent γ is equal to 1, Eq. 2.17 refers normal (conventional) diffusion in the matrix and natural fracture regions. In other words, the MSD of the particle and time has a linear relationship. Normal diffusion is usually valid for homogeneous porous media. In this case, Brownian motion of individual particles behaves Gaussian distribution. On the other hand, if α is not equal to 1, the process is anomalous diffusion. This means that the diffusion process is either slower or faster. The anomalous diffusion is displayed in disordered and heterogeneous reservoirs.

$$\begin{array}{ll} \gamma = 1 & Normal\ Diffusion \\ \gamma \neq 1 & Anomalous\ Diffusion \\ \gamma < 1 & Subdiffusion \\ \gamma > 1 & Superdiffusion \end{array} \tag{2.18}$$

It can be seen that diffusion has a power law relationship, and fluid particles obey a Continuous Time Random Walk (CTRW) behavior (Raghavan, 2011). In CTRW model, the fluid particles change the position between two points. If there is an impediment or obstacle for flux, the diffusion process goes slower. As a result, the diffusion process is called subdiffusion. On the other side of the coin, if particles change their position in a smaller time scale or jump longer than normal displacement, this process is called superdiffusion. For example, highly conductive and well-connected paths supply longer jump for particles. For instance, Redner (1989) presented the superdiffusion model, and Cloot and Botha (2006) studied on extremely conductive paths.

2.2.2 Anomalous diffusion model proposed by Metzler

In 1994, Metzler et al. proposed new diffusion equation for the fluid flow in fractal porous media. The main difference is that Metzler et al. introduced fractional calculus for the behavior of transport process in fractal porous media. Park et al. (2000) explained the main idea of Metzler's study. That is, the root idea is that Chang and Yortsos's study fails to capture the history of the diffusion process and the nonlocality. Hence, Metzler incorporates the memory effect by applying the fractional derivative. The mass balance for the differential shell (Figure 2.3) is that:

$$\begin{Bmatrix} Amount\ of \\ Mass\ Input \end{Bmatrix} - \begin{Bmatrix} Amount\ of \\ Mass\ Output \end{Bmatrix} = \begin{Bmatrix} Increment\ of\ Mass\ Content \\ of\ Fractal\ loops\ in\ matrix \end{Bmatrix} \tag{2.19}$$

The diffusivity equation in the dimensionless domain can be expressed by the above mass balance:

$$\frac{\partial^\alpha p_D(r_D, t_D)}{\partial t_D^\alpha} = \frac{1}{r_D^{d_f-1}} \frac{\partial}{\partial r_D}\left(r_D^{d_f-\theta-1} \frac{\partial p_D(r_D, t_D)}{\partial r_D}\right) \tag{2.20}$$

or

$$\frac{\partial^\alpha p_D}{\partial t_D^\alpha} = \frac{1}{r_D^{d_f-1}} \frac{\partial}{\partial r_D}\left(r_D^\beta \frac{\partial p_D}{\partial r_D}\right), \tag{2.21}$$

where $\alpha = \frac{2}{2+\theta}$, α is the anomalous diffusion exponent, and r_D, t_D and p_D are given in Eqs. 2.10, 2.11 and 2.12, respectively.

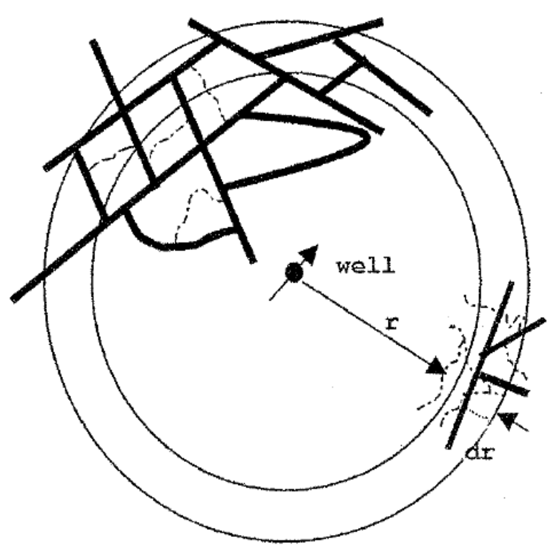

Figure 2.3 Flow across from backbone fracture to the fractal loops and to the production well (Park et al., 2000).

Metzler et al. used the same dimensionless radius, time, and pressure with Chang and Yortsos. In dimensional coordinate system, the diffusivity equation for flow of a slightly compressible fluid in a fractured network is given (Raghavan, 2011):

$$\frac{1}{\tilde{\eta}}\frac{\partial p^{\alpha}(r,t)}{\partial t^{\alpha}} = \frac{1}{r^{d_f-1}}\frac{\partial}{\partial r}\left(r^{\beta}\frac{\partial p(r,t)}{\partial r}\right), \tag{2.22}$$

where

$$\tilde{\eta} = \frac{1}{\Gamma(1-\alpha)A_{\alpha}}\frac{m}{c_t\mu} \tag{2.23}$$

and

$$A_{\alpha} = \left(\frac{\mu c_t r_w^{\theta+2}}{m}\right)^{\alpha-1}. \tag{2.24}$$

2.2.3 Anomalous diffusion model proposed by Raghavan

In 2011, Raghavan compared Chang and Yortsos's study and Metzler's study. Raghavan partially agreed with Metzler's study. However, he claimed that Metzler's approaches partially correct because Metzler derived the diffusivity equation (Eq. 2.22) by using conventional form of Darcy's law which is

$$q(\bar{x},t) = -\frac{k}{\mu}\nabla p(\bar{x},t). \tag{2.25}$$

In addition, Metzler did not change the convolved form of the continuity equation. Therefore, Raghavan asserted that it is not possible to obtain Eq. 2.22 by using conventional Darcy law and convolved form of the continuity equation. Either flux term or continuity equation has to be modified. Therefore, Raghavan (2011) proposed a new flux term:

$$q(\bar{x},t) = -\frac{k_{\alpha}}{\mu}\frac{d}{dt}\int_0^t dt'\frac{1}{(t-t')^{1-\alpha}}\nabla p(\bar{x},t). \tag{2.26}$$

Then, Raghavan updated the flux term in 2013.

$$q(\bar{x},t) = -\frac{k_\alpha}{\mu}\frac{\partial^{1-\alpha}}{\partial t^{1-\alpha}}[\nabla p(\bar{x},t)]. \tag{2.27}$$

Eq. 2.26 and Eq. 2.27 are the same and serve for the same purpose. He just changed the notation. Furthermore, Raghavan prefer using Caputo (1967) fractional operator to take the Laplace transform of fractional derivative. The Caputo fractional operator is

$${}_0^cD_t^\alpha x(t) = \frac{1}{\Gamma(n-\alpha)}\int_0^t dt'(t-t')^{n-\alpha-1}\frac{d^n}{dt'^n}f(t') \ . \tag{2.28}$$

The Laplace transform of Caputo fractional operator is (Liang et al., 2015):

$$\int_0^\infty e^{-st}\,{}_0^cD_t^\alpha f(t)dt = s^\alpha f(s) - s^{\alpha-1}f(0), \tag{2.29}$$

where $0 \leq \alpha < 1$. Therefore, Laplace transform of Eq. 2.26 with respect to t is

$$\bar{q}(\bar{x},s) = -s^{1-\alpha}\frac{k_\alpha}{\mu}\nabla\bar{p}(\bar{x},s). \tag{2.30}$$

It is fact that the Laplace transform of Eq. 2.27 is also equal to Eq. 2.30. Moreover, Raghavan derived the diffusivity equation for the flow of a slightly compressible liquid to a well in the radial coordinate system by using the conservation equation given by:

$$\frac{\partial q(r,t)}{\partial r} = \phi c_t\frac{\partial p(r,t)}{\partial t}. \tag{2.31}$$

Then, taking the Laplace transform of Eq. 2.31 with respect to t gives

$$\frac{\partial\bar{q}(r,s)}{\partial r} = \phi c_t[s\bar{p}(r,s) - p(r,t=0)]. \tag{2.32}$$

Next, putting Eq. 2.30 into Eq. 2.32 gives us

$$\frac{\partial}{\partial r}\left(s^{1-\alpha}\frac{k_\alpha}{\mu}\frac{\partial}{\partial r}\bar{p}(r,s)\right) = \phi c_t[s\bar{p}(r,s) - p(r,t=0)] \tag{2.33}$$

or

$$s^{1-\alpha}\frac{\partial}{\partial r}\left(\frac{k_\alpha}{\mu}\frac{\partial}{\partial r}\bar{p}(r,s)\right)=\phi c_t[s\bar{p}(r,s)-p(r,t=0)]. \tag{2.34}$$

Divide left and right-hand side with $s^{1-\alpha}$, so

$$\frac{\partial}{\partial r}\left(\frac{k_\alpha}{\mu}\frac{\partial}{\partial r}\bar{p}(r,s)\right)=\frac{\phi c_t[s\bar{p}(r,s)-p(r,t=0)]}{s^{1-\alpha}} \tag{2.35}$$

or

$$\frac{\partial}{\partial r}\left(\frac{k_\alpha}{\mu}\frac{\partial}{\partial r}\bar{p}(r,s)\right)=\phi c_t[s^\alpha\bar{p}(r,s)-s^{\alpha-1}p(r,t=0)]. \tag{2.36}$$

Taking the inverse Laplace transform of Eq. 2.36 provides the diffusivity equation for the anomalous diffusion model proposed by Raghavan.

$$\frac{\partial}{\partial r}\left(\frac{k_\alpha}{\mu}\frac{\partial}{\partial r}p(r,t)\right)=\phi c_t\frac{\partial^\alpha p(r,t)}{\partial t^\alpha} \tag{2.37}$$

or

$$\nabla\left(\frac{k_\alpha}{\mu}\nabla p(r,t)\right)=\phi c_t\frac{\partial^\alpha p(r,t)}{\partial t^\alpha} \tag{2.38}$$

or

$$\nabla[\lambda(r)\nabla p(r,t)]=\phi c_t\frac{\partial^\alpha p(r,t)}{\partial t^\alpha}, \tag{2.39}$$

where $\lambda(r)=\lambda_\alpha r^{-\theta}=\frac{k_\alpha}{\mu}r^{-\theta}$. In addition, Raghavan showed that Eq. 2.39 can be written as

$$\frac{1}{r^{n-1}}\frac{\partial}{\partial r}\left[r^{n-1}\lambda(r)\frac{\partial p(r,t)}{\partial r}\right]=\phi c_t\frac{\partial^\alpha p(r,t)}{\partial t^\alpha}. \tag{2.40}$$

Eq. 2.27 is applicable for subdiffusion. Therefore, Chen and Raghavan (2015) modified the flux term in order to solve superdiffusion condition.

$$q(x,t)=-\frac{k_{\alpha,\beta}}{\mu}\frac{\partial^{1-\alpha}}{\partial t^{1-\alpha}}\left[\frac{\partial^\beta}{\partial x^\beta}p(x,t)\right] \tag{2.41}$$

or

$$q(x,t) = -\lambda_{\alpha,\beta} \frac{\partial^{1-\alpha}}{\partial t^{1-\alpha}} \left[\frac{\partial^{\beta}}{\partial x^{\beta}} p(x,t) \right]. \quad (2.42)$$

Chen and Raghavan (2015) presented the subdiffusion flow with a time fractional derivative and described the superdiffusion flow with a space fractional derivative. Therefore, they defined both time fractional derivative and space fractional derivative with Caputo fractional operator

$$\frac{\partial^{\alpha}}{\partial t^{\alpha}} f(t) = \frac{1}{\Gamma(1-\alpha)} \int_0^t dt'(t-t')^{-\alpha} \frac{d}{dt'} f(t') \quad (2.43)$$

and

$$\frac{\partial^{\beta}}{\partial x^{\beta}} f(x) = \frac{1}{\Gamma(1-\beta)} \int_0^x dx'(x-x')^{-\beta} \frac{d}{dx'} f(x'), \quad (2.44)$$

where $0 < \alpha < 1$ and $0 < \beta < 1$. In conclusion, we study with subdiffusion in this thesis, so we assume $\beta = 1$, and α is changed in the given range.

CHAPTER 3

SOLUTIONS OF DIFFUSIVITY EQUATIONS FOR PRESSURE TRANSIENT WELL TESTS BASED ON FRACTAL AND ANOMALOUS DIFFUSION MODELS

In this chapter, we present analytical solutions of diffusivity equations for fractal and anomalous diffusion models. We describe the initial boundary value problem (IBVP) for each of the models. The solution of each model is presented for constant rate, constant pressure, and variable rate/variable bottomhole pressure in the Laplace space. Then, the fractal model and Metzler anomalous diffusion models are compared when $\Theta = 0$. After that, the effect of fractal dimension and topology of the network are investigated for each model. Next, the dimensionless pressure response in the reservoir is analyzed. Finally, the influence of fractal dimension d_f for Metzler anomalous model and n for Raghavan anomalous model is studied.

3.1 Fractal Model

In this part, constant rate, constant bottomhole pressure, and variable rate/variable bottomhole pressure are solved for an entirely fractal reservoir by using fractal model. Firstly, the initial condition, inner boundary condition, and outer boundary condition are given in dimensionless. The diffusivity equation is already given in Chapter 2. Laplace space analytical solutions are found in dimensionless coordinate. Finally, the solution is converted from dimensionless to dimensional by using scaling property.

3.1.1 Constant rate

In this section, the solution of the diffusivity equation is solved for constant rate condition. The diffusivity equation is given in Section 2.

$$\frac{\partial p_D}{\partial t_D} = \frac{1}{r_D^{d_f-1}} \frac{\partial}{\partial r_D}\left(r_D^{\beta} \frac{\partial p_D}{\partial r_D}\right), \tag{2.13}$$

where $\beta = d_f - \Theta - 1$. The initial condition is,

$$p_D(r_D, t_D = 0) = 0. \tag{3.1}$$

The inner boundary condition for a finite wellbore is

$$\left(r_D^{\beta} \frac{\partial p_D}{\partial r_D}\right)_{r_D=1} = -1. \tag{3.2}$$

The outer boundary condition is

$$\lim_{r_D \to \infty} p_D(r_D, t_D) = 0. \tag{3.3}$$

Let us start with taking the Laplace transform of the diffusivity equation, and applying the initial condition:

$$s\overline{p_D}(r_D, s) = \frac{1}{r_D^{d_f-1}} \frac{d}{dr_D}\left(r_D^{\beta} \frac{d\overline{p_D}}{dr_D}\right). \tag{3.4}$$

The above equation can be written as

$$s\overline{p_D}(r_D, s) = \frac{1}{r_D^{\beta+\Theta}} \frac{d}{dr_D}\left(r_D^{\beta} \frac{d\overline{p_D}}{dr_D}\right). \tag{3.5}$$

Next, the Laplace transform of the inner boundary condition is

$$\left(r_D^{\beta} \frac{\partial \overline{p_D}}{\partial r_D}\right)_{r_D=1} = -\frac{1}{s}, \tag{3.6}$$

and the outer boundary condition in the Laplace domain is

$$\lim_{r_D \to \infty} \overline{p_D}(r_D, s) = 0. \tag{3.7}$$

Before, applying the outer and inner boundary conditions, Eq. 3.4 is rearranged to find a general solution,

$$r_D^2 \frac{d^2\overline{p_D}}{dr_D^2} + \beta r_D \frac{d\overline{p_D}}{dr_D} - r_D^{\theta+2} s\overline{p_D}(r_D, s) = 0. \tag{3.8}$$

The details of this section are given in Appendix A. The general solution of Eq. 3.8 is

$$\overline{p_D}(r_D, s) = r_D^{\frac{\theta+2}{2}\nu} \left\{ A I_\nu \left[\frac{2\sqrt{s}}{\theta+2} r_D^{\frac{\theta+2}{2}} \right] + B K_\nu \left[\frac{2\sqrt{s}}{\theta+2} r_D^{\frac{\theta+2}{2}} \right] \right\}, \tag{3.9}$$

where $\nu = \frac{1-\beta}{\theta+2}$. Next, the inner and outer boundary conditions are applied to find A and B. While A is equal to zero because of the infinite-acting outer boundary condition given by Eq. 3.7, B is then determined by applying the inner boundary condition given by Eq. 3.6 as

$$B = \frac{1}{s\sqrt{s} K_{\nu-1}\left(\frac{2\sqrt{s}}{\theta+2}\right)}. \tag{3.10}$$

Consequently, the result is

$$\overline{p_D}(r_D, s) = r_D^{\frac{\theta+2}{2}\nu} \frac{K_\nu \left[\frac{2\sqrt{s}}{\theta+2} r_D^{\frac{\theta+2}{2}} \right]}{s\sqrt{s}\ K_{\nu-1}\left[\frac{2\sqrt{s}}{\theta+2} \right]}, \tag{3.11}$$

or

$$\overline{p_D}(r_D, s) = r_D^{\frac{1-\beta}{2}} \frac{K_\nu \left[\frac{2\sqrt{s}}{\theta+2} r_D^{\frac{\theta+2}{2}} \right]}{s\sqrt{s}\ K_{\nu-1}\left[\frac{2\sqrt{s}}{\theta+2} \right]}. \tag{3.12}$$

Next, pressure change, Δp, is found by using Eqs. 2.11 and 2.12 in the SI unit.

$$t_D = \frac{k(r_w)t}{\phi(r_w)c_t \mu\, r_w^2} \tag{2.11}$$

and

$$p_D = \frac{k(r_w)h}{2\pi qB\mu}(p_i - p) = \frac{k(r_w)h}{2\pi qB\mu}\Delta p. \tag{2.12}$$

Eq. 2.11 can be written as

$$t_D = \eta^* t, \tag{3.13}$$

where

$$\eta^* = \frac{k(r_w)}{\phi(r_w)c_t\mu r_w^2}. \tag{3.14}$$

Then, Eq. 2.12 in the Laplace space is given by,

$$\overline{\overline{p_D}}(s) = \frac{kh}{2\pi qB\mu}\overline{\overline{\Delta p}}(r,s), \tag{3.15}$$

where $\overline{\overline{p_D}}(s)$ is the Laplace transform of $p_D(t_D)$ with respect to time t, and $\overline{\overline{\Delta p}}(s)$ represents the Laplace transform of $\Delta p(t)$ with respect to t. Applying scaling property helps us to find $\overline{\overline{p_D}}(s)$,

$$\overline{\overline{p_D}}(r_D,s) = r_D^{\frac{\theta+2}{2}\nu}\left(\frac{K_\nu\left[\frac{2\sqrt{\frac{s}{\eta^*}}}{\theta+2}r_D^{\frac{\theta+2}{2}}\right]}{s\sqrt{\frac{s}{\eta^*}}\;K_{\nu-1}\left[\frac{2\sqrt{\frac{s}{\eta^*}}}{\theta+2}\right]}\right). \tag{3.16}$$

The details of scaling property operation are given in Appendix B. As a result, $\overline{\overline{\Delta p}}(s)$ is found as:

$$\overline{\overline{\Delta p}}(r,s) = \frac{2\pi qB\mu}{kh}r_D^{\frac{\theta+2}{2}\nu}\left(\frac{K_\nu\left[\frac{2\sqrt{\frac{s}{\eta^*}}}{\theta+2}r_D^{\frac{\theta+2}{2}}\right]}{s\sqrt{\frac{s}{\eta^*}}\;K_{\nu-1}\left[\frac{2\sqrt{\frac{s}{\eta^*}}}{\theta+2}\right]}\right). \tag{3.17}$$

3.1.2 Constant bottomhole pressure

In this section, the solution of the diffusivity equation of the fractal model is solved for constant bottomhole pressure condition. The details of the derivation are given in Appendix C. The diffusivity equation is given Eq. 2.13, in Section 2. Moreover, the same initial and outer boundary condition is used for this section. On the other hand, the inner boundary condition is changed as:

$$p_D(r_D = 1, t_D) = 1. \tag{3.18}$$

The Laplace transform of inner boundary condition is

$$\overline{p_D}(r_D = 1, s) = \frac{1}{s}. \tag{3.19}$$

Note that dimensionless time and dimensionless radius are defined in Eqs. 2.10 and 2.11. On the other hand, dimensionless pressure is defined differently for constant bottomhole pressure:

$$p_D = \frac{p_i - p}{p_i - p_{wf}} = \frac{\Delta p(r,t)}{\Delta p_{wf}}. \tag{3.20}$$

After taking the Laplace transform of the diffusivity equation and applying derivation, we obtain the general solution which is the same as the constant rate solution.

$$\overline{p_D}(r_D, s) = r_D^{\frac{\theta+2}{2}\nu} \left\{ A I_\nu \left[\frac{2\sqrt{s}}{\theta+2} r_D^{\frac{\theta+2}{2}} \right] + B K_\nu \left[\frac{2\sqrt{s}}{\theta+2} r_D^{\frac{\theta+2}{2}} \right] \right\}. \tag{3.9}$$

As we consider an infinite-acting reservoir, the outer boundary condition is the same with the constant rate solution, which is given by Eq. 3.7. Thus, A must be zero due to the outer boundary condition given by Eq. 3.7, but B should not be zero. As a result, the general solution reduces to

$$\overline{p_D}(r_D, s) = r_D^{\frac{\theta+2}{2}\nu} B K_\nu \left[\frac{2\sqrt{s}}{\theta+2} r_D^{\frac{\theta+2}{2}} \right]. \tag{3.21}$$

The inner boundary condition in the Laplace space is applied to Eq. 3.21 to find B,

$$B = \frac{1}{sK_\nu\left[\frac{2\sqrt{s}}{\theta + 2}\right]} . \tag{3.22}$$

Consequently, the dimensionless pressure in the Laplace domain is

$$\overline{p_D}(r_D, s) = r_D^{\frac{\theta+2}{2}\nu} \frac{K_\nu\left[\frac{2\sqrt{s}}{\theta + 2} r_D^{\frac{\theta+2}{2}}\right]}{sK_\nu\left[\frac{2\sqrt{s}}{\theta + 2}\right]} \tag{3.23}$$

or

$$\overline{p_D}(r_D, s) = r_D^{\frac{1-\beta}{2}} \frac{K_\nu\left[\frac{2\sqrt{s}}{\theta + 2} r_D^{\frac{\theta+2}{2}}\right]}{sK_\nu\left[\frac{2\sqrt{s}}{\theta + 2}\right]} . \tag{3.24}$$

Next, the pressure change, Δp, is found by using Eqs. 3.13 and 3.14. The details of derivation are given in Appendix D. Taking the Laplace transform of Eq. 3.20 yields

$$\overline{\overline{p_D}}(s) = \frac{1}{\Delta p_{wf}} \overline{\overline{\Delta p}}(r, s). \tag{3.25}$$

Applying the scaling property helps us find

$$\overline{\overline{p_D}}(s) = \mathcal{L}_t[p_D(\eta^* t)] = r_D^{\frac{\theta+2}{2}\nu} \frac{K_\nu\left[\frac{2\sqrt{\frac{s}{\eta^*}}}{\theta + 2} r_D^{\frac{\theta+2}{2}}\right]}{sK_\nu\left[\frac{2\sqrt{\frac{s}{\eta^*}}}{\theta + 2}\right]} . \tag{3.26}$$

Finally, pressure change in the Laplace space with respect to t is

$$\overline{\overline{\Delta p}}(s) = \frac{\Delta p_{wf}}{s} r_D^{\frac{\theta+2}{2}\nu} \left(\frac{K_\nu \left[\frac{2\sqrt{\frac{s}{\eta^*}}}{\theta+2} r_D^{\frac{\theta+2}{2}} \right]}{K_\nu \left[\frac{2\sqrt{\frac{s}{\eta^*}}}{\theta+2} \right]} \right). \tag{3.27}$$

3.1.3 Variable rate/Variable bottomhole pressure

In this section, we present production at a specified variable rate and bottomhole pressure. Up to this section, we found the constant rate and bottomhole pressure solution for fractal model. Now, we use these solutions in this section. Firstly, we explain the solution of variable rate case. Pressure change is explained by using a superposition equation assuming a piecewise step rate function in each time interval.

$$p_i - p(r,t) = \sum_{j=1}^{N} (q_j - q_{j-1}) \Delta p_u(r, t - t_{j-1}), \tag{3.28}$$

where N means the total number of flow rate steps. Note that $q_0 = 0$ and $t_0 = 0$. Pressure is described as

$$p(r,t) = \begin{cases} p_w(r,t) & for\ r = r_w, \\ p_{ow}(r,t) & for\ r_w < r < r_e, \end{cases} \tag{3.29}$$

where p_w and p_{ow} are the pressure response at the well and inside the reservoir, respectively. Next,

$$\Delta p_u(r,t) = \begin{cases} \Delta p_{wu}(r,t) & for\ r = r_w, \\ \Delta p_{owu}(r,t) & for\ r_w < r < r_e, \end{cases} \tag{3.30}$$

where $\Delta p_{wu}(r,t)$ and $\Delta p_{owu}(r,t)$ is the unite rate pressure change solution at r is at the well, and outside of the well, respectively. We previously presented the constant rate solution Eq. 3.17 in Section 3.1.1. When $qB = 1$, the solutions provide the unit rate pressure solutions ($\Delta p_{wu}(r,t)$ and

$\Delta p_{owu}(r,t)$). Furthermore, to take the inverse Laplace transform, we use Stehfest algorithm (Stehfest, 1970) with $N_{Stef} = 12$.

Secondly, we show how to find specified variable bottomhole pressure. In this case, the pressure change is described by using superposition equation considering piecewise step bottomhole pressure function in each time interval.

$$p_i - p(r,t) = \sum_{j=1}^{N} \left(\Delta p_{wf,j} - \Delta p_{wf,j-1}\right) \Delta p_{cp,u}\left(r, t - t_{j-1}\right), \tag{3.31}$$

where N means the total number of bottomhole pressure change steps. Note that $q_0 = 0$ and $t_0 = 0$. Pressure is described as

$$p(r,t) = \begin{cases} p_w(r,t) & for\ r = r_w \\ p_{ow}(r,t) & for\ r_w < r < r_e \end{cases} \tag{3.32}$$

and

$$\Delta p_{cp,u}(r,t) = \begin{cases} \Delta p_{cp,wu}(r,t) & for\ r = r_w, \\ \Delta p_{cp,owu}(r,t) & for\ r_w < r < r_e, \end{cases} \tag{3.33}$$

where $\Delta p_{cp,wu}(r,t)$ and $\Delta p_{cp,owu}(r,t)$ symbolize the unit pressure change solutions at r is the well and inside the reservoir, respectively. We previously presented the constant bottomhole pressure solution Eq. 3.27 in Section 3.1.2. if $\Delta p_{wf} = 1$, then the unit pressure change solutions ($\Delta p_{cp,wu}(r,t)$ and $\Delta p_{cp,owu}(r,t)$) are found.

3.2 Anomalous Models

In this part, constant rate, constant bottomhole pressure, and variable rate/variable bottomhole pressure are solved for anomalous models. As mentioned before, there are two anomalous models. The first one is proposed by Metzler et al. (1994), and the second one is introduced by Raghavan (2011). In this part, it is assumed that subdiffusion exists, and space fractional exponent (β) is equal to 1. Firstly, we derive the analytical solution of Metzler anomalous model for dimensionless pressure in Laplace space. Then, dimensionless pressure is converted to pressure change in Laplace space by using scaling property. Next, we present Raghavan's anomalous model for pressure change solution in the SI unit. After, we convert the solution from pressure change to dimensionless pressure in the Laplace domain. In addition, the initial condition, inner boundary condition, and outer boundary condition are given separately for both Metzler anomalous model and Raghavan anomalous model. Each solution is presented individually in Laplace space.

3.2.1 Constant rate for Metzler anomalous model

In this part, the solution of diffusivity equation for Metzler anomalous model is solved for constant rate condition. Dimensionless variables are defined in Eqs. 2.10, 2.11 and 2.12. The details of derivation are expressed in Appendix E. Previously, the diffusivity equation is already given in Section 2:

$$\frac{\partial^\alpha p_D}{\partial t_D^\alpha} = \frac{1}{r_D^{d_f-1}} \frac{\partial}{\partial r_D}\left(r_D^\beta \frac{\partial p_D}{\partial r_D}\right), \tag{2.21}$$

where $\alpha = \frac{2}{2+\theta}$. The same initial condition, inner and outer boundary conditions (Eqs. 3.1, 3.2 and 3.3, respectively) are used in this section. Initially, we take the Laplace transform of the diffusivity equation.

$$s^\alpha \overline{p_D}(r_D, s) - s^{\alpha-1} p_D(r_D, t_D = 0) = \frac{1}{r_D^{d_f-1}} \frac{d}{dr_D}\left(r_D^\beta \frac{d\overline{p_D}}{dr_D}\right). \tag{3.34}$$

After applying the initial condition, and the derivation part, Eq. 3.34 is equal to

$$\frac{1}{r_D^{\theta}}\frac{d^2\overline{p_D}}{dr_D^2}+\frac{\beta}{r_D^{\theta+1}}\frac{d\overline{p_D}}{dr_D}-s^{\alpha}\overline{p_D}(r_D,s)=0. \tag{3.35}$$

The general solution of above equation is found as,

$$\overline{p_D}(r_D,s)=r_D^{\frac{\theta+2}{2}\nu}\left\{AI_\nu\left[\frac{2\sqrt{s^\alpha}}{\theta+2}r_D^{\frac{\theta+2}{2}}\right]+BK_\nu\left[\frac{2\sqrt{s^\alpha}}{\theta+2}r_D^{\frac{\theta+2}{2}}\right]\right\}, \tag{3.36}$$

where $\nu=\frac{1-\beta}{\theta+2}$. As you can see the order (ν) is the same with fractal model. After applying outer and inner boundary conditions, respectively, we obtain that while A must be zero, B is equal to

$$B=\frac{1}{s\sqrt{s^\alpha}K_{\nu-1}\left[\frac{2\sqrt{s^\alpha}}{\theta+2}\right]}. \tag{3.37}$$

Consequently, the dimensionless pressure is found as

$$\overline{p_D}(r_D,s)=r_D^{\frac{\theta+2}{2}\nu}\frac{K_\nu\left[\frac{2\sqrt{s^\alpha}}{\theta+2}r_D^{\frac{\theta+2}{2}}\right]}{s\sqrt{s^\alpha}\;K_{\nu-1}\left[\frac{2\sqrt{s^\alpha}}{\theta+2}\right]}. \tag{3.38}$$

Next, scaling property is used to find pressure change in the Laplace space. The derivation process is given in Appendix F. Eq. 3.15 is used to find pressure change ($\Delta p(r,s)$). As you know $\overline{\overline{p_D}}(s)$ is the Laplace transform of $p_D(t_D)$ with respect to time t, and $\overline{\overline{p_D}}(s)$ can be described as

$$\overline{\overline{p_D}}(s)=\mathcal{L}_t[p_D(\eta^* t)]=\frac{1}{\eta^*}\overline{p_D}\left(\frac{s}{\eta^*}\right). \tag{3.39}$$

So,

$$\overline{\overline{p_D}}(s)=r_D^{\frac{\theta+2}{2}\nu}\left(\frac{K_\nu\left[\frac{2\sqrt{\frac{s^\alpha}{\eta^*}}}{\theta+2}r_D^{\frac{\theta+2}{2}}\right]}{s\sqrt{\frac{s^\alpha}{\eta^*}}\;K_{\nu-1}\left[\frac{2\sqrt{\frac{s^\alpha}{\eta^*}}}{\theta+2}\right]}\right). \tag{3.40}$$

As a consequence, the pressure change is equal to

$$\overline{\overline{\Delta p}}(r_D, s) = \frac{2\pi q B \mu}{kh} r_D^{\frac{\theta+2}{2}\nu} \left(\frac{K_\nu \left[\frac{2\sqrt{\frac{s^\alpha}{\eta^*}}}{\theta+2} r_D^{\frac{\theta+2}{2}} \right]}{s\sqrt{\frac{s^\alpha}{\eta^*}} \;\; K_{\nu-1}\left[\frac{2\sqrt{\frac{s^\alpha}{\eta^*}}}{\theta+2} \right]} \right). \tag{3.41}$$

3.2.2 Constant bottomhole pressure for Metzler anomalous model

In this part, the solution of the diffusivity equation for Metzler anomalous model is solved for constant bottomhole pressure condition. The details of derivation are expressed in Appendix G. The diffusivity equation is already given in Eq. 2.21, in Section 2. Furthermore, the same initial and outer boundary conditions are utilized to calculate the analytical solution of Metzler anomalous model for constant bottomhole pressure conditions. However, we change the inner boundary condition. It is given in Section 3.1.2:

$$p_D(r_D = 1, t_D) = 1. \tag{3.18}$$

The Laplace transform of the inner boundary condition is also given in Section 3.1.2,

$$\overline{p_D}(r_D = 1, s) = \frac{1}{s}. \tag{3.19}$$

It is note that dimensionless pressure for constant bottomhole pressure is defined in Eq. 3.20. Then, the Laplace transform of the diffusivity equation of Metzler anomalous model is taken, and the general solution is given previously,

$$\overline{p_D}(r_D, s) = r_D^{\frac{\theta+2}{2}\nu} \left\{ A I_\nu \left[\frac{2\sqrt{s^\alpha}}{\theta+2} r_D^{\frac{\theta+2}{2}} \right] + B K_\nu \left[\frac{2\sqrt{s^\alpha}}{\theta+2} r_D^{\frac{\theta+2}{2}} \right] \right\}, \tag{3.36}$$

where $\nu = \frac{1-\beta}{\theta+2}$. It is clearly seen that the same general solution and order are obtained in Metzler anomalous model for constant rate condition. Next, the outer and inner boundary conditions are applied to general solution, respectively. As a result of calculation process, it is found that A is zero, and B is

$$B = \frac{1}{sK_\nu\left[\frac{2\sqrt{s^\alpha}}{\theta + 2}\right]}. \tag{3.42}$$

Consequently, Eq. 3.36 develops into

$$\overline{p_D}(r_D, s) = r_D^{\frac{\theta+2}{2}\nu} \frac{K_\nu\left[\frac{2\sqrt{s^\alpha}}{\theta + 2} r_D^{\frac{\theta+2}{2}}\right]}{sK_\nu\left[\frac{2\sqrt{s^\alpha}}{\theta + 2}\right]}. \tag{3.43}$$

Next, we find pressure change ($\Delta p(r, s)$) by applying scaling rule. The details of solution procedure are given in Appendix H.

$$\overline{\overline{\Delta p}}(r_D, s) = \frac{\Delta p_{wf}}{s} r_D^{\frac{\theta+2}{2}\nu} \left(\frac{K_\nu\left[\frac{2\sqrt{\frac{s^\alpha}{\eta^*}}}{\theta + 2} r_D^{\frac{\theta+2}{2}}\right]}{K_\nu\left[\frac{2\sqrt{\frac{s^\alpha}{\eta^*}}}{\theta + 2}\right]} \right). \tag{3.44}$$

3.2.3 Constant rate for Raghavan anomalous model

In this part, the analytical solution of Raghavan anomalous model is studied for constant rate condition. The main purpose of this part is to find pressure change in Laplace space. Therefore, we use different initial condition, inner and outer boundary conditions. The details of derivation are explained in Appendix I. As you know, the diffusivity equation for Raghavan anomalous model is

$$\frac{1}{r^{n-1}}\frac{\partial}{\partial r}\left[r^{n-1}\lambda(r)\frac{\partial p(r,t)}{\partial r}\right]=\phi c_t\frac{\partial^{\alpha}p(r,t)}{\partial t^{\alpha}}, \tag{2.40}$$

where $\lambda(r)=\lambda_{\alpha}r^{-\theta}=\frac{k_{\alpha}}{\mu}r^{-\theta}$. The above equation can be rewritten as for pressure change

$$\frac{1}{r^{n-1}}\frac{\partial}{\partial r}\left(r^{n-1-\theta}\lambda_{\alpha}\frac{\partial\Delta p}{\partial r}\right)=\phi c_t\frac{\partial^{\alpha}\Delta p(r,t)}{\partial t^{\alpha}}. \tag{3.45}$$

The initial condition is

$$\Delta p(r,t=0)=0. \tag{3.46}$$

The outer boundary condition is

$$\lim_{r\to\infty}\Delta p(r,t)=0, \tag{3.47}$$

and the inner boundary condition for a finite wellbore case

$$\lim_{r\to r_w}\left(r^{n-1-\theta}\frac{\partial^{1-\alpha}}{\partial t^{1-\alpha}}\frac{\partial\Delta p}{\partial r}\right)=-\frac{q_{sc}B}{\alpha_n\lambda_{\alpha}h}. \tag{3.48}$$

Next, Laplace transform of diffusivity equation with respect to t is found, and initial boundary condition is applied to get the general solution,

$$\frac{1}{r^{n-1}}\frac{\partial}{\partial r}\left(r^{n-1-\theta}\frac{\partial\overline{\Delta p}}{\partial r}\right)=\frac{\phi c_t}{\lambda_{\alpha}}s^{\alpha}\overline{\Delta p}(r,s). \tag{3.49}$$

Note that λ_{α} is constant. To simply the equation, let us define new variables,

$$\beta=n-1-\theta \tag{3.50}$$

and

$$\eta_i=\frac{\lambda_{\alpha}}{\phi c_t}. \tag{3.51}$$

So, the diffusivity equation develops into

$$\frac{1}{r^{\beta+\theta}}\frac{d}{dr}\left(r^{\beta}\frac{d\overline{\Delta p}}{dr}\right)=\frac{1}{\eta_i}s^{\alpha}\overline{\Delta p}(r,s). \tag{3.52}$$

The general solution of the above equation is

$$\overline{\Delta p}(r,s)=r^{-\frac{\theta+2}{2}\nu}\left\{CI_{\nu'}\left[\frac{2\sqrt{\frac{s^{\alpha}}{\eta_i}}}{\theta+2}r^{\frac{\theta+2}{2}}\right]+DK_{\nu'}\left[\frac{2\sqrt{\frac{s^{\alpha}}{\eta_i}}}{\theta+2}r^{\frac{\theta+2}{2}}\right]\right\}, \tag{3.53}$$

where C and D are the arbitrary constants to be determine from the outer and inner boundary conditions. Note that

$$\nu'=\frac{n}{d_w}-1=\frac{\beta-1}{\theta+2}. \tag{3.54}$$

Observe that, the order of Bessel I and Bessel K function is different than Chang and Yortsos and Metzler's solution,

$$\nu=-\nu'. \tag{3.55}$$

The negative reflection rule says that $K_{\nu}(z)=\mathrm{K}_{-\nu}(z)$, so $K_{\nu}(z)=\mathrm{K}_{\nu'}(z)$. Hence, there is no difference between the orders. After applying outer and inner boundary conditions, it is found that when $C=0$

$$D=\frac{q_{sc}B}{\alpha_n\lambda_\alpha hs^{2-\frac{\alpha}{2}}}\frac{\sqrt{\eta_i}}{r_w^{\frac{d_w(\nu\prime+1)}{2}}K_{\nu\prime+1}\left[2s^{\frac{\alpha}{2}}\left(\frac{r_w^{d_w}}{\eta_i d_w^2}\right)^{\frac{1}{2}}\right]}\ , \tag{3.56}$$

where $\alpha_n=\frac{2\pi^{\frac{n}{2}}}{\Gamma\left(\frac{n}{2}\right)}$ and $n=2$. In conclusion, the diffusivity equation for Raghavan's anomalous model in the Laplace space is

$$\overline{\Delta p}(r,s)=\frac{q_{sc}B}{\alpha_n\lambda_\alpha h s^{2-\frac{\alpha}{2}}}\frac{\sqrt{\eta_i}}{r_w^{\frac{d_w(\nu\prime+1)}{2}}K_{\nu\prime+1}\left[2s^{\frac{\alpha}{2}}\left(\frac{r_w^{d_w}}{\eta_i d_w^2}\right)^{\frac{1}{2}}\right]}r^{-\frac{d_w}{2}\nu\prime}K_{\nu\prime}\left[2s^{\frac{\alpha}{2}}\left(\frac{r^{d_w}}{\eta_i d_w^2}\right)^{\frac{1}{2}}\right].\qquad(3.57)$$

After, we find the dimensionless pressure. The dimensionless pressure is introduced by Raghavan (2011),

$$p_D(r_D,t_D)=\frac{\alpha_n k_\alpha h}{q_{sc}\alpha_p \mu}\Delta p(r,t),\qquad(3.58)$$

where

$$\alpha_p=\left(\frac{1}{\eta_i d_w^2}\right)^{\frac{1}{\alpha}-1}r_w^{d_w\left(\frac{1}{\alpha}-\xi\right)},\qquad(3.59)$$

where $\xi=\frac{n}{d_w}$. Moreover, dimensionless time is expressed as

$$t_D=\frac{\eta_i}{r^{d_w}}t^\alpha.\qquad(3.60)$$

Taking Laplace transform of Eq. 3.58 supplies to

$$\overline{p_D}=\frac{\alpha_n k_\alpha h}{q_{sc}\alpha_p \mu B}\overline{\Delta p}(r,s)\qquad(3.61)$$

or

$$\overline{\Delta p}(r,s)=\frac{q_{sc}\alpha_p \mu B}{\alpha_n k_\alpha h}\overline{p_D},\qquad(3.62)$$

where $\overline{p_D}(r,s)$ is the Laplace transform of $p_D(r_D,t_D)$ with respect to t. Equalizing Eq. 3.57 and Eq. 3.62 develops into

$$\frac{q_{sc}\alpha_p \mu B}{\alpha_n k_\alpha h}\overline{p_D}$$

$$= \frac{q_{sc}B}{\alpha_n \lambda_\alpha h s^{2-\frac{\alpha}{2}}} \frac{\sqrt{\eta_i}}{r_w^{\frac{d_w(\nu\prime+1)}{2}} K_{\nu\prime+1}\left[2s^{\frac{\alpha}{2}}\left(\frac{r_w^{d_w}}{\eta_i d_w^2}\right)^{\frac{1}{2}}\right]} r^{-\frac{d_w}{2}\nu\prime} K_{\nu\prime}\left[2s^{\frac{\alpha}{2}}\left(\frac{r^{d_w}}{\eta_i d_w^2}\right)^{\frac{1}{2}}\right]. \tag{3.63}$$

Consequently, dimensionless pressure is equal to

$$\overline{p_D}(r,s) = \frac{1}{\left(\frac{1}{\eta_i d_w^2}\right)^{\frac{1}{\alpha}-1} r_w^{d_w\left(\frac{1}{\alpha}-\xi\right)}} \frac{1}{s^{2-\frac{\alpha}{2}}}$$
$$\frac{\sqrt{\eta_i}}{r_w^{\frac{d_w(\nu\prime+1)}{2}} K_{\nu\prime+1}\left[2s^{\frac{\alpha}{2}}\left(\frac{r_w^{d_w}}{\eta_i d_w^2}\right)^{\frac{1}{2}}\right]} r^{-\frac{d_w}{2}\nu\prime} K_{\nu\prime}\left[2s^{\frac{\alpha}{2}}\left(\frac{r^{d_w}}{\eta_i d_w^2}\right)^{\frac{1}{2}}\right]. \tag{3.64}$$

3.2.4 Constant bottomhole pressure for Raghavan anomalous model

In this part, we present the analytical solution of Raghavan anomalous model for constant bottomhole pressure condition. The details of derivation are given in Appendix J. Initially, the same PDE, initial condition and outer boundary condition (Eqs. 3.45, 3.46 and 3.47) are used. The new inner boundary condition is introduced as

$$\Delta p(r = r_w, t) = \Delta p_w = constant. \tag{3.65}$$

The Laplace transform of the inner boundary condition is

$$\overline{\Delta p}(r = r_w, s) = \frac{\Delta p_w}{s}\ . \tag{3.66}$$

After taking the Laplace transform of the diffusivity equation, and applying the outer and inner boundary conditions, respectively, we obtain that the general solution is

$$\overline{\Delta p}(r = r_w, s) = \frac{\Delta p_w}{s} \frac{r^{-\frac{d_w}{2}\nu'}}{r_w^{-\frac{d_w}{2}\nu'}} \frac{K_{\nu'}\left(2s^{\frac{\gamma}{2}}\left(\frac{r^{d_w}}{\eta_i d_w^2}\right)^{\frac{1}{2}}\right)}{K_{\nu'}\left(2s^{\frac{\gamma}{2}}\left(\frac{r_w^{d_w}}{\eta_i d_w^2}\right)^{\frac{1}{2}}\right)}. \tag{3.67}$$

3.2.5 Variable rate/Variable bottomhole pressure for anomalous models

In this section, the analytical solution of a specified variable rate and bottomhole pressure is presented. The constant rate and the constant bottomhole pressure solution for Metzler anomalous model and Raghavan anomalous model are expressed in previous sections. Let us start with variable rate case. Pressure change is explained by using superposition equation assuming piecewise step rate function in each time interval.

$$p_i - p(r,t) = \sum_{j=1}^{N} (q_j - q_{j-1}) \Delta p_u(r, t - t_{j-1}), \tag{3.68}$$

where N means the total number of flow rate steps. Note that $q_0 = 0$ and $t_0 = 0$. Pressure is described as

$$p(r,t) = \begin{cases} p_w(r,t) & for\ r = r_w, \\ p_{ow}(r,t) & for\ r_w < r < r_e, \end{cases} \tag{3.69}$$

where p_w and p_{ow} are the pressure response at the well and inside the reservoir, respectively. Next,

$$\Delta p_u(r,t) = \begin{cases} \Delta p_{wu}(r,t) & for\ r = r_w, \\ \Delta p_{owu}(r,t) & for\ r_w < r < r_e, \end{cases} \tag{3.70}$$

where $\Delta p_{wu}(r,t)$ and $\Delta p_{owu}(r,t)$ is the unit rate pressure change solution at r is at the well, and outside of the well, respectively. This part is also shown in Section 3.1.3. However, the constant rate solution for Metzler anomalous model (Eq. 3.41) and Raghavan anomalous model (3.57) are different than fractal model. Therefore, when $qB = 1$, the solutions provide the different unit rate pressure solutions ($\Delta p_{wu}(r,t)$ and $\Delta p_{owu}(r,t)$). In addition, we use Stehfest algorithm (Stehfest, 1970) with $N_{Stef} = 12$ to take the inverse Laplace transform.

Next, the specified variable bottomhole pressure solution is found. In this case, the pressure change is described by using superposition equation considering piecewise step bottomhole pressure function in each time interval.

$$p_i - p(r,t) = \sum_{j=1}^{N} \left(\Delta p_{wf,j} - \Delta p_{wf,j-1}\right) \Delta p_{cp,u}\left(r, t - t_{j-1}\right), \tag{3.71}$$

where N means the total number of bottomhole pressure change steps. Note that $q_0 = 0$ and $t_0 = 0$. Pressure is described as

$$p(r,t) = \begin{cases} p_w(r,t) & for\ r = r_w \\ p_{ow}(r,t) & for\ r_w < r < r_e \end{cases} \tag{3.72}$$

and

$$\Delta p_{cp,u}(r,t) = \begin{cases} \Delta p_{cp,wu}(r,t) & for\ r = r_w, \\ \Delta p_{cp,owu}(r,t) & for\ r_w < r < r_e, \end{cases} \tag{3.73}$$

where $\Delta p_{cp,wu}(r,t)$ and $\Delta p_{cp,owu}(r,t)$ symbolize the unit pressure change solutions at r is the well and inside the reservoir, respectively. If $\Delta p_{wf} = 1$, then the unit pressure change solutions ($\Delta p_{cp,wu}(r,t)$ and $\Delta p_{cp,owu}(r,t)$) are found. The unit pressure change solution can be calculated by using Eq. 3.44 for Metzler anomalous model and Eq. 3.67 for Raghavan anomalous model.

3.3 Verification for Fractal and Anomalous Models

In this part, we present the relationship between fractal and anomalous models. In other words, we prove that fractal model is a special case of anomalous models. Furthermore, we show the effect of the topology of the network and fractal dimension for each model. Then, the pressure responses with respect to different distance are demonstrated for each model and compared between the models.

3.3.1 Relationship between fractal and anomalous model

In this part, we validate that the fractal model is a special case for Metzler anomalous model. Previously, the governing equation is given for both fractal model and Metzler anomalous model in Section 2. The PDE of fractal model is

$$\frac{\partial p_D}{\partial t_D} = \frac{1}{r_D^{d_f-1}} \frac{\partial}{\partial r_D}\left(r_D^{\beta} \frac{\partial p_D}{\partial r_D}\right), \tag{2.13}$$

and Metzler anomalous model diffusivity equation is

$$\frac{\partial^{\alpha} p_D}{\partial t_D^{\alpha}} = \frac{1}{r_D^{d_f-1}} \frac{\partial}{\partial r_D}\left(r_D^{\beta} \frac{\partial p_D}{\partial r_D}\right). \tag{2.21}$$

Camacho (2008) claims that if $\alpha = 1$, the diffusivity equation for Metzler model is the same as fractal model. Camacho (2008) studied constant bottomhole pressure condition. In this section, we firstly look at the constant rate condition. Then, we examine the constant bottomhole pressure case. Initially, we draw a graph for $\alpha = 1$ and $\Theta = 0$ for different fractal dimension at the wellbore ($r = r_w$) and in the reservoir ($r = 100r_w$) to show the behavior of the models. We use Stehfest algorithm (Stehfest, 1970) with $N_{Stef} = 12$ to take the inverse Laplace transform of dimensionless pressure.

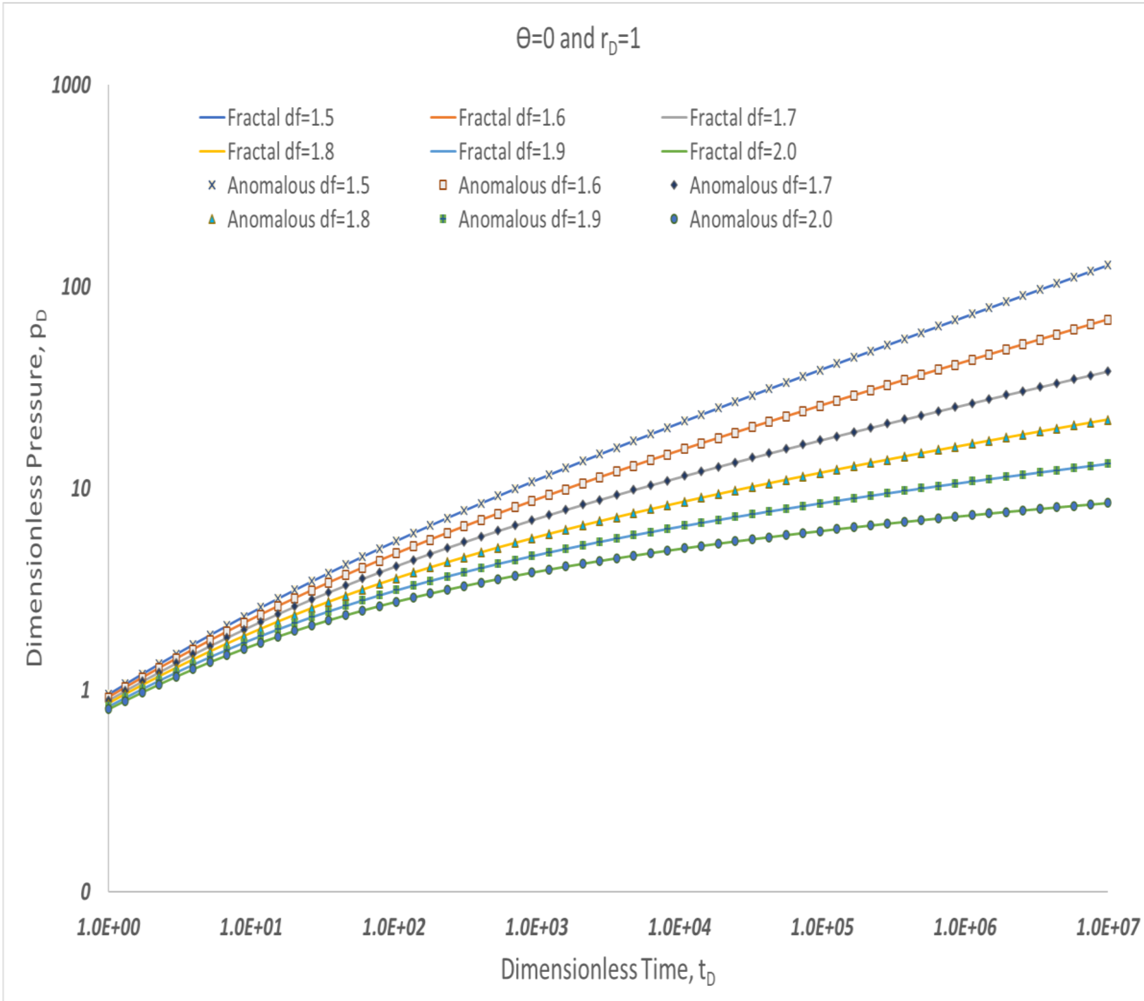

Figure 3.1 Fractal Model vs Metzler Anomalous Model dimensionless pressure responses for

$\alpha = 1$ and at $r = r_w$ case.

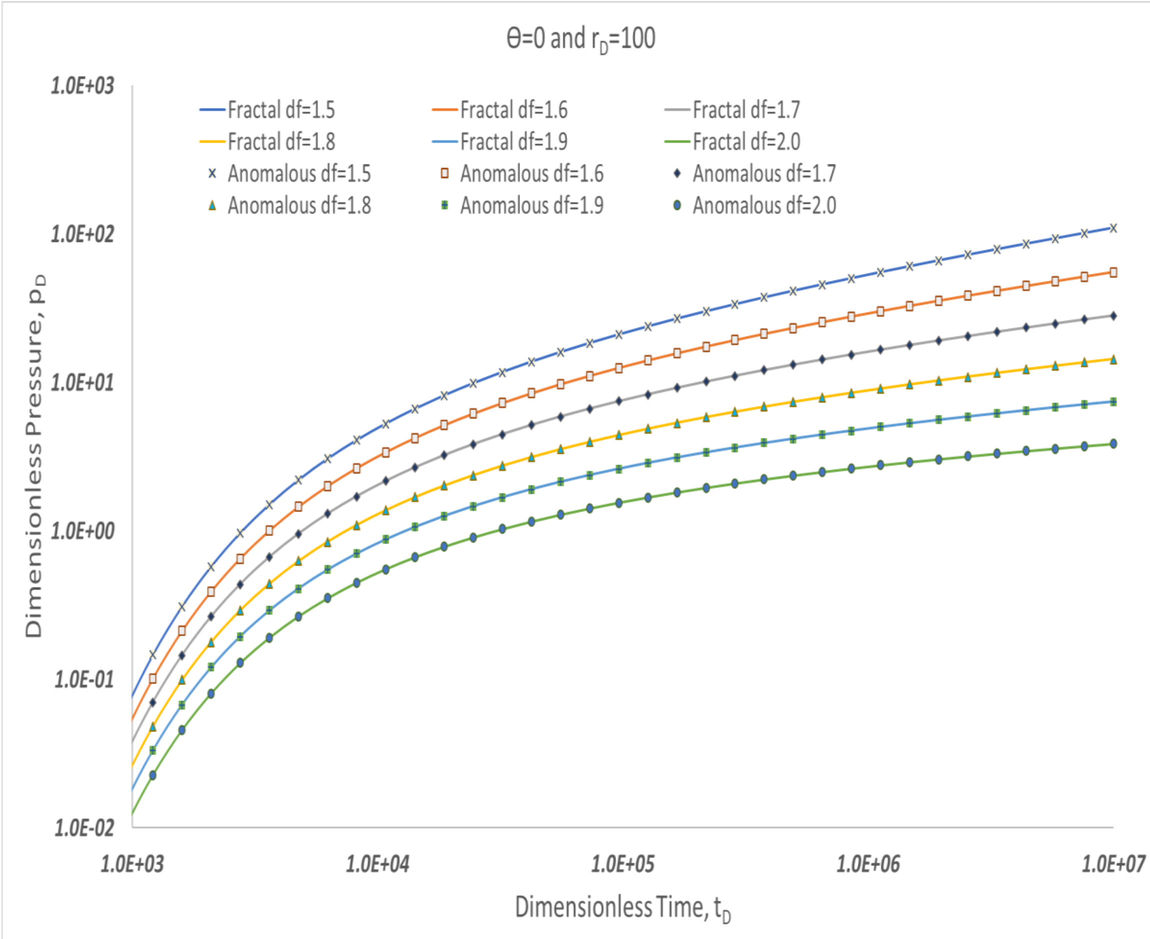

Figure 3.2 Fractal Model vs Metzler Anomalous Model dimensionless pressure responses for $\alpha = 1$ and at $r = 100r_w$ case.

Figures 3.1 and 3.2 are derived by using constant rate solution. It is clearly seen that although the fractal dimension and dimensionless radius change, the dimensionless pressure response of the fractal model is the same as Metzler anomalous model. Furthermore, the fractal dimension affects the dimensionless pressure. As the fractal dimension approaches 2, the dimensionless pressure value decreases significantly. Dimensionless radius also influences the dimensionless pressure. As dimensionless radius increases, the dimensionless pressure reduces. In addition, we check the derivative response of for both methods at the wellbore ($r = r_w$) and in the reservoir ($r = 100r_w$).

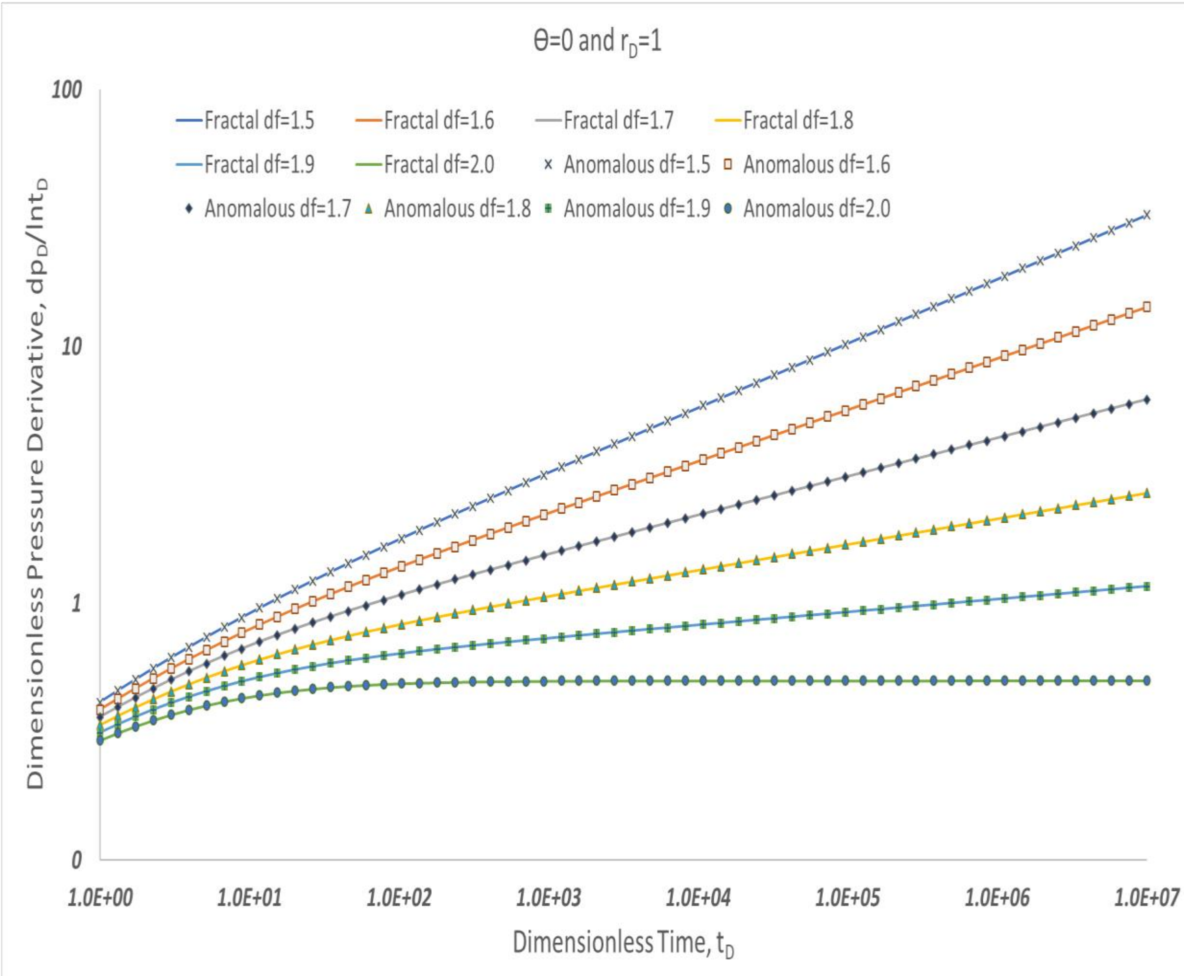

Figure 3.3 Fractal Model vs Metzler Anomalous Model dimensionless pressure derivative responses for $\alpha = 1$ and at $r = r_w$ case.

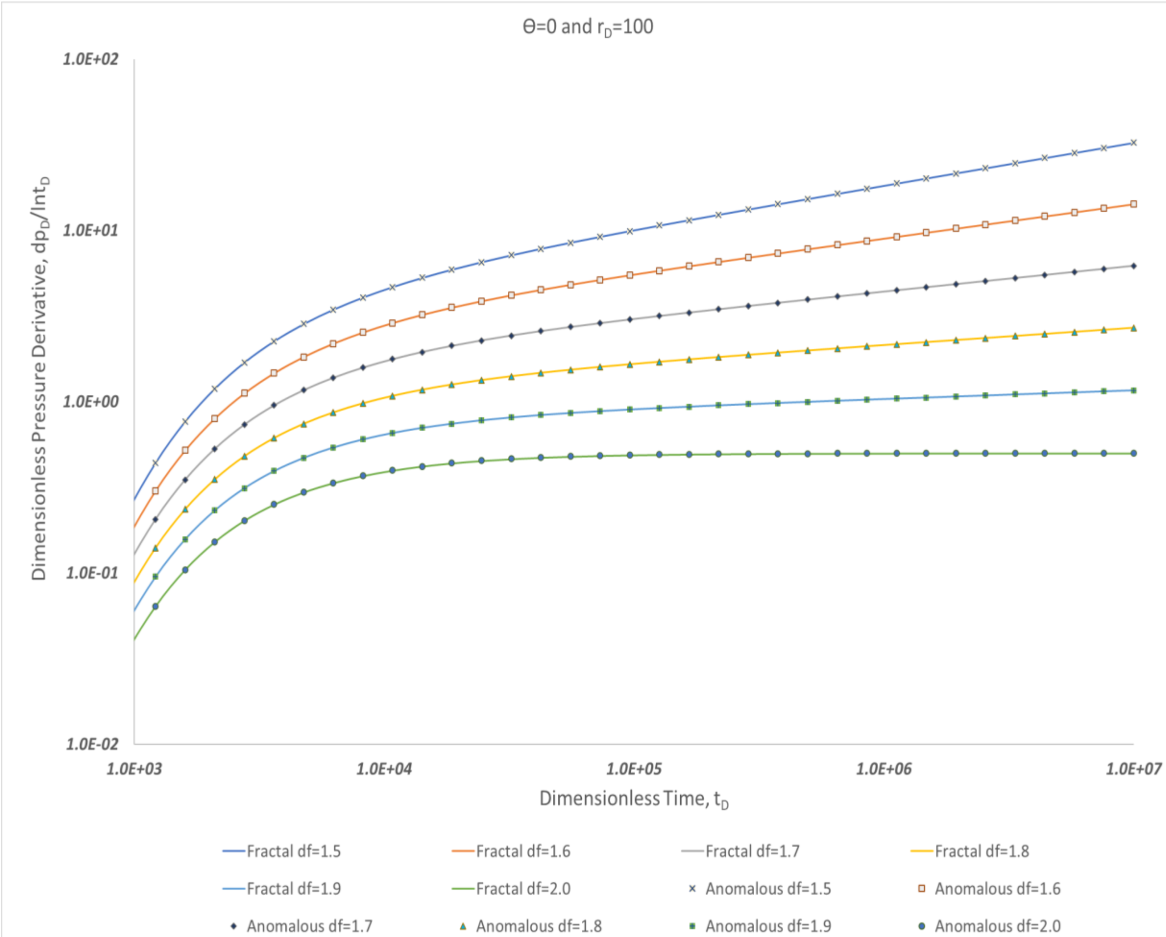

Figure 3.4 Fractal Model vs Metzler Anomalous Model dimensionless pressure derivative responses for $\alpha = 1$ and at $r = 100r_w$ case.

Figures 3.3 and 3.4 are derived by using constant rate solution. It is obvious that there is a perfect match between the fractal and Metzler anomalous model derivative responses for constant rate case. Hence, we confirm Camacho's (2008) assertion that the fractal model is the special case of Metzler anomalous model for constant rate condition. Furthermore, dimensionless pressure responses decrease when the fractal dimensions increase. Dimensionless pressure responses at $r = 100r_w$ are smaller than dimensionless pressure in the wellbore.

Next, we look at the dimensionless pressure and dimensionless pressure derivative behaviors for both the fractal model and Metzler anomalous model at the constant bottomhole pressure case when $r = 100r_w$. Note that we do not analyze for $r = r_w$ because dimensionless pressure response is equal to 1 at the wellbore.

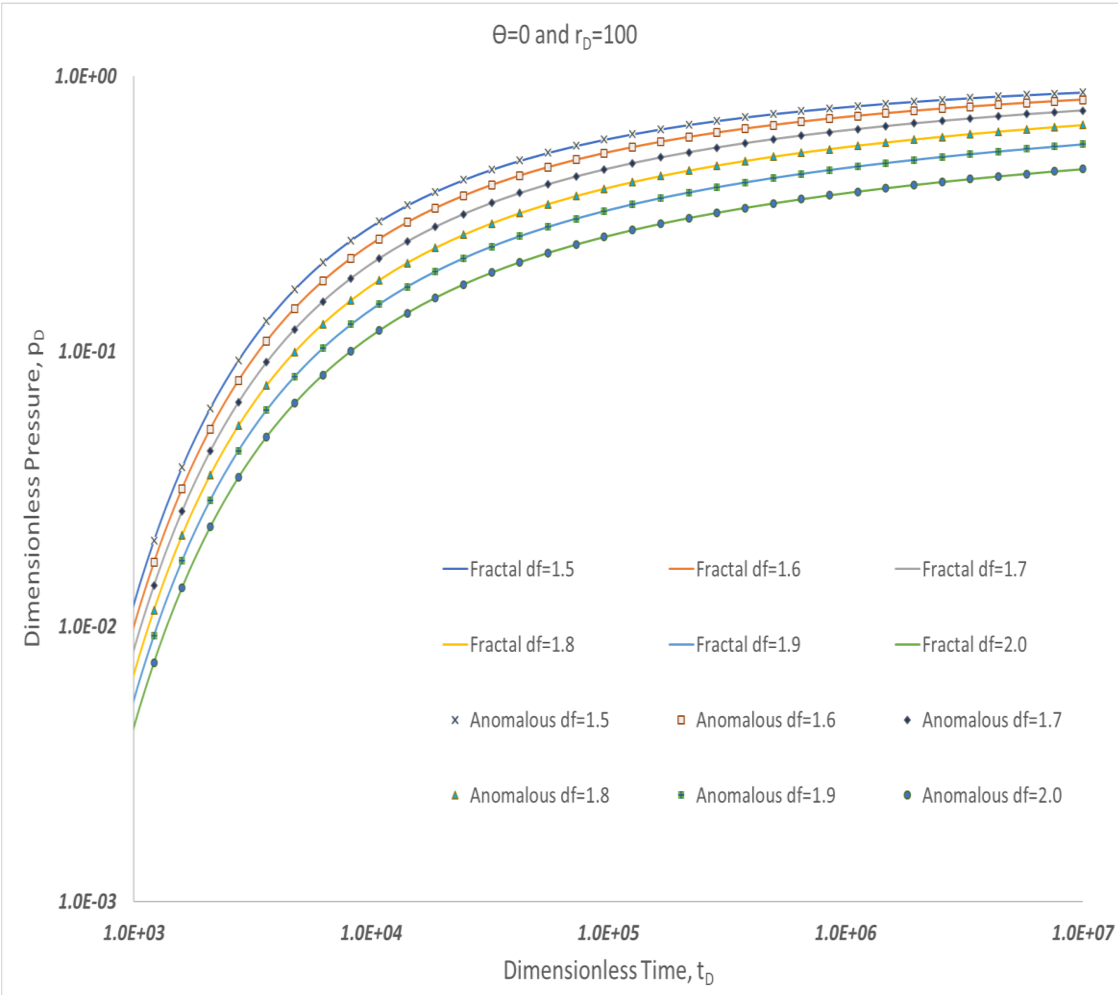

Figure 3.5 Fractal Model vs Metzler Anomalous Model dimensionless pressure responses at the constant bottomhole pressure condition for $\alpha = 1$ and at $r = 100r_w$ case.

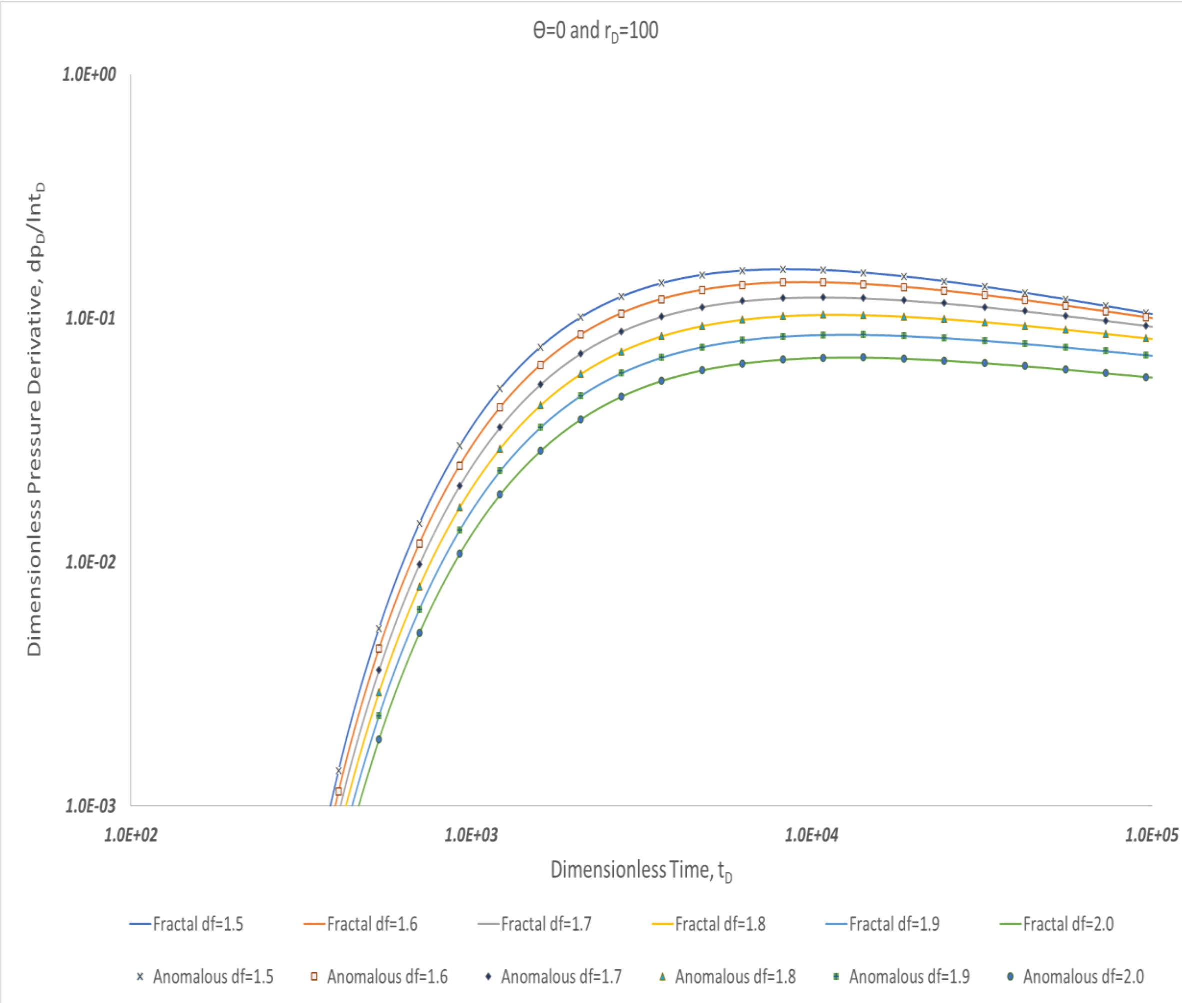

Figure 3.6 Fractal Model vs Metzler Anomalous Model dimensionless pressure derivative responses at the constant bottomhole pressure condition for $\alpha = 1$ and at $r = 100r_w$ case.

Figures 3.5 and 3.6 refer constant bottomhole pressure condition. As the fractal dimension changes, both the fractal model and Metzler anomalous model generate the same dimensionless pressure and dimensionless pressure derivative. To conclude, fractal model is the special case of Metzler anomalous model.

3.3.2 Effect of d_f for fractal model and Metzler anomalous model

In this section, we observe effect of fractal dimension d_f for fractal model and Metzler anomalous model. We cannot include Raghavan anomalous model because that model uses n (integer number) instead of d_f (noninteger number). We study on three different fractal dimensions (1.50, 1.75 and 2.00), and two different topologies of the network ($\theta = 0.25\ and\ 0.50$). Stehfest algorithm (Stehfest, 1970) with $N_{Stef} = 12$ is used to take the inverse Laplace transform. Firstly, dimensionless pressure responses are observed, and then, dimensionless pressure derivative responses are investigated with respect to dimensionless time.

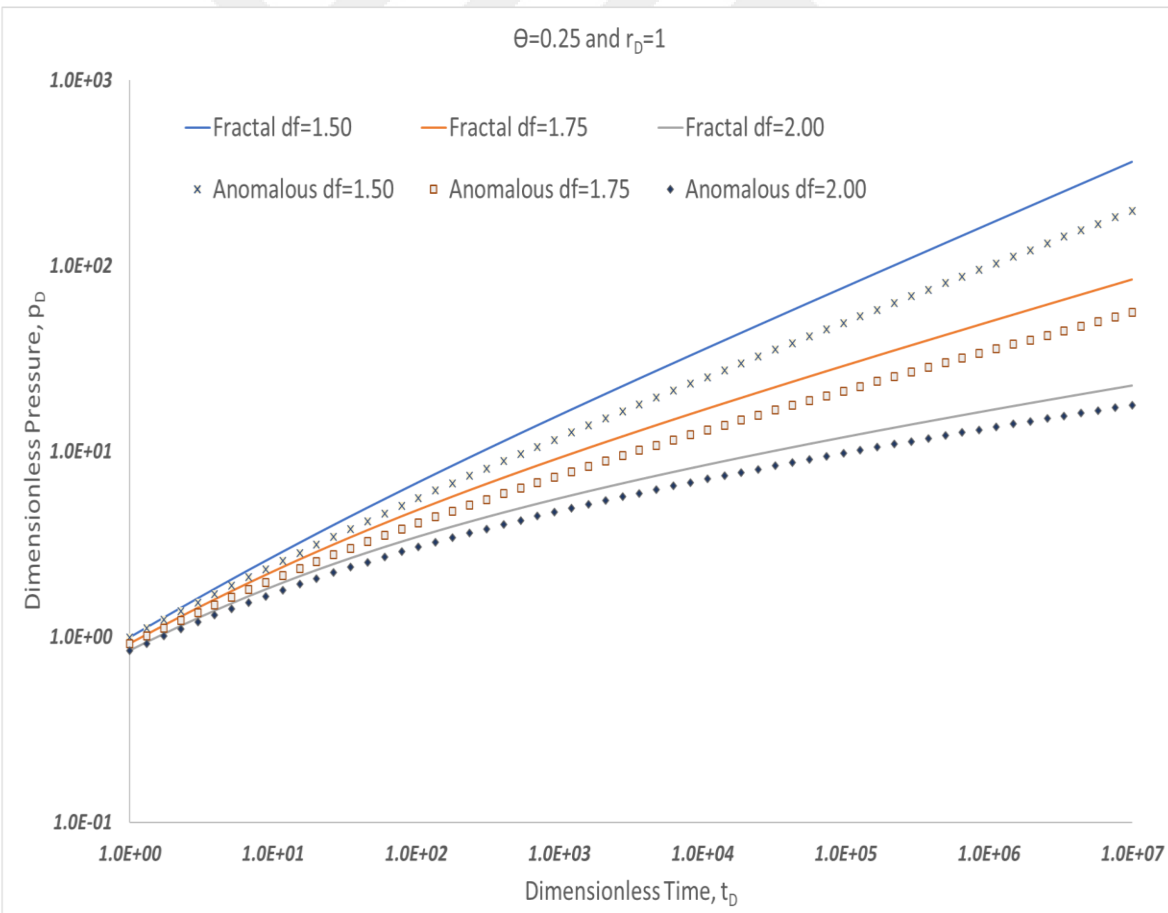

Figure 3.7 Fractal Model vs Metzler Anomalous Model dimensionless pressure responses at the wellbore for constant rate solution when $\theta = 0.25$.

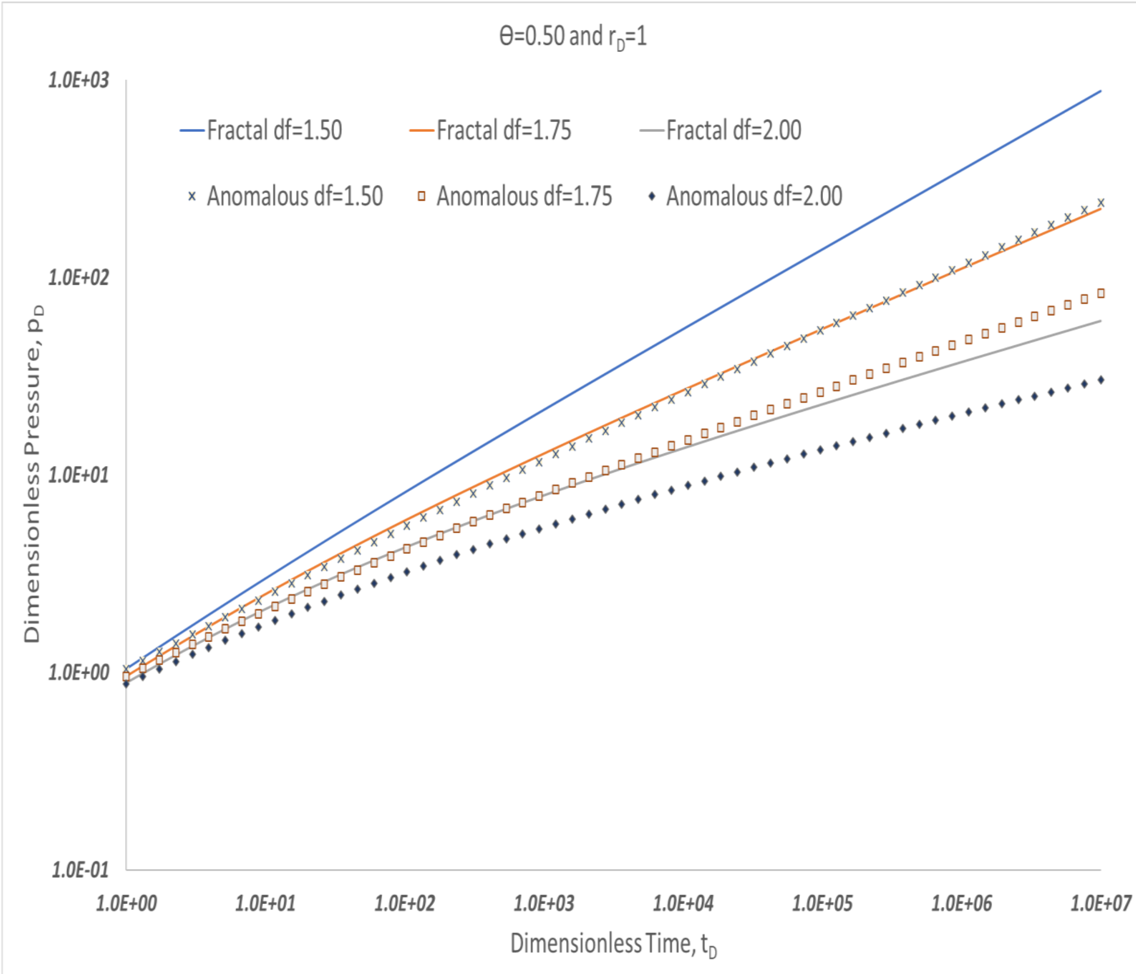

Figure 3.8 Fractal Model vs Metzler Anomalous Model dimensionless pressure responses at the wellbore for constant rate solution when $\theta = 0.50$.

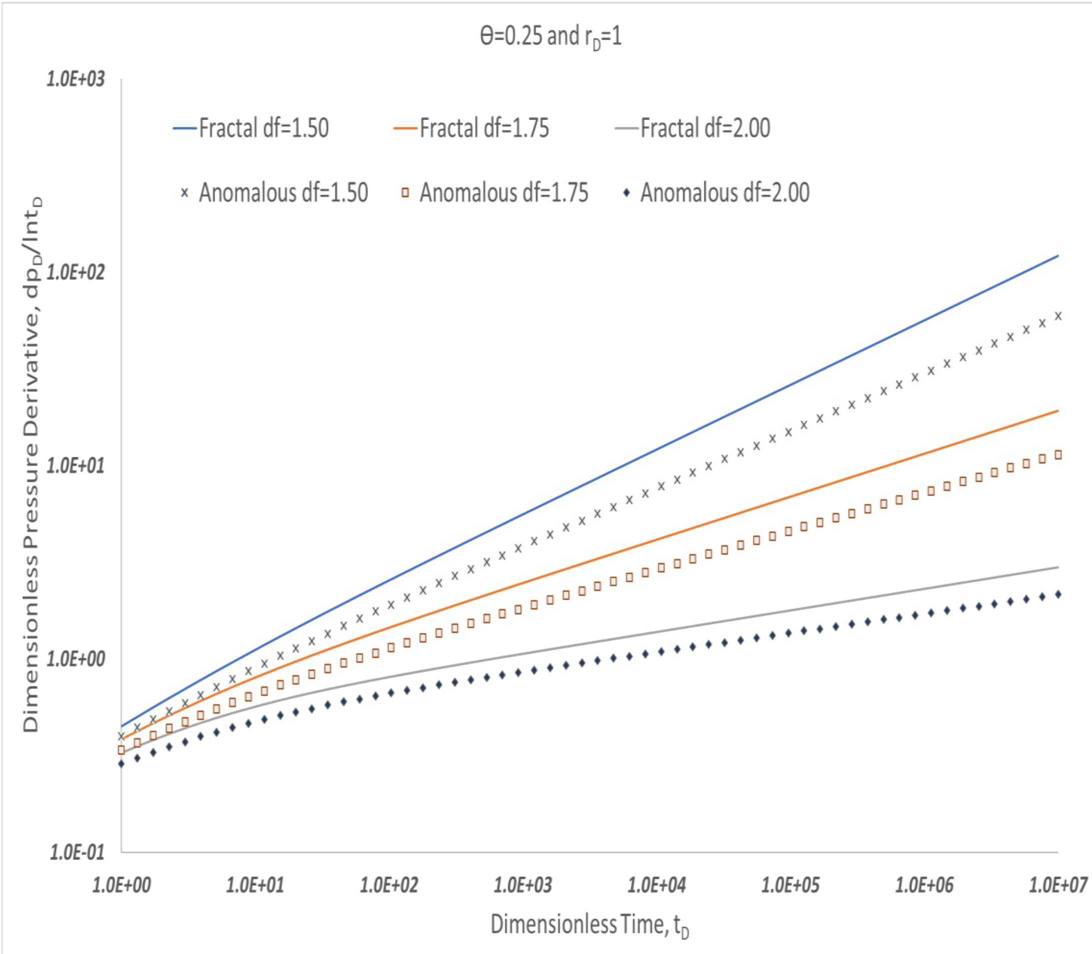

Figure 3.9 Fractal Model vs Metzler Anomalous Model dimensionless pressure derivative responses at the wellbore for constant rate solution when $\theta = 0.25$.

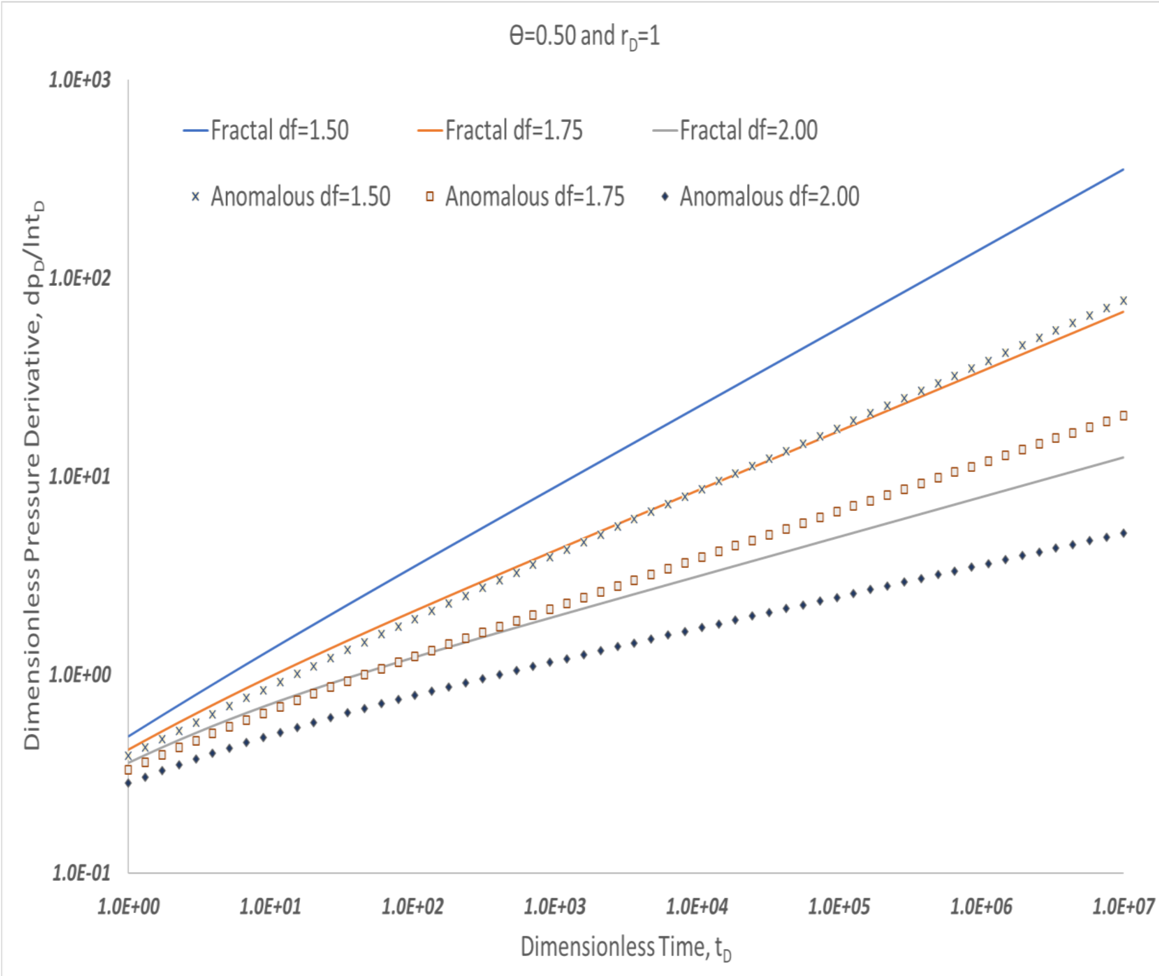

Figure 3.10 Fractal Model vs Metzler Anomalous Model dimensionless pressure derivative responses at the wellbore for constant rate solution when $\theta = 0.50$.

Initially, we compare the effect of fractal dimension for each model in itself. According to Figure 3.7, as the fractal dimension increases, the fractal model generates less dimensionless pressure at the wellbore for the constant $\theta = 0.25$. Moreover, Metzler anomalous model behaves the same, too. Secondly, we compare the behavior of the models. Fractal model causes higher dimensionless pressure than Metzler anomalous model when fractal dimension and topology of the network are constant. In other words, it is obvious that the Metzler anomalous model generates less dimensionless pressure than fractal model for each d_f. According to Figure 3.8, it is seen that as the topology of the network rises, the difference between the fractal model and Metzler anomalous model goes up. For example, the fractal model dimensionless pressure response for $d_f = 1.75$ is nearly same as the Metzler anomalous model pressure response for $d_f = 1.50$ at the late dimensionless time. Another example is that the fractal model for $d_f = 2.00$ generates approximately the same as Metzler anomalous model for $d_f = 1.75$ at the early dimensionless time. The similar conclusions are applicable for the dimensionless pressure derivative responses.

3.3.3 Effect of θ for fractal model and anomalous models

In this section, we observe the effect of fractal dimension θ for the fractal model and anomalous models at the constant rate condition. It is note that Raghavan anomalous model defines the dimensionless time different than fractal model and Metzler anomalous model.

$$t_D = \frac{\eta_i}{r^{d_w}} t^{\alpha}, \tag{3.60}$$

where $d_w = 2 + \theta$ and $\alpha = \frac{2}{2+\theta}$. In this part, we use Eq. 3.64 to find dimensionless pressure solution for Raghavan anomalous method. Most importantly, when we use Stehfest algorithm to find the inverse Laplace transform of Raghavan anomalous model solution, we take the inverse Laplace transform with respect to time t because of Eq. 3.64 definition. However, the graph is drawn with respect to dimensionless time t_D in the x axis. Consequently, we consider both time and dimensionless time for Raghavan anomalous model. On the other hand, we only calculate dimensionless time for fractal model (Eq. 3.12) and Metzler anomalous model (Eq. 3.38). Furthermore, we examine three different topologies of the network $\theta = 0.25, 0.50$ and 0.75 for each method.

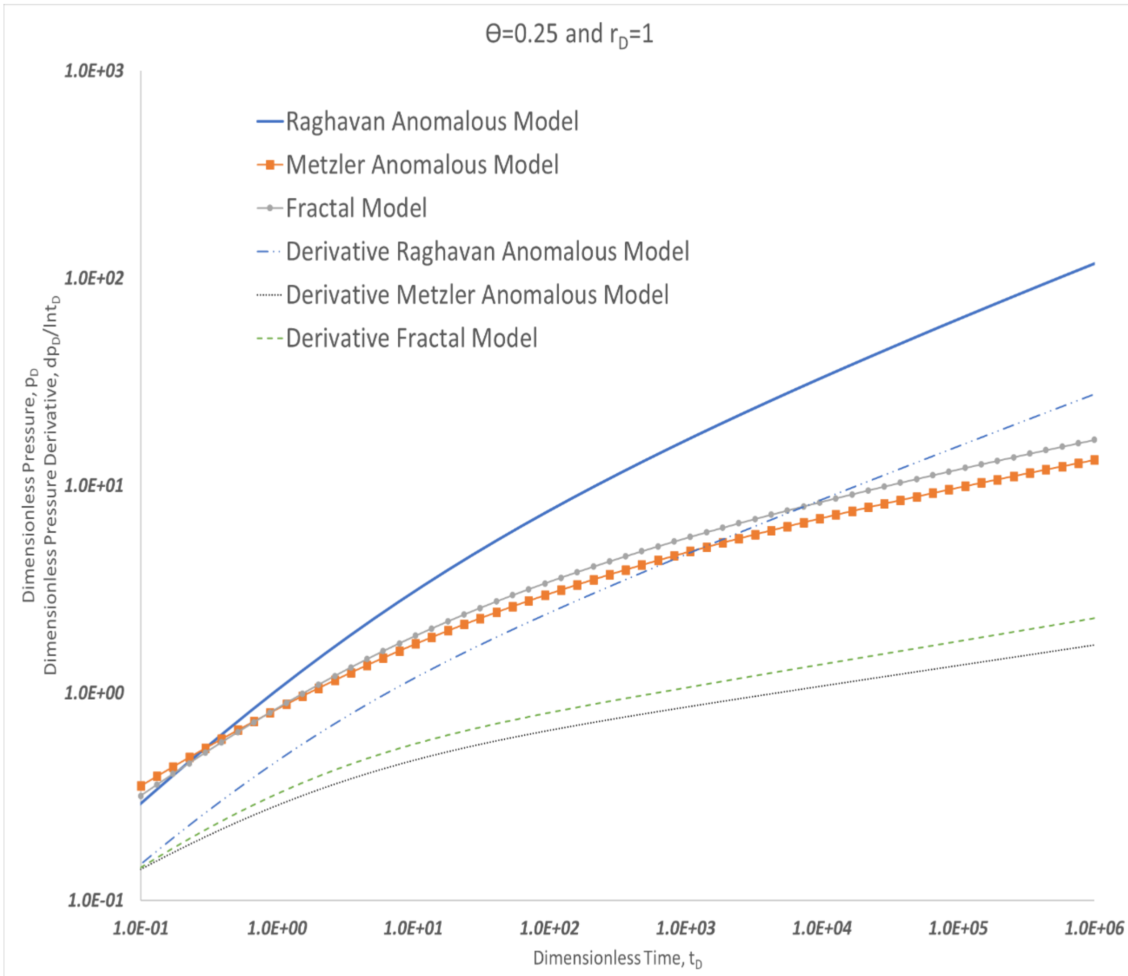

Figure 3.11 Fractal Model vs Metzler Anomalous Model vs Raghavan Anomalous model for constant rate solution when $\theta = 0.25$ and $r = r_w$.

Figure 3.11 is derived for each method at the constant rate solution, and finite wellbore case is considered. Figure 3.11 depicts for both dimensionless pressure and dimensionless pressure derivative responses. Fractal dimension d_f is assumed 2 for the fractal model and Metzler anomalous model. On the other hand, n is equal to 2 for Raghavan anomalous model. θ is assumed 0.25 for all model. As you can see all the methods behave similarly at the early time. However, as dimensionless time goes up, the difference between Raghavan anomalous model and others raises tremendously. In addition, when we compare fractal and Metzler anomalous model at the early time, Metzler anomalous model generates a slightly higher dimensionless pressure response than fractal model. Nevertheless, dimensionless pressure for fractal model overtakes Metzler anomalous model after early dimensionless time. While dimensionless time rises, the difference between fractal and anomalous model increases gradually. Furthermore, if we compare dimensionless pressure derivative responses for all methods, they are nearly the same at the initial dimensionless time. While dimensionless time is increasing, difference between the Raghavan anomalous model and others goes up noticeably. On the other hand, the difference between the fractal model and Metzler anomalous model for dimensionless pressure derivative responses grows slightly when $\theta = 0.25$.

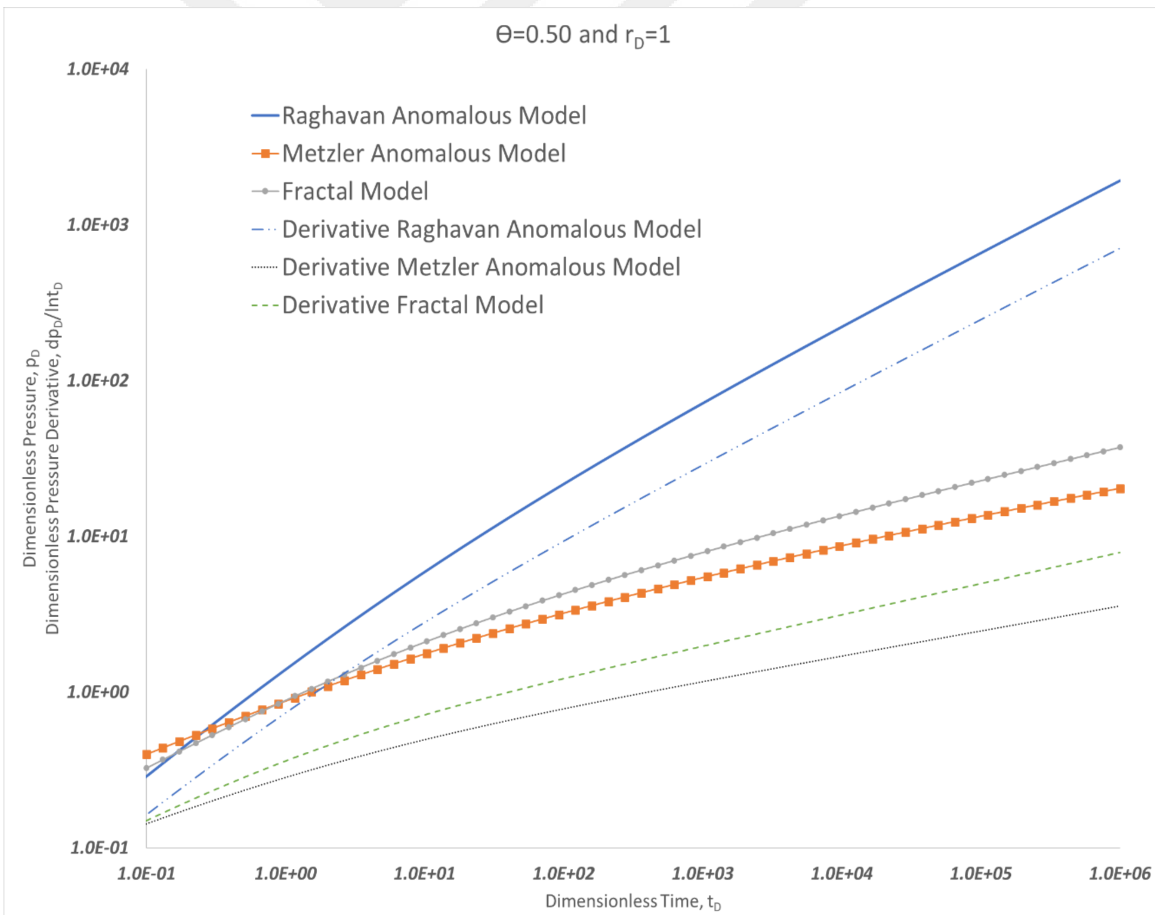

Figure 3.12 Fractal Model vs Metzler Anomalous Model vs Raghavan Anomalous model for constant rate solution when $\theta = 0.50$ and $r = r_w$.

Figure 3.12 is derived by assuming θ is assumed 0.50. When we compare Figure 3.11 and 3.12, the dimensionless pressure and dimensionless pressure derivative responses are almost the same at the early time. Nonetheless, while the dimensionless time rises, the difference between the models grows markedly for both dimensionless pressure and dimensionless pressure derivative. Again, Metzler anomalous model generates a slightly higher dimensionless pressure response than fractal model at the early dimensionless time. However, fractal model overtakes Metzler anomalous model after early dimensionless time and generates the higher difference than $\theta = 0.25$. Moreover, the difference between fractal model and Metzler anomalous model for dimensionless pressure derivative is slightly higher than $\theta = 0.25$.

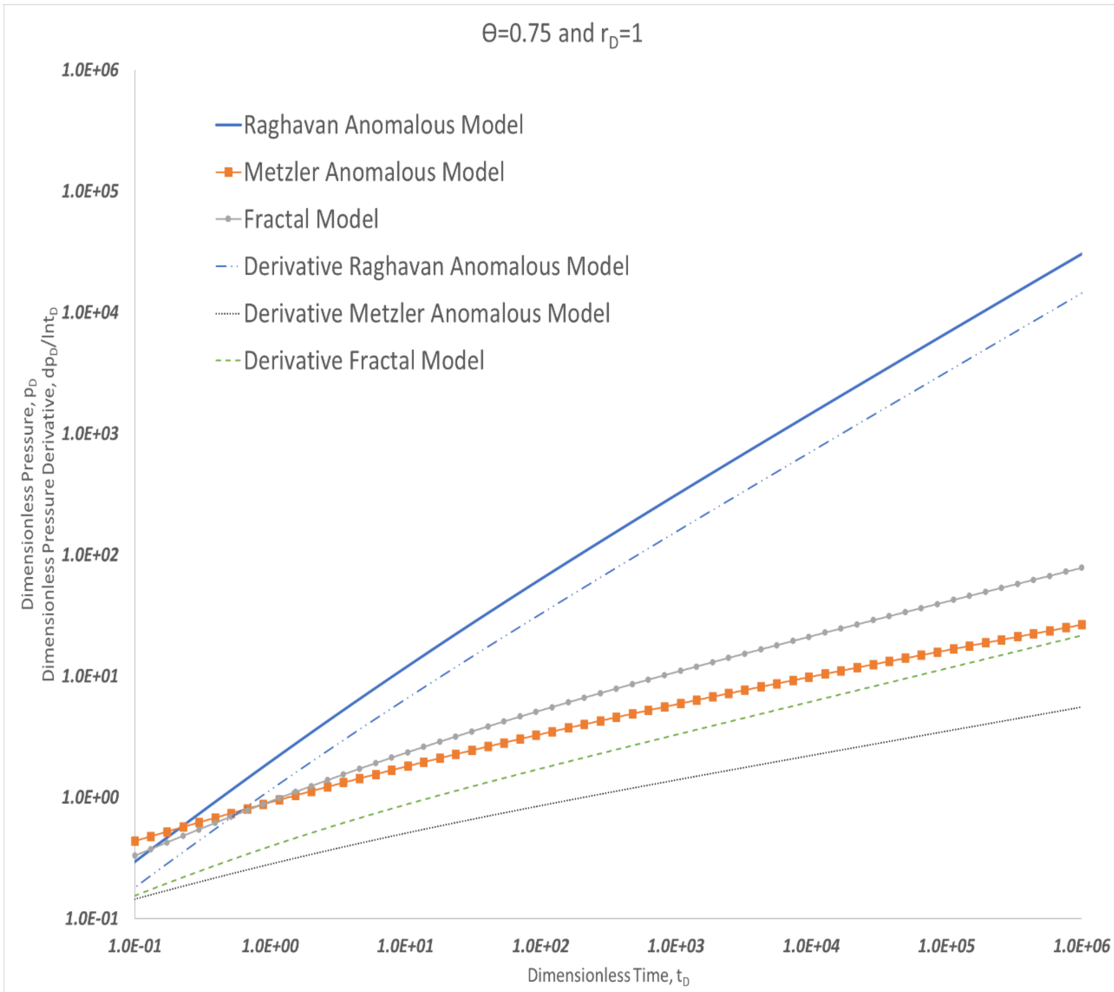

Figure 3.13 Fractal Model vs Metzler Anomalous Model vs Raghavan Anomalous model for constant rate solution when $\theta = 0.75$ and $r = r_w$.

Figure 3.13 is formed by assuming θ is assumed 0.75. When we compare Figure 3.13 with Figures 3.11 and 3.12, it is seen that each model forms a steeper line for both dimensionless pressure and dimensionless pressure derivative because of higher θ. Moreover, the fractal model forms minimally less dimensionless pressure than Metzler anomalous model at the early dimensionless time. In addition to that, dimensionless pressure derivative responses are quite similar at the initial dimensionless time like $\theta = 0.25$ *and* 0.50. Then, while dimensionless time goes up, the difference between models rises dramatically. To sum up, as the topology of the network and dimensionless time increase, the dimensionless pressure and dimensionless pressure derivative responses difference grow remarkably. While Raghavan anomalous model always creates higher dimensionless pressure than other models, Metzler anomalous model usually generates less dimensionless pressure response. As the topology of the network increases, each model generates higher dimensionless pressure and dimensionless pressure derivative responses at the late dimensionless time.

3.3.4 Dimensionless pressure and dimensionless pressure derivative response in the reservoir for fractal model and anomalous models

In this section, we analyze the dimensionless pressure response in the reservoir for each model. Fractal dimension and n are assumed 2, and topology of the network is used as 0.25. We investigate the dimensionless pressure and dimensionless pressure derivative response at dimensionless radius r_D is equal to 10 and 100. It is important to say that we calculate the dimensionless time for Raghavan anomalous model individually for each r_D.

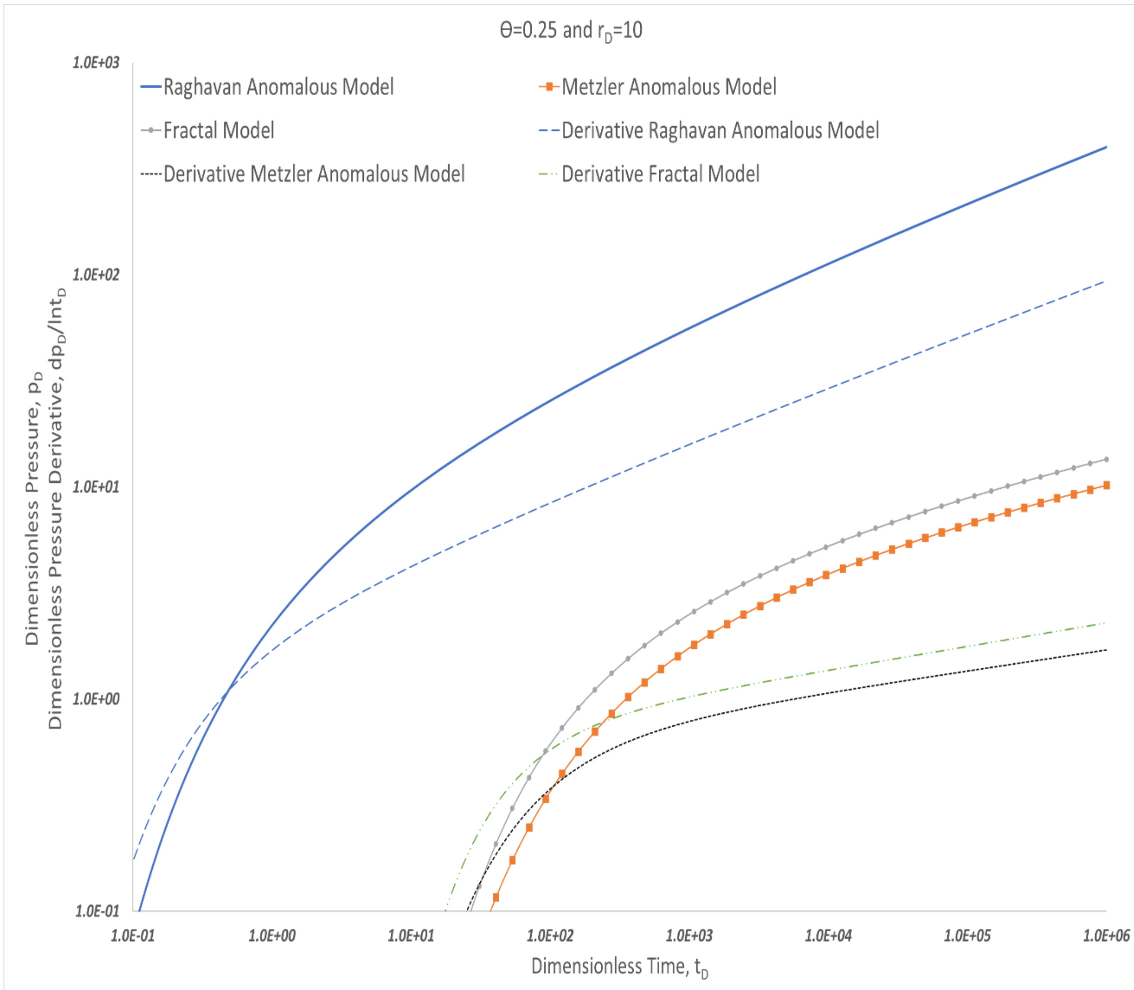

Figure 3.14 Fractal Model vs Metzler Anomalous Model vs Raghavan Anomalous model for constant rate solution when $\theta = 0.25$ and $r = 10r_w$.

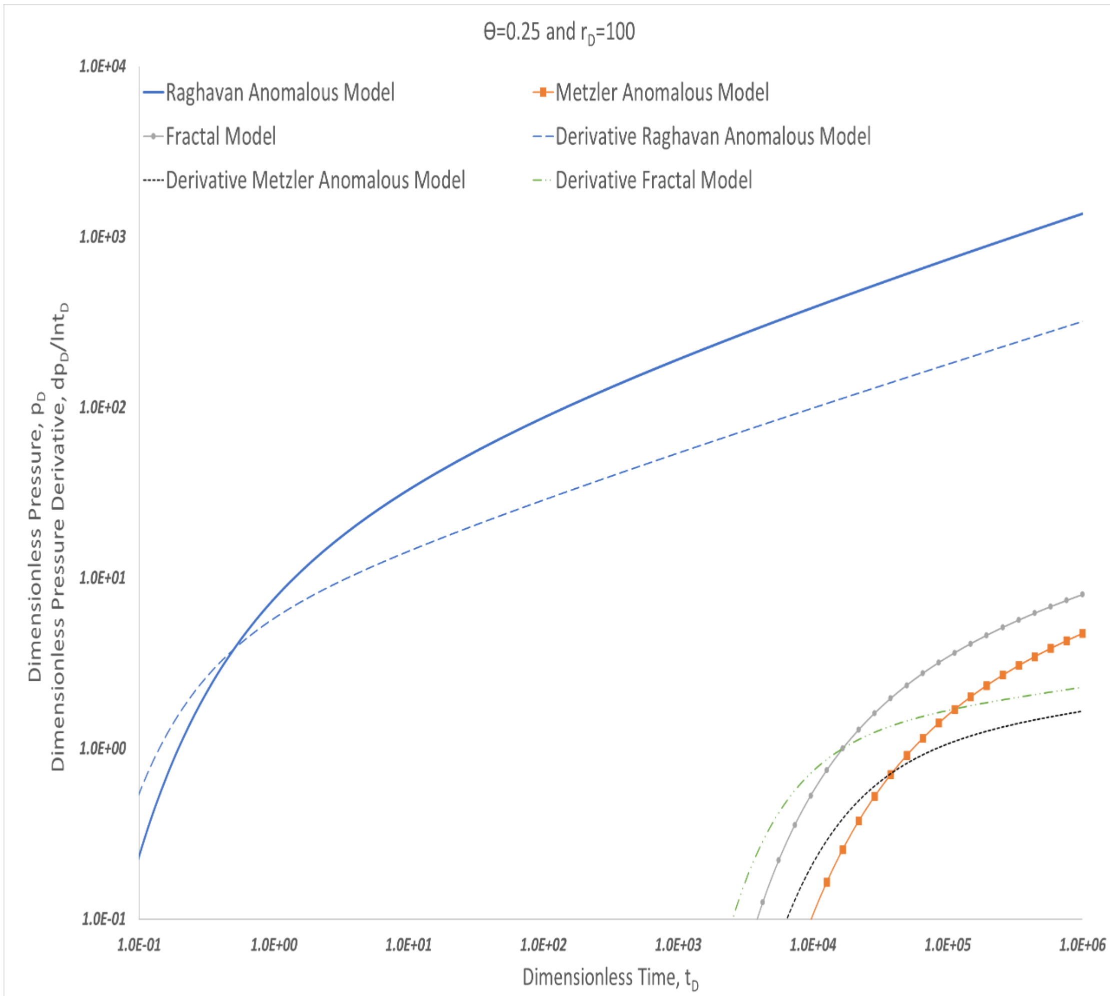

Figure 3.15 Fractal Model vs Metzler Anomalous Model vs Raghavan Anomalous model for constant rate solution when $\theta = 0.25$ and $r = 100r_w$.

Figures 3.14 and 3.15 are derived for constant θ, and different dimensionless radiuses. According to these figures, Raghavan anomalous model generates dimensionless pressure and dimensionless pressure derivative responses earlier than fractal model and Metzler anomalous model. In addition, as the dimensionless radius increases, the difference between the models rises significantly.

3.3.5 Verification of n value for Raghavan (2011) anomalous model

In this section, we study on Raghavan (2011) paperwork. He compared the production at the constant bottomhole pressure for both Metzler anomalous model and his model. He took as a reference Camacho (2008) study for the Metzler anomalous model. In Figure 3.16, Raghavan drew a graph for dimensionless rate (q_{wD}) at the wellbore vs dimensionless time (t_D).

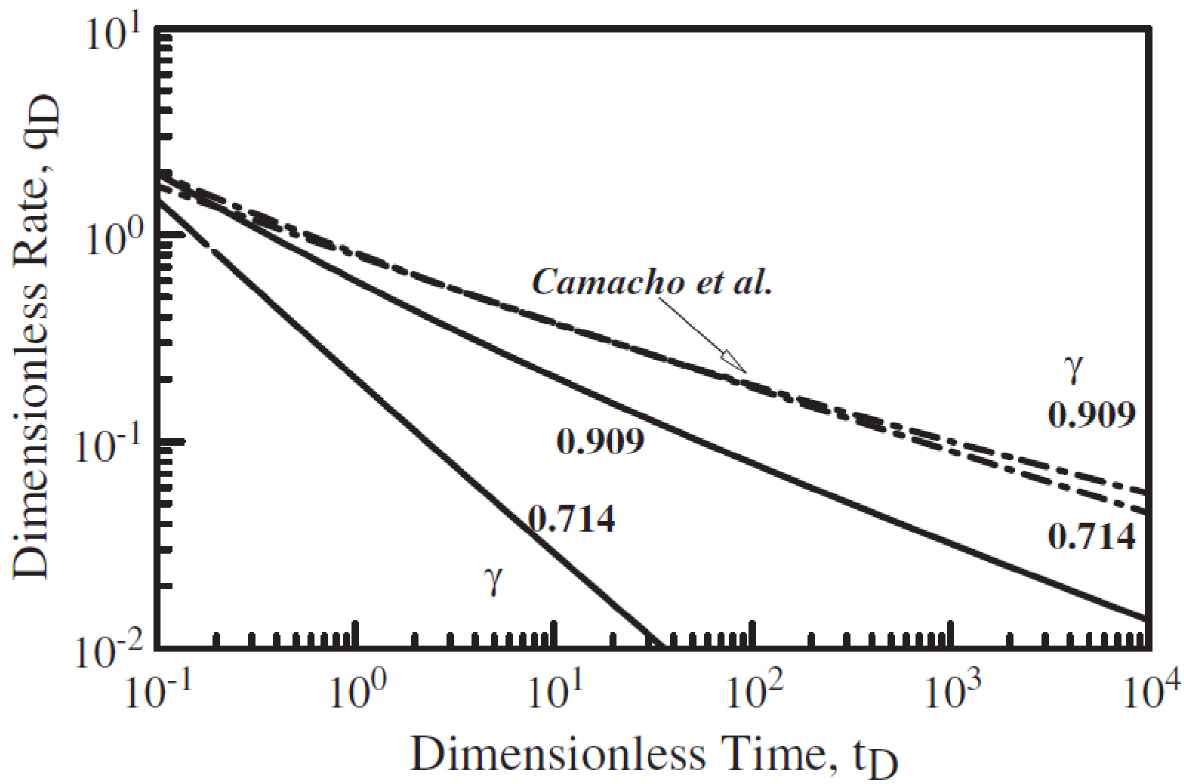

Figure 3.16 Well response for constant pressure production. The top two lines correspond to that of Camacho – Velazquez et al. (Raghavan, 2011).

Raghavan (2011) described γ as $\frac{2}{2+\theta}$. Hence, γ is equal to α in this thesis. Raghavan drew Figure 3.16 for $\gamma = 0.909$ and 0.714 which means topologies of the network is equal to $\theta = 0.20$ and 0.80, respectively. To draw Figure 3.16, we firstly need to derive dimensionless rate. The details of derivation for dimensionless flow rate are given in Appendix K.

$$\overline{q_D}(r_D, s) = d_w r_D^{-d_w\left(\frac{1}{\alpha}-\frac{1+\xi}{2}\right)} \left(\frac{r^{d_w}}{\eta_i d_w^2}\right)^{\frac{1}{\alpha}-\frac{1}{2}} s^{-\frac{\alpha}{2}} \frac{K_{\nu'+1}\left[2s^{\frac{\alpha}{2}}\left(\frac{r^{d_w}}{\eta_i d_w^2}\right)^{\frac{1}{2}}\right]}{K_{\nu'}\left[2s^{\frac{\alpha}{2}}\left(\frac{r_w^{d_w}}{\eta_i d_w^2}\right)^{\frac{1}{2}}\right]}. \tag{3.74}$$

At the wellbore ($r = r_w$), dimensionless flow rate is

$$\overline{q_{wD}}(s) = d_w \left(\frac{r_w^{d_w}}{\eta_i d_w^2}\right)^{\frac{1}{\alpha}-\frac{1}{2}} s^{-\frac{\alpha}{2}} \frac{K_{\nu'+1}\left[2s^{\frac{\alpha}{2}}\left(\frac{r_w^{d_w}}{\eta_i d_w^2}\right)^{\frac{1}{2}}\right]}{K_{\nu'}\left[2s^{\frac{\alpha}{2}}\left(\frac{r_w^{d_w}}{\eta_i d_w^2}\right)^{\frac{1}{2}}\right]}. \tag{3.75}$$

Furthermore, Camacho found the dimensionless flow rate at the wellbore for constant bottomhole pressure condition by using Duhamel's principle,

$$\overline{q_{wD}}(s) = \frac{-\nu(\Theta+2)K_\nu\left[\frac{2\sqrt{s^\alpha}}{\theta+2}\right] + s^{\frac{\alpha}{2}} K_{\nu+1}\left[\frac{2\sqrt{s^\alpha}}{\theta+2}\right]}{sK_\nu\left[\frac{2\sqrt{s^\alpha}}{\theta+2}\right]}. \tag{3.76}$$

As you can see Raghavan compared his method with Camacho study which demonstrates Metzler anomalous model. Raghavan claims that he drew the Figure 3.16 by assuming $n = 2$ and $d_f = 1.65$. To check his study, we reproduce Figure 3.16 by assuming the same n and d_f.

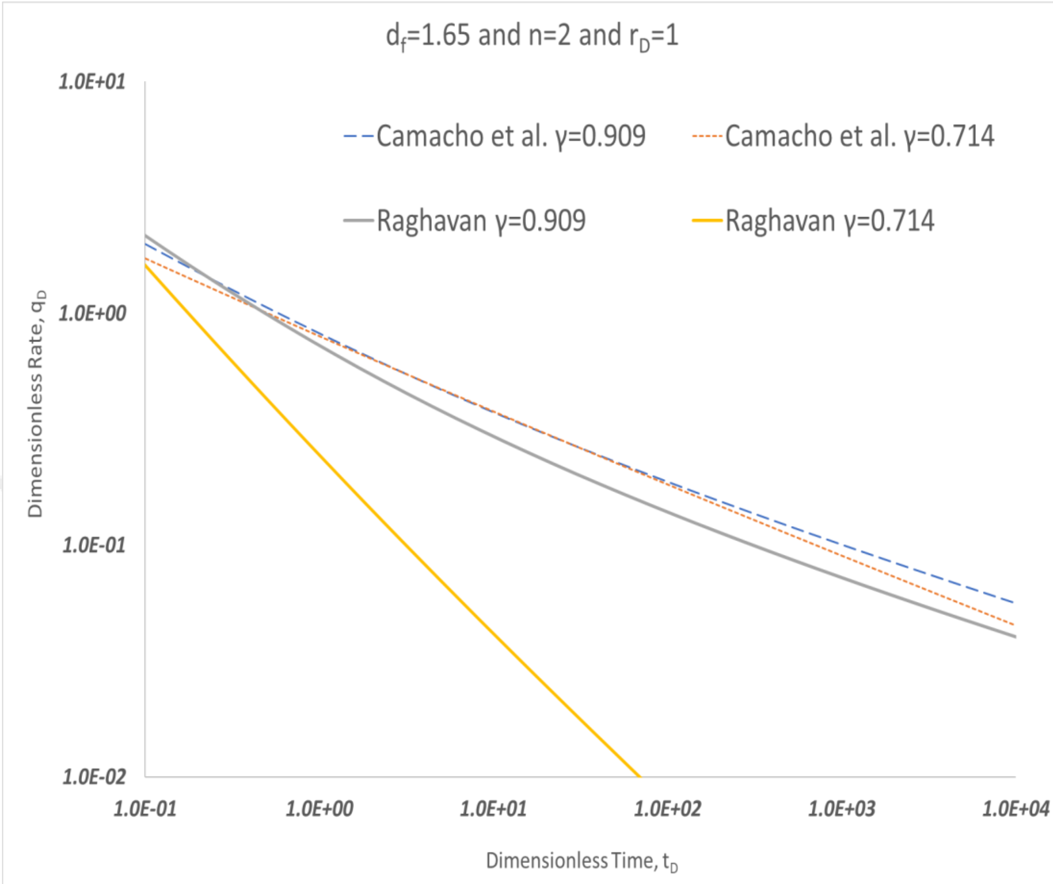

Figure 3.17 Camacho et al. vs Raghavan for constant bottomhole pressure when $n = 2$ and $d_f = 1.65$.

It is clearly seen that Figure 3.17 is different than Figure 3.16. Although we draw the same Camacho et al. lines, Raghavan lines are different. In other words, Raghavan anomalous model generates higher flow rate at the wellbore when $n = 2$. This is what we expect. To draw the same Figure 3.16, we use the same d_f, but we change the n value. It is assumed that d_f and n are 1.65.

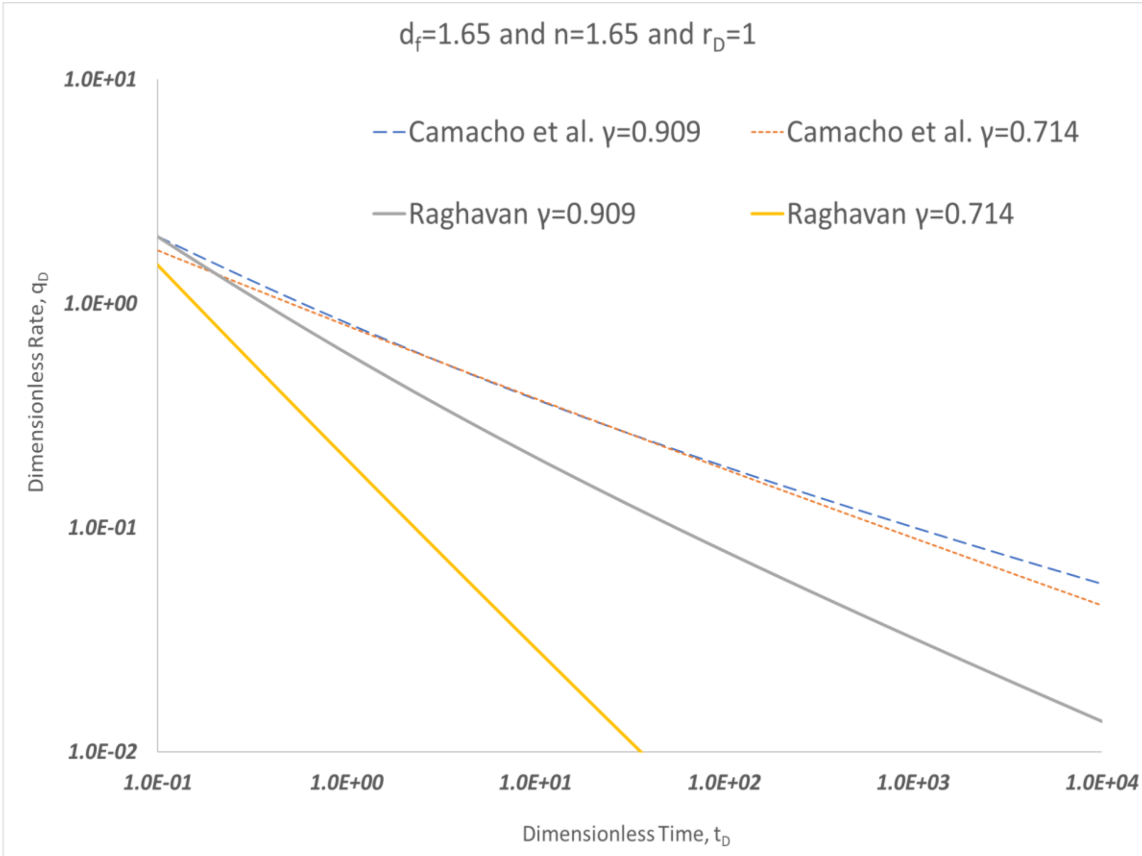

Figure 3.18 Camacho et al. vs Raghavan for constant bottomhole pressure when $n = 1.65$ and $d_f = 1.65$.

It is obvious that Figure 3.16 and Figure 3.18 are the same. Even though Raghavan emphasized $n = 2$, he used $n = 1.65$ to draw the Figure 3.16. On the other hand, Raghavan (2011 and 2012) asserted that n is the integer and cannot be noninteger value. To conclude, Raghavan anomalous model cannot be compared with Metzler anomalous model unless n and d_f are equal. In addition to this analysis, dimensionless flow rate derivative responses are observed for both $n = 2$ and $n = 1.65$. Again, d_f is equal to 1.65 for Camacho's study. It is important to say that dimensionless rate derivative values are negative because of production decline. Therefore, the absolute values of dimensionless rate derivative are used to draw the following graphs.

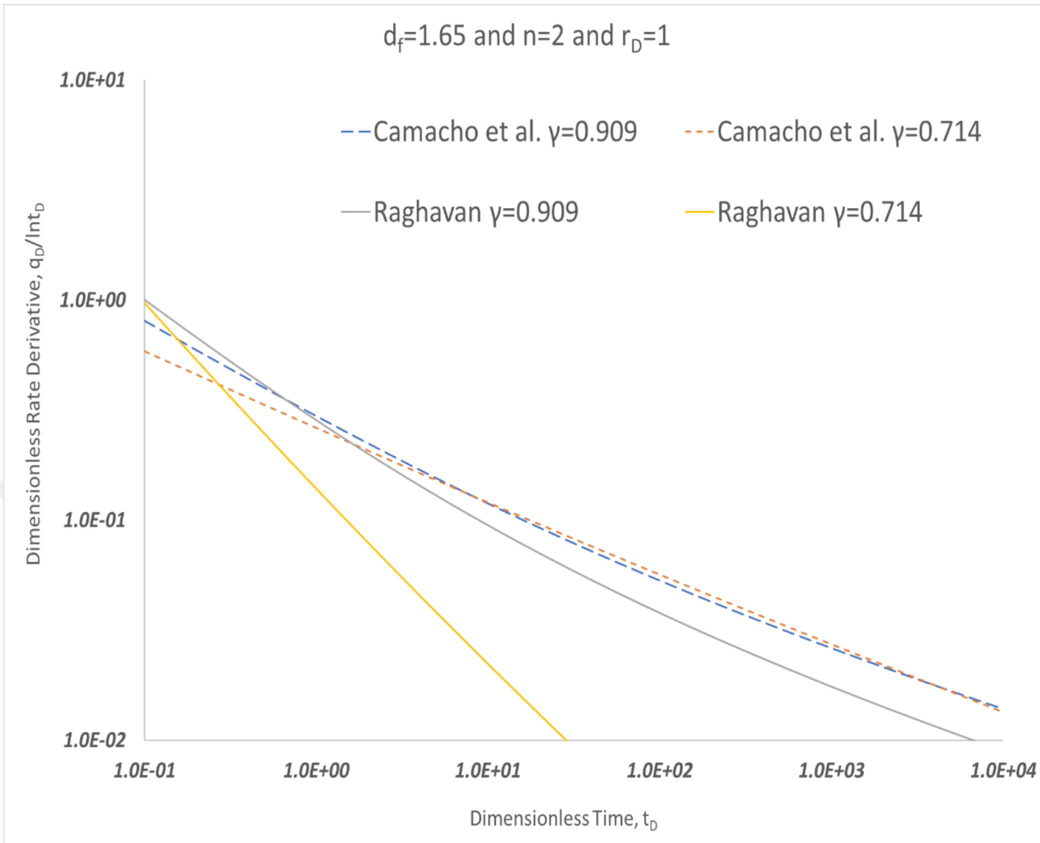

Figure 3.19 Comparison for dimensionless flow rate derivative for constant bottomhole pressure when $n = 2.00$ and $d_f = 1.65$.

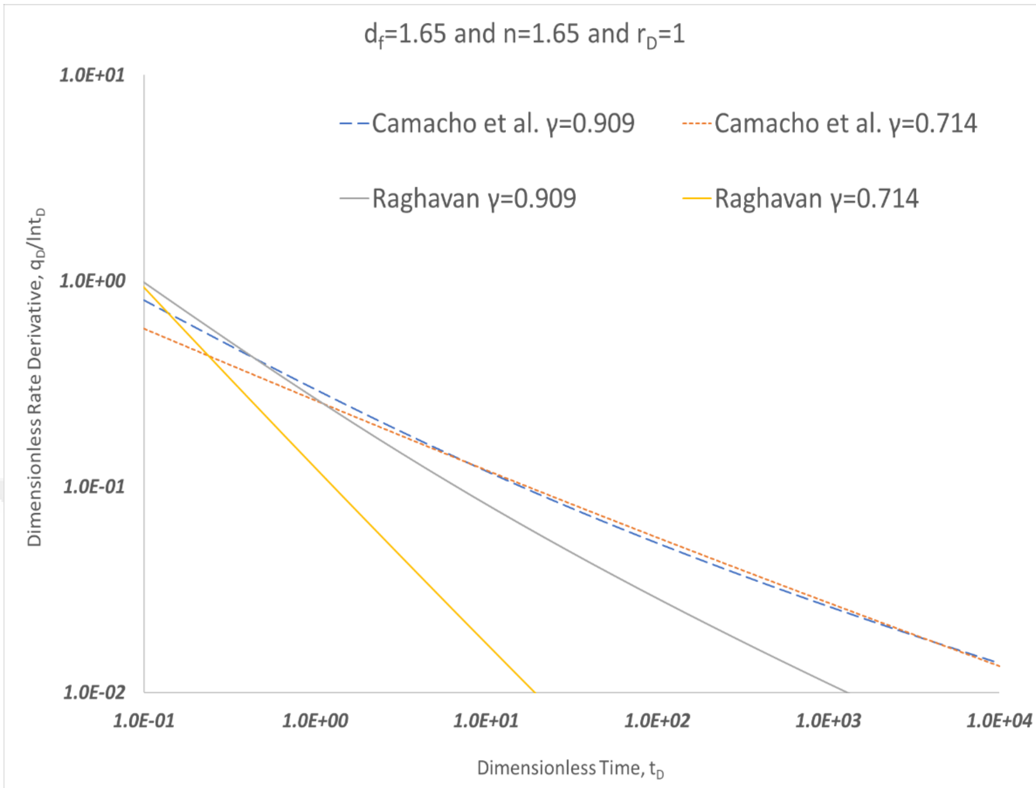

Figure 3.20 Comparison for dimensionless flow rate derivative for constant bottomhole pressure when $n = 1.65$ and $d_f = 1.65$.

According to Figures 3.19 and 3.20, it is clearly seen that dimensionless flow rate derivative for Camacho's study are the same because of the same d_f. On the other hand, the dimensionless flow rate derivatives for Raghavan anomalous model are quite different due to the different n values. As the n value increases, higher dimensionless flow rate derivatives are obtained for both $\gamma = \alpha = \frac{2}{2+\theta}$. Moreover, although dimensionless flow rate derivatives for Camacho's study are slightly lower than dimensionless flow rate derivatives produced by Raghavan anomalous model at the initial dimensionless time, Camacho's study generates higher dimensionless flow rate derivative responses at the higher dimensionless time.

CHAPTER 4

EXAMPLE FIELD DATA APPLICATIONS

In this chapter, we apply fractal model and anomalous models to real field well-test data. The main goal is to solve the reservoir history – matching problem. We analyze pressure changes to obtain reservoir characteristics (kh and $\phi c_t h$) for two different fields: Kizildere, in Turkey and Kamojang, in Indonesia. Therefore, the ensemble smoother with multiple data assimilation (ES-MDA) is used for both fields.

4.1 The Ensemble Smoother with Multiple Data Assimilation (ES – MDA)

History matching is kind of changing the uncertain parameters in the assimilation process. Ensemble – based methods have been used in the last two decades for history matching applications. In this chapter, we use the ensemble smoother with multiple data assimilation (ES – MDA), which is developed by Emerick and Reynolds (2013), is one of the most popular for history-matching applications. ES – MDA is used for nonlinear problems to estimate the parameters. This method assimilates parameters in multiple steps at the same time and iterative methods are used to improve the assimilation.

$$m_j^{a,i} = m_j^{f,i} + C_{MD}^i \left[C_{DD}^i + \alpha_i C_D\right]^{-1} (d_{uc,j}^i - d_j^{f,i}), \tag{4.1}$$

where $j = 1,2, \dots, N_e$ and $i = 1,2, \dots, N_a$. While N_e is the number of ensemble members, N_a represents the total number of data assimilation steps. m_j $(N_m \times N_e)$ is referred as model parameters matrix. That is, this matrix consists of uncertain model parameters. $d_{uc,j}^i (N_d \times N_e)$ is a sample from the normal distribution $N(d_{obs}, \alpha_i C_D)$ where $d_{obs}(1 \times N_d)$ is the observed data vector. $d_j(N_d \times N_e)$ is the simulated data matrix. In addition, α is the inflation factor. The main drawback of ES – MDA is the determining inflation factor. Therefore, we choose the inflation factors ($\alpha_i = N_a$) to simplify the process. Furthermore, C_D is the covariance of the measurement errors. When the data are uncorrelated, C_D should be diagonal matrix:

$$C_D = \begin{bmatrix} \sigma & \dots & 0 \\ 0 & \ddots & 0 \\ 0 & 0 & \sigma \end{bmatrix}_{N_d \times N_d}, \tag{4.2}$$

where σ is the standard deviation. C_{MD} is the cross – covariance matrix ($N_m \times N_d$) between the parameters, and C_{DD} is the auto – covariance matrix ($N_d \times N_d$) for the simulated data. While N_m is the number of model parameters, N_d denotes the number of data. C_{MD} and C_{DD} are described as

$$C_{MD} = \Delta M^i \left(\Delta D^i\right)^T \tag{4.3}$$

and

$$C_{DD} = \Delta D^i \left(\Delta D^i\right)^T, \tag{4.4}$$

ΔM and ΔD are defined as

$$\Delta M^i = \frac{1}{\sqrt{N_e - 1}} \left[m_1^f - \overline{m}_1^f, \dots, m_{Ne}^f - \overline{m}_1^f\right] \tag{4.5}$$

and

$$\Delta D^i = \frac{1}{\sqrt{N_e - 1}} \left[d_1^f - \bar{d}_1^f, \dots, d_{Ne}^f - \bar{d}_1^f\right], \tag{4.6}$$

where $\overline{m}^f = \frac{1}{N_e} \sum_{j=1}^{N_e} m_j^f$ and $\bar{d}^f = \frac{1}{N_e} \sum_{j=1}^{N_e} d_j^f$.

4.2 Kizildere Geothermal Field, Well KD – 21 Interference Test

Kizildere is located in Saraykoy, which is located west part of Denizli, Turkey. The Kizildere geothermal field is placed in the east part of the Buyuk Menderes graben, where it intersects the Gediz and Cukursu grabens (Onur et al, 2003). Kizildere geothermal field is an active region in terms of tectonic movements. This field temperature is between 195 and 240 °C and it is a liquid-dominated geothermal field.

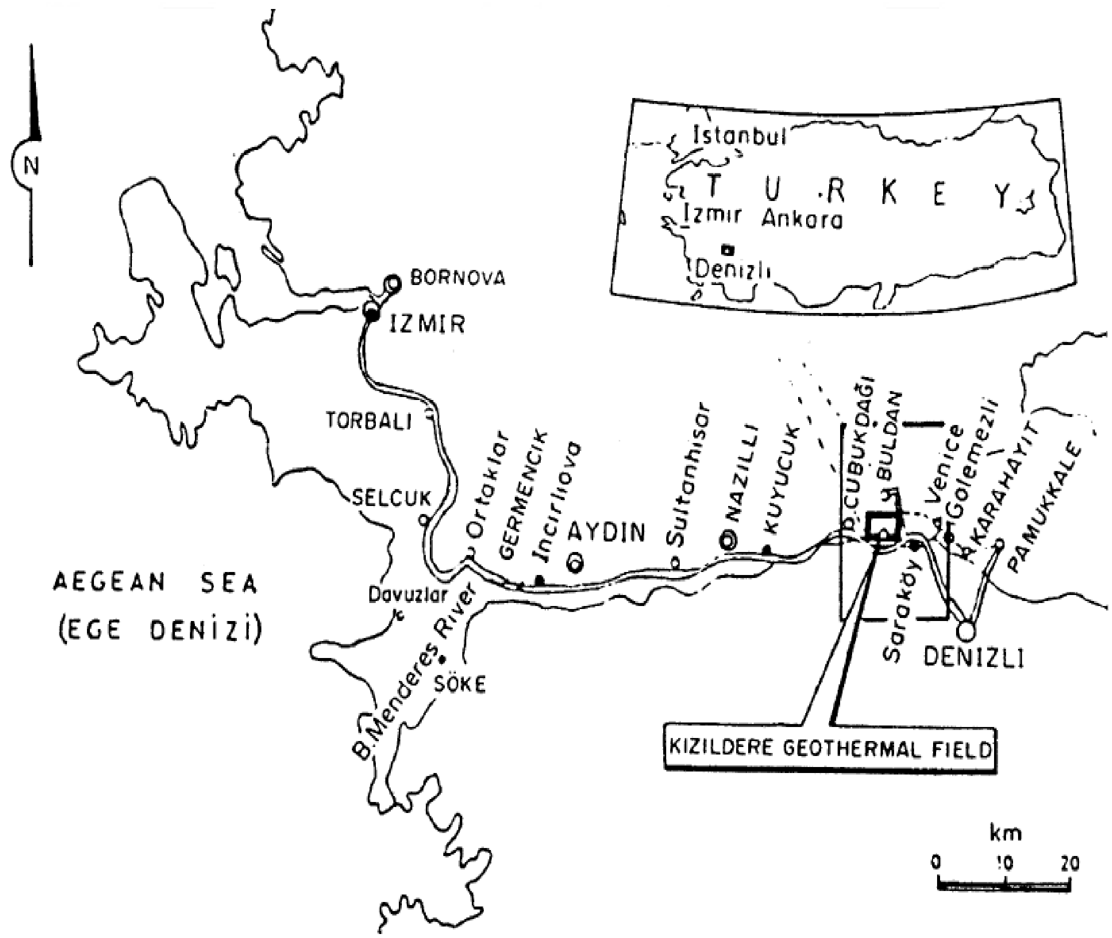

Figure 4.1 Kizildere Geothermal Field (Onur et al., 2003).

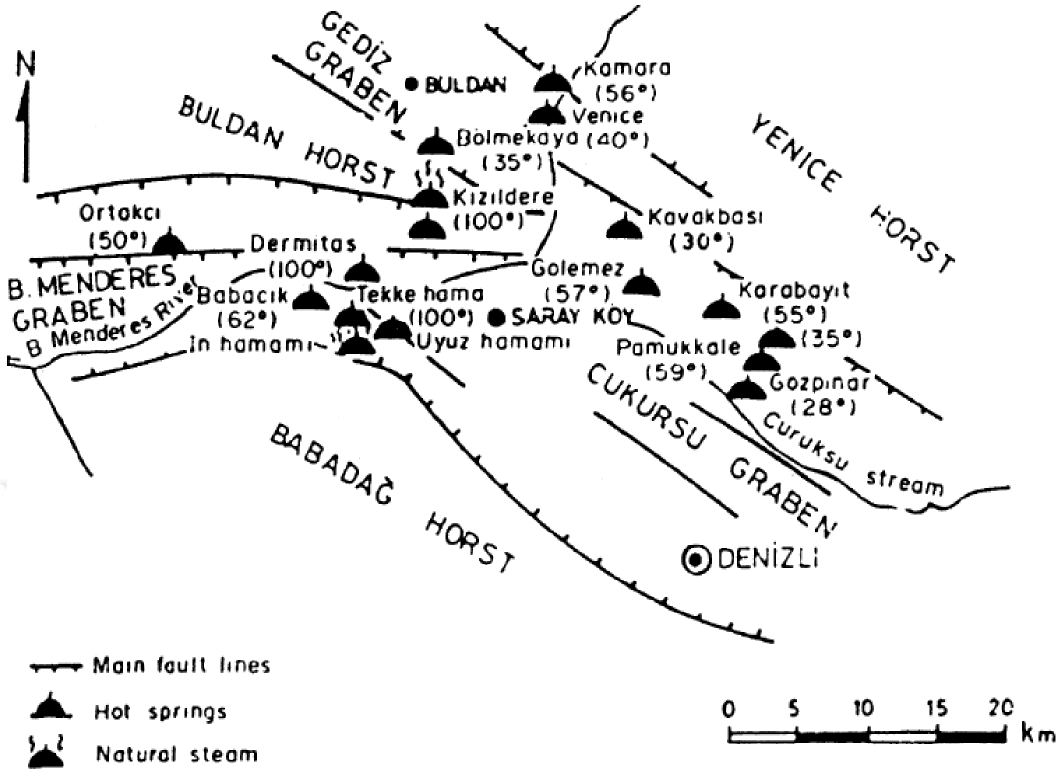

Figure 4.2 Main fault lines Saraykoy – Buldan area (Onur et al., 2003).

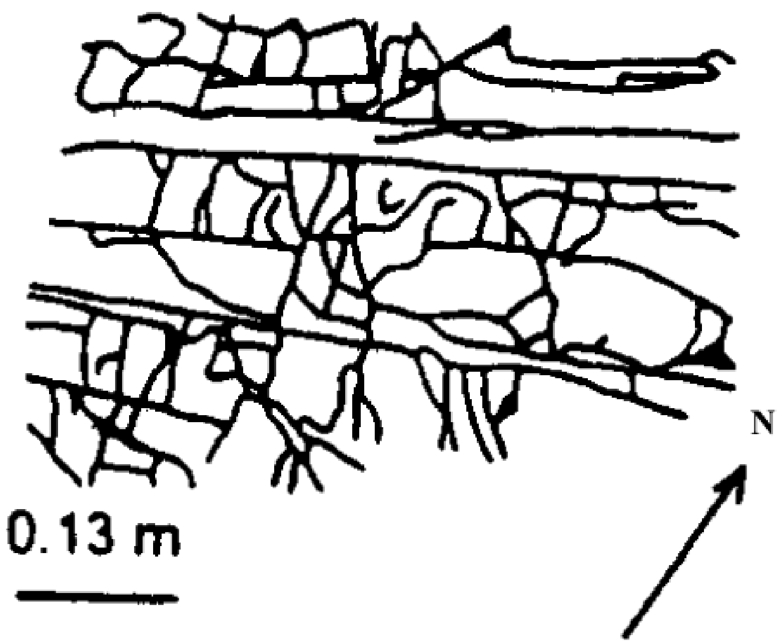

Figure 4.3 Fracture patterns in the Kizildere geothermal field (Onur et al., 2003).

There are many wells drilled to produce geothermal energy. In this thesis, KD – 21 well is analyzed by using pressure transient test. KD – 21 has a depth of 898 m. A maximum temperature of this well was recorded up to 205 °C. The interference test between wells KD – 21 (observation well) and KD – 22 was conducted in 1988 (Onur et al., 2003), and KD – 22 was the active well which produced at a constant rate of 87 t/h hot water. The interference test took 43.5 hours. The required well, reservoir, and fluid property data are given in the following table.

Table 4.1 KD – 21 and KD – 22 well, reservoir, and fluid property data for the interference test.

Parameter	***Value***
Flow rate (qB)	87 t/h
Reservoir thickness (h)	350 m
Fluid Viscosity (μ)	1.5x10^{-4} Pa s
Wellbore radius (r_w)	0.108 m
Bottomhole Temperature (T)	205 °C
Distance between wells (r_b)	200 m

In this section, KD – 21 well is examined for fractal model and anomalous models. We analyze each model in two cases. In the first case, it is assumed that the exponent related to the topology of the network, $\theta = 2.33$ and the fractal dimension, $d_f = 1.3$. These values are determined by Onur et al. (2003) who used the fractal dimension data provided Babadagli et al. (1997) and a log – log plot of pressure change and derivative of interference pressure test data versus time (see Fig. 4.4). Babadagli et al. (1997) determined the fractal dimension range $1.25 \leq d_f \leq 1.57$ from outcrop and satellite studies using the box-counting method. According to Figure 4.4, log – log plots of the pressure and derivative data demonstrates almost the same slope value of 0.7, especially between 2.5 and 31.5 h. In addition, the separation distance between the straight lines is 0.16. The slope and separation values show that the reservoir consists of fractal (fracture network) system with $\delta < 1$ $(i.e., d_f < 2 + \Theta)$ because that slope cannot be explained with commonly used homogeneous models. Furthermore, the slope value of 0.7 yields $\delta = 0.3$ because slope is equal to $1 - \delta$ and indicates that $d_f < 2$ for reported values of Θ in the literature. Note that $\delta = d_f/2 + \Theta$ (Zeybek, 2000). In addition, there are other values of d_f and Θ that can satisfy δ value obtained from log – log plot of Figure 4.4. For instance, $\Theta = 0.50$ and $d_f = 0.75$ or $\Theta = 1.78$ and $d_f = 1.14$, respectively. The main purpose of this section is to determine kh and $\phi c_t h$ for each diffusion model by using ES – MDA. The Stehfest algorithm is used to take the inverse Laplace transform of the general solution, and the algorithm is implemented in MATLAB. Moreover, the pressure changes with time for KD – 21 interference test is:

Table 4.2 Pressure change for the interference test in KD – 21 well.

Time (hours)	*Pressure Changes (kPa)*
0.499	2.986
1.000	5.962
1.504	8.972
2.501	16.407
3.500	17.860
4.515	22.326
5.520	27.473
6.499	30.000
7.509	32.352
8.487	36.456
9.532	38.944
10.471	43.337
11.437	44.441
12.527	47.473
13.550	50.554
16.515	58.419
19.566	65.624
22.536	73.487
25.472	78.997
28.521	86.265
31.536	91.000
34.327	97.517
37.599	104.499
40.926	111.630
43.716	121.518

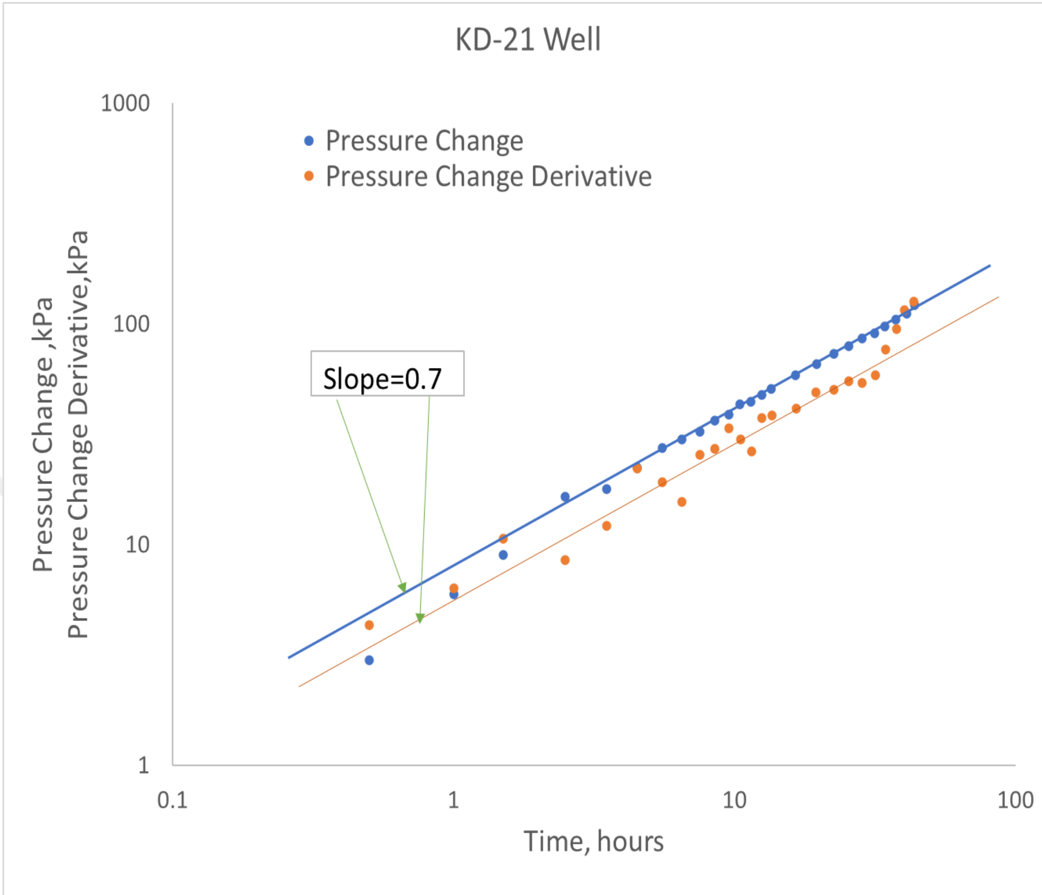

Figure 4.4 Pressure Change and Pressure Change Derivative with time for KD – 21 interference test.

According to the given information, the required data for ES – MDA can be interpreted as for both case 1 (θ=*2.33* and d_f=*1.3)* and case 2 (θ=*0.5* and d_f=*0.75)*.

Table 4.3 ES – MDA input for KD – 21 well.

Input	***Value***
N_m	2
N_a	8
N_d	25
N_e	100

4.2.1 Kizildere Geothermal Field Nonlinear Regression for θ=2.33 and d_f=1.3

After the applying ES – MDA, kh and $\phi c_t h$ is found for the given minimum and maximum value. n is 2 for Raghavan anomalous model. For Raghavan anomalous model, n represent Euclidean dimension. Thus, n should be used as an integer. The goal is to get the smallest Root Mean Square (RMS). The following table shows kh and $\phi c_t h$ matching result, and the following figures demonstrate both prior and assimilated results. It is important to note that the unit of kh for Raghavan's anomalous model is different than fractal and Metzler's anomalous model. Raghavan describes the dimensionless time in Eq. 3.60 different than the others. According to Eq. 3.60, the unit of k_α is $L^{2+\theta}T^{1-\alpha}$. In addition, Raghavan anomalous model describes the mobility at any point r in the reservoir,

$$\lambda(r) = \lambda_\alpha r^{-\theta} = \frac{k(r)}{\mu} = \frac{k_\alpha}{\mu} r^{-\theta}, \tag{4.7}$$

where the unit of $k(r)$ is $L^2T^{1-\alpha}$. As a result, the unit of kh for Raghavan anomalous model is $L^3T^{1-\alpha}$ in the following table. Note that $\alpha = \frac{2}{2+\theta}$.

Table 4.4 Nonlinear Regression Result for θ=2.33 and d_f=1.3.

	Fractal Model	***Metzler Anomalous Model***	***Raghavan Anomalous Model***
kh, m³	8.67×10^{-11} (2.9×10^{-11} – 1.4×10^{-10})	4.76×10^{-13} (2×10^{-13} – 8×10^{-13})	7.97×10^{-9} * (7×10^{-9} – 9×10^{-9})
$\phi c_t h$, m/Pa	3.64×10^{-8} (2.2×10^{-8} – 3.7×10^{-8})	1.55×10^{-10} (1.1×10^{-10} – 2.2×10^{-10})	5.31×10^{-8} (4×10^{-8} – 6×10^{-8})
RMS, kPa	1.238	2.617	3.838

* The unit is $L^3T^{1-\alpha}$.

RMS is defined as

$$RMS = \sqrt{\frac{1}{N_d}\sum_{i=1}^{N_d}(\Delta P_{measured} - \Delta P_{model})^2}. \qquad (4.8)$$

It is important to note that RMS represents the root mean square of the ensemble mean in the Table 4.4 and following tables.

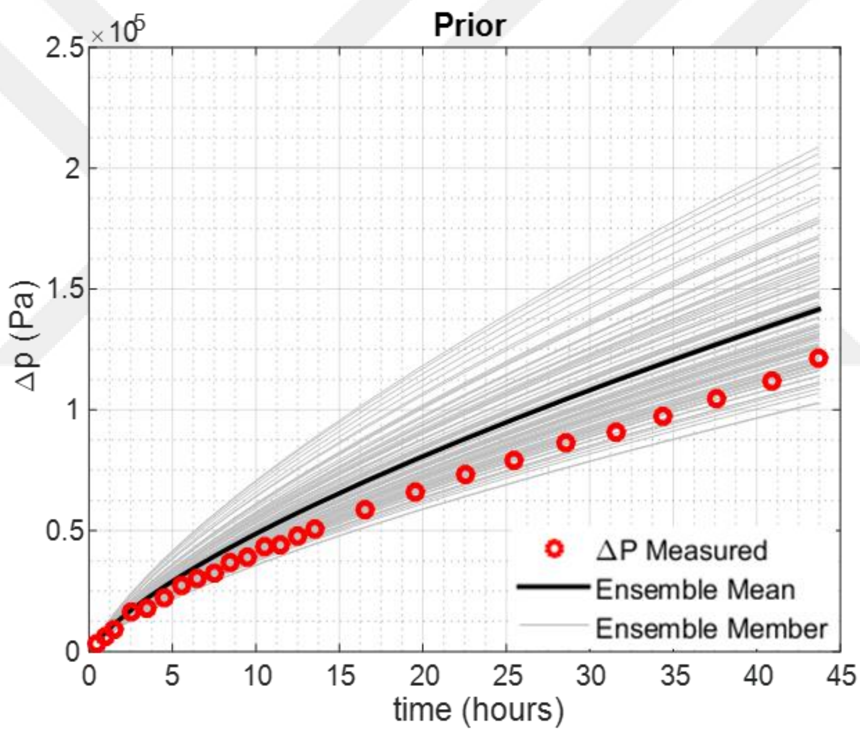

Figure 4.5 Fractal Model for Prior Results.

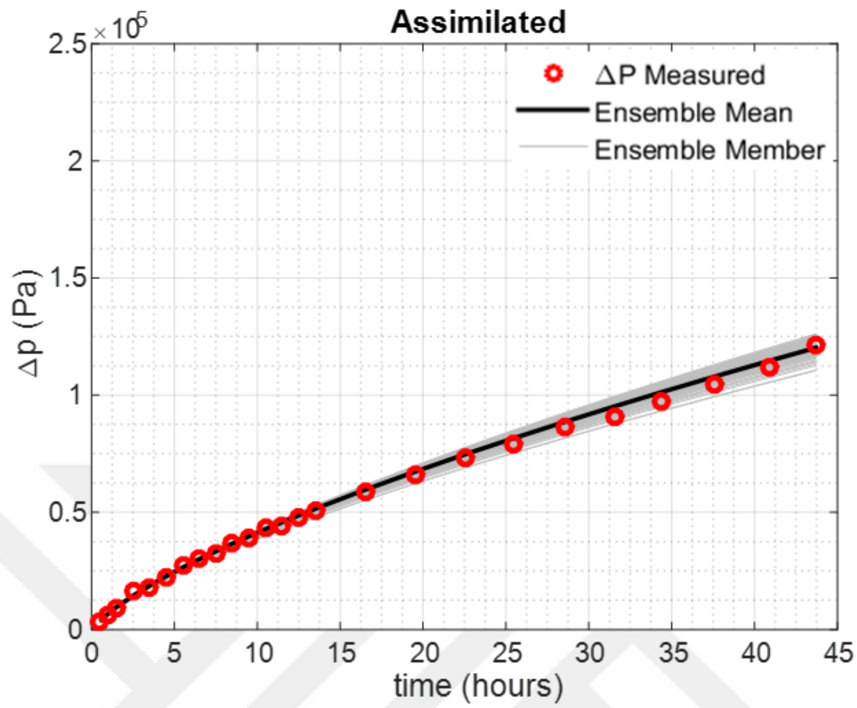

Figure 4.6 Fractal Model for Assimilated Results.

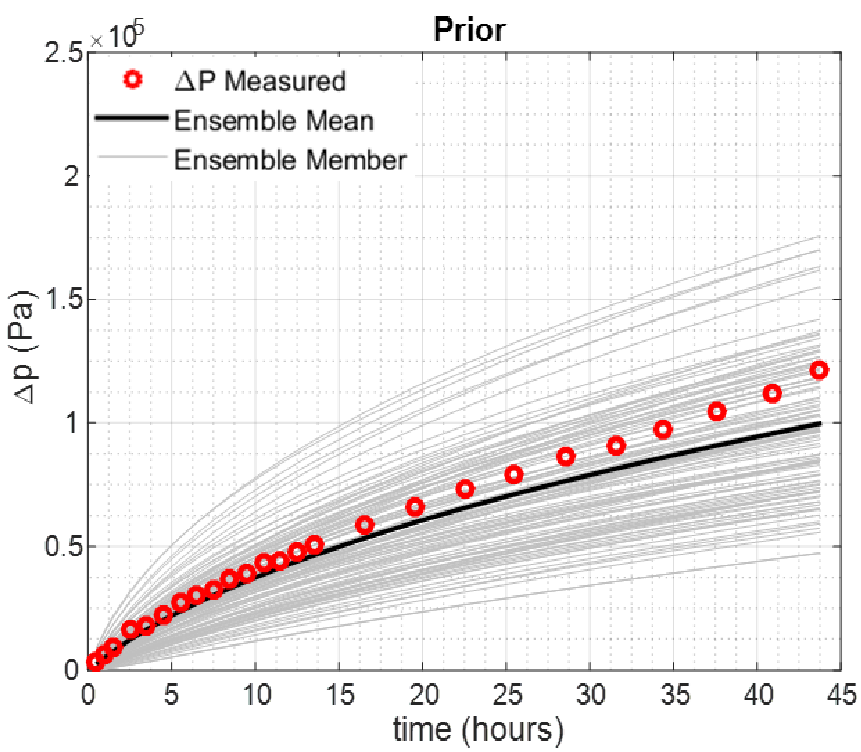

Figure 4.7 Metzler Anomalous Model for Prior Results.

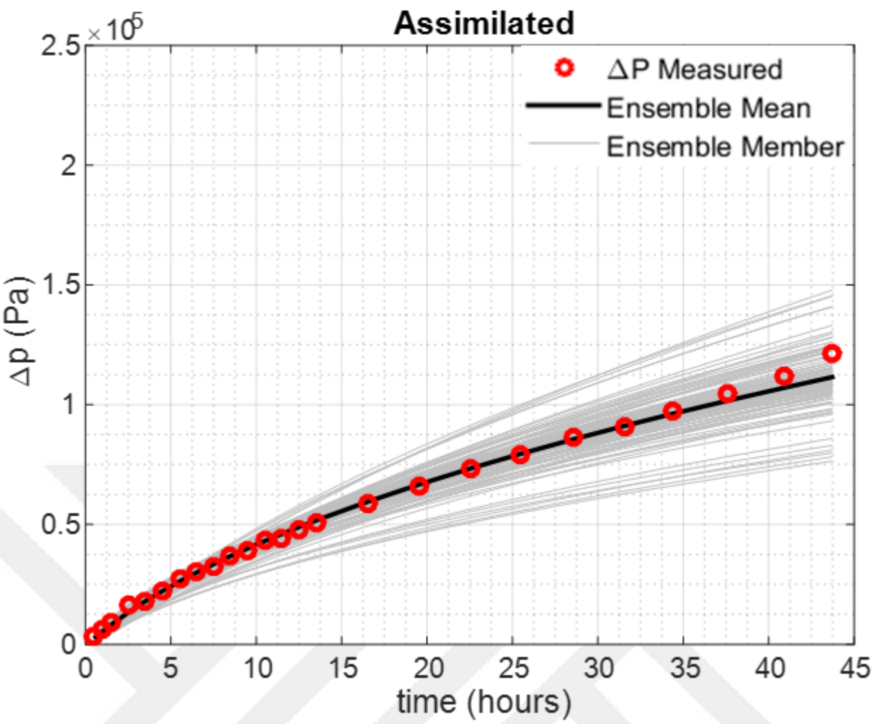

Figure 4.8 Metzler Anomalous Model for Assimilated Results.

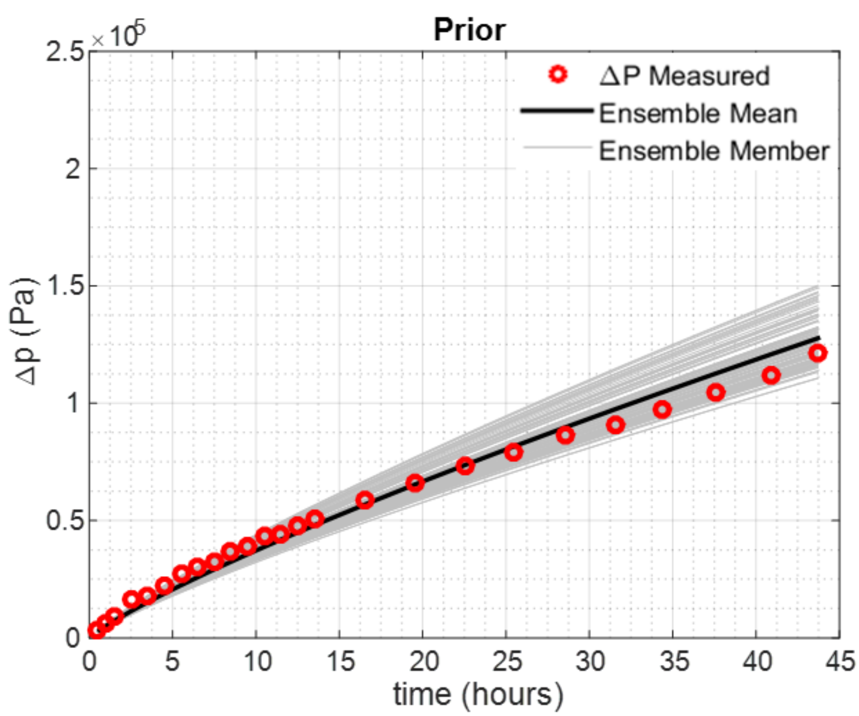

Figure 4.9 Raghavan Anomalous Model for Prior Results.

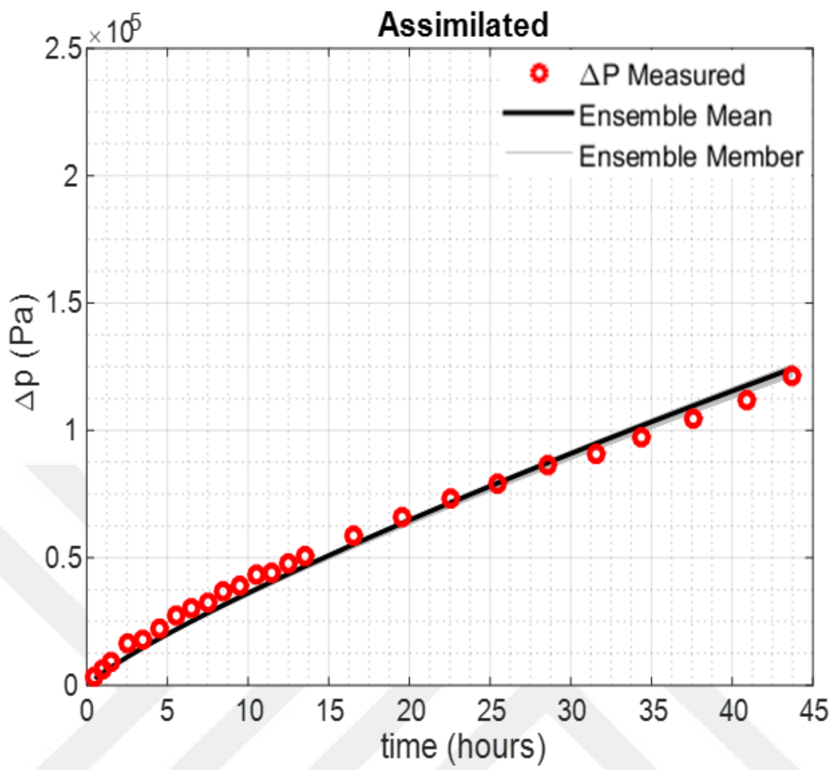

Figure 4.10 Raghavan Anomalous Model for Assimilated Results.

According to Table 4.4 and the figures above, fractal model obtains the best match and the least RMS. In other words, the ensemble mean of fractal model approaches to measured pressure change data so closely. Although Metzler anomalous model's RMS is smaller than Raghavan anomalous model's RMS, Raghavan anomalous model assimilates better than Metzler anomalous model. Perhaps, Raghavan anomalous model fits better than others if the given range is changed. Moreover, fractal model gets along with both early time and late time. On the other hand, Metzler anomalous model suits very well at the early time. Nevertheless, as time goes on, Metzler anomalous model's result moves away from the measured data at the late time. In addition, while Raghavan anomalous model underestimates at the early time, it overestimates at the late time. To conclude, each model finds different results. Raghavan anomalous model and fractal model get approximately the same result for $\phi c_t h$. Metzler anomalous model results for both kh and $\phi c_t h$

are the smallest values. We cannot compare kh result for Raghavan anomalous model with other models because of the definition.

4.2.2 Kizildere Geothermal Field Nonlinear Regression for θ=0.50 and d_f=0.75

In this part, Kizildere geothermal field is examined using another topology of the network and fractal dimension value. These values are taken from Onur et al. (2003). kh and $\phi c_t h$ are analyzed by using ES – MDA. n is 2 for Raghavan anomalous model. The main aim is to get the best match. Hence, acquiring the smallest RMS is the most important criteria. Table 4.5 demonstrates the ranges and the nonlinear regression result for the Case 2.

Table 4.5 Nonlinear Regression Result for θ=0.5 and d_f=0.75.

	Fractal Model	***Metzler Anomalous Model***	***Raghavan Anomalous Model***
kh, m³	$1.47\text{x}10^{-10}$ ($4.9\text{x}10^{-11} – 2.4\text{x}10^{-10}$)	$1.26\text{x}10^{-11}$ ($6\text{x}10^{-12} – 2\text{x}10^{-11}$)	$7.34\text{x}10^{-11}$ * ($6\text{x}10^{-11} – 9\text{x}10^{-11}$)
$\phi c_t h$, m/Pa	$2.13\text{x}10^{-8}$ ($1.3\text{x}10^{-8} – 2.2\text{x}10^{-8}$)	$4.62\text{x}10^{-9}$ ($3\text{x}10^{-9} – 6\text{x}10^{-9}$)	$5.43\text{x}10^{-8}$ ($4\text{x}10^{-8} – 7\text{x}10^{-8}$)
RMS, kPa	1.212	2.111	2.579

* The unit is $L^3T^{1-\alpha}$.

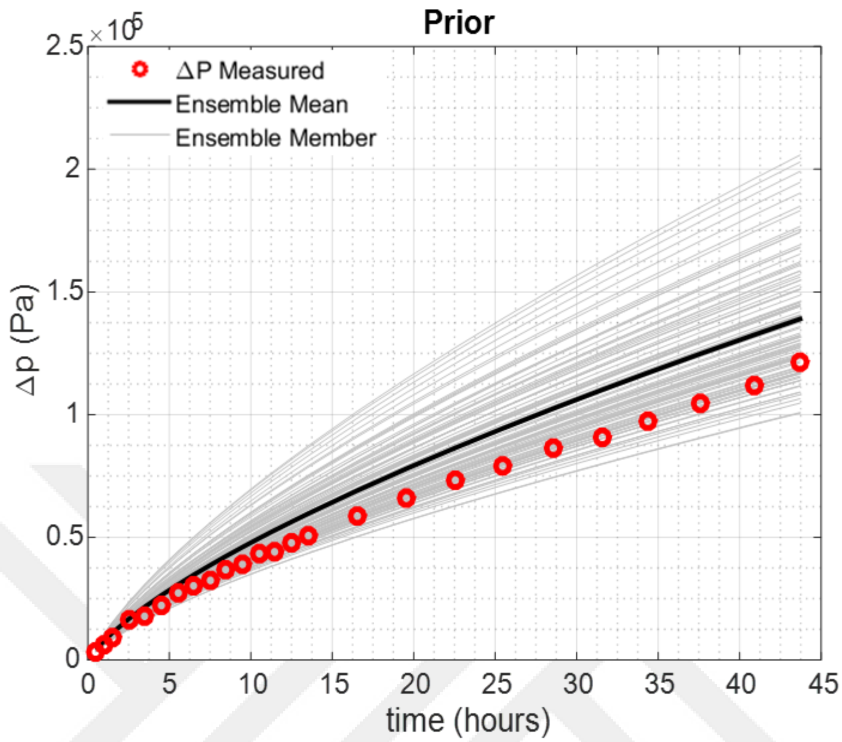

Figure 4.11 Fractal Model for Prior Results.

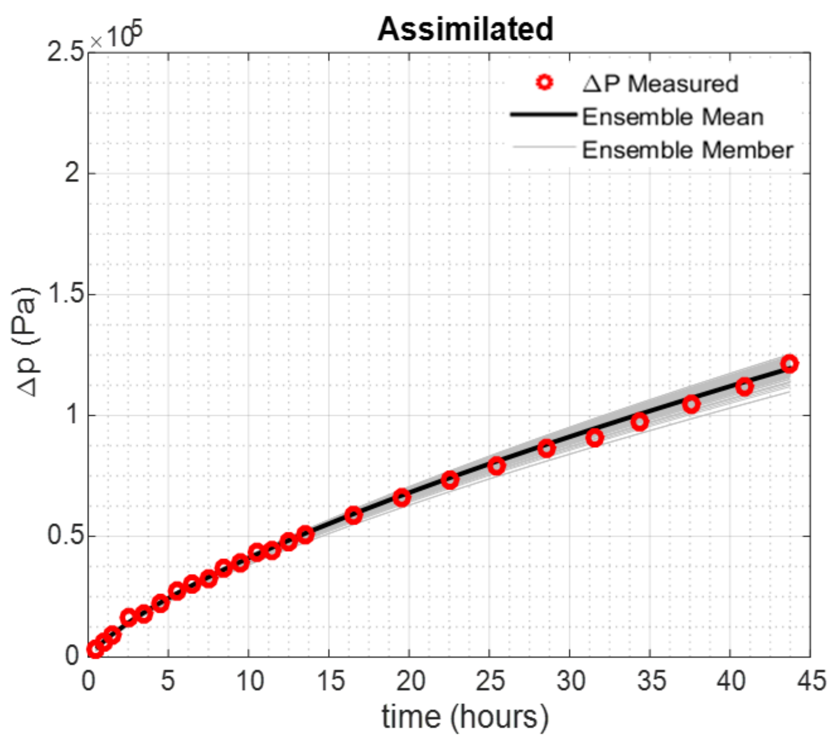

Figure 4.12 Fractal Model for Assimilated Results.

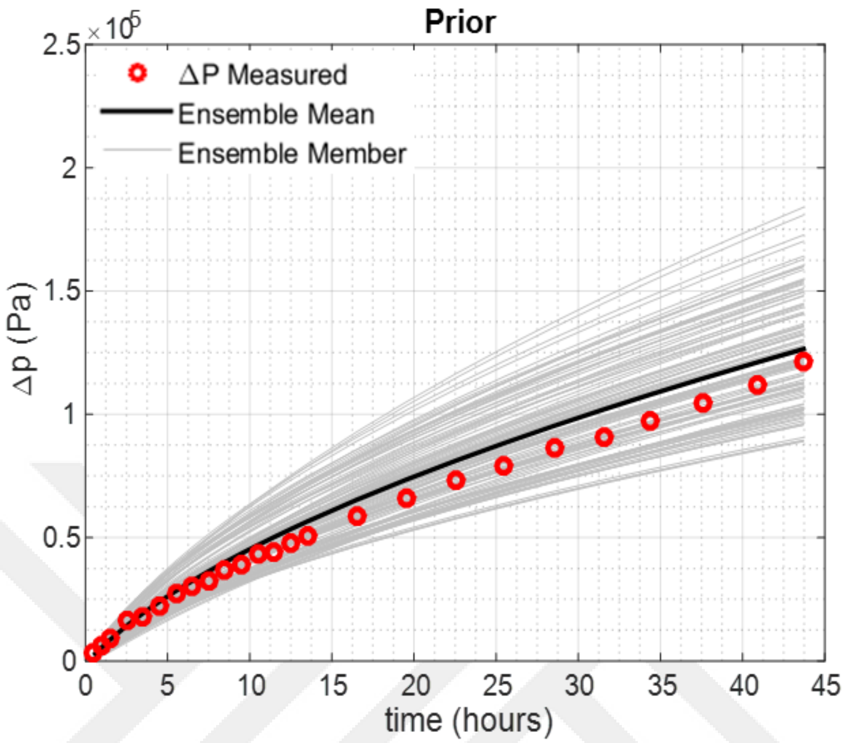

Figure 4.13 Metzler Anomalous Model for Prior Results.

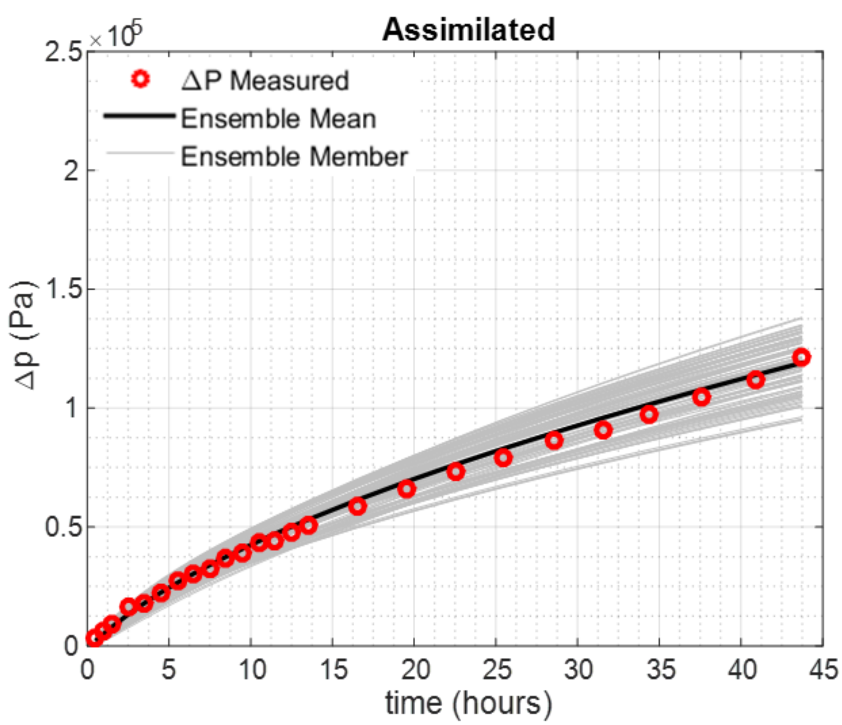

Figure 4.14 Metzler Anomalous Model for Assimilated Results.

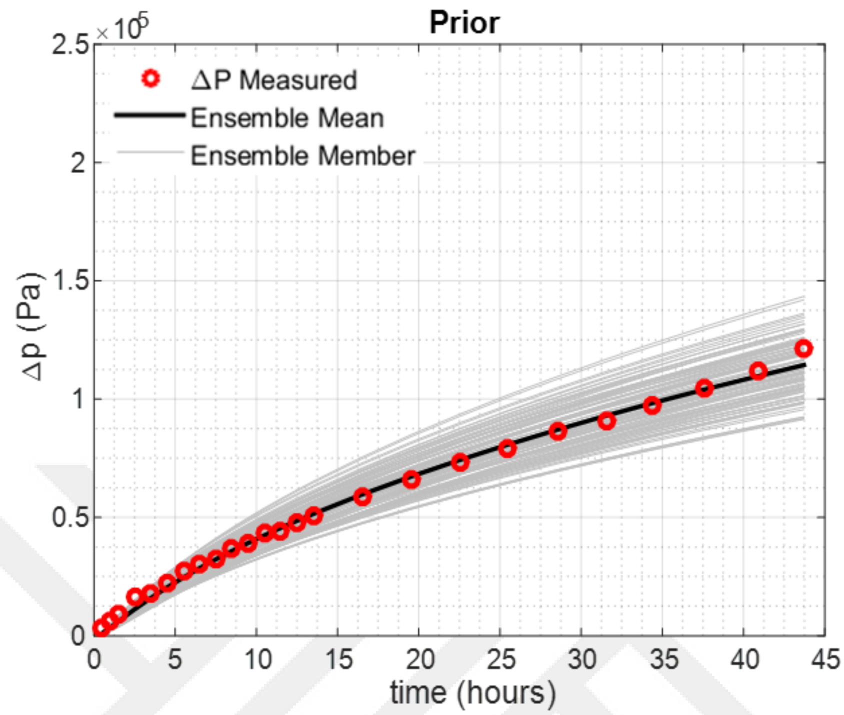

Figure 4.15 Raghavan Anomalous Model for Prior Results.

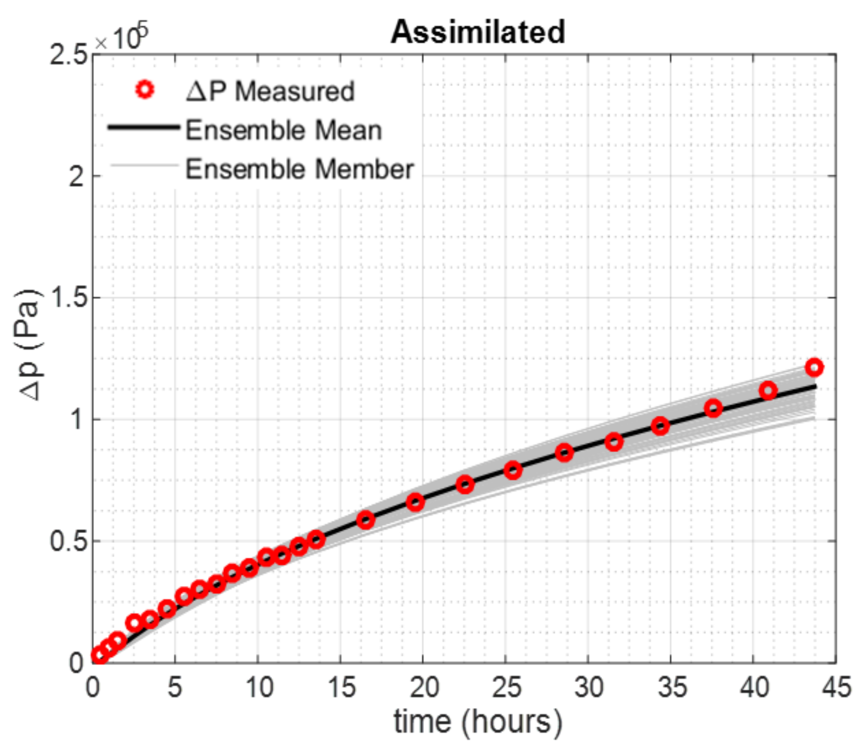

Figure 4.16 Raghavan Anomalous Model for Assimilated Results.

According to Table 4.5 and the figures above, fractal model again performs better than other models. On the other hand, Raghavan anomalous model fits better than Case 1. If we compare Case 1 and Case 2 results, it is clearly seen that each model obtain different outcomes for each case. Therefore, we can say that topology of the network and fractal dimension influence remarkably. Consequently, the box-counting method is critically important to determine fractal parameters. Fractal model fits perfectly both at early and late time. On the other side of the coin, Metzler anomalous model performs very well at the early time. However, this is not applicable for the late time response. Furthermore, Raghavan anomalous model underestimates at the early time. Nevertheless, this model fits very good as time increases. Then, the model results moves away from the measured data. In addition, Metzler anomalous model disperses more than other models for prior results for both cases. However, this model acquires less errors than Raghavan anomalous model. The reason may be because of the difference between d_f and n. In other words, even though d_f values 0.75 and 1.3 are used for fractal model and Metzler anomalous model, n value 2 is used for Raghavan for both cases. This may cause a difference. To sum up, the fractal model shows better performance than other models and gathers close to the measured data pretty good.

4.3 Kamojang Geothermal Field, Well KMJ – 40 Interference Test

Kamojang is in Indonesia. The Kamojang reservoir is vapor-dominated. Two separate interference test was run. The first interference test is that KMJ – 37 is the signal well, and KMJ – 28 and KMJ – 33 are the monitor wells. In the second interference test, while KMJ – 46 is the signal well, KMJ – 40 is the monitor well (Aprilian et al., 1993). In this section, we focus on the second interference test. The pressure transient test data is analyzed with the fractal model and anomalous models in this study. Aprilian et al. (1993) examined the field by using fractal model.

Furthermore, Camacho et al. (2011) analyzed the interference data using with Metzler anomalous model. In this section, we reanalyze the field for both method, and investigate with Raghavan anomalous model, and then compare the results. We analyze each model in two cases. In the first case, it is assumed $\theta = 0.50$ and $d_f = 1.6$. These values are taken from Camacho et al. (2011). In the second case, θ and d_f are assumed as 0.25 and 1.575, respectively. The second case values can be found in Aprilian et al. (1993).

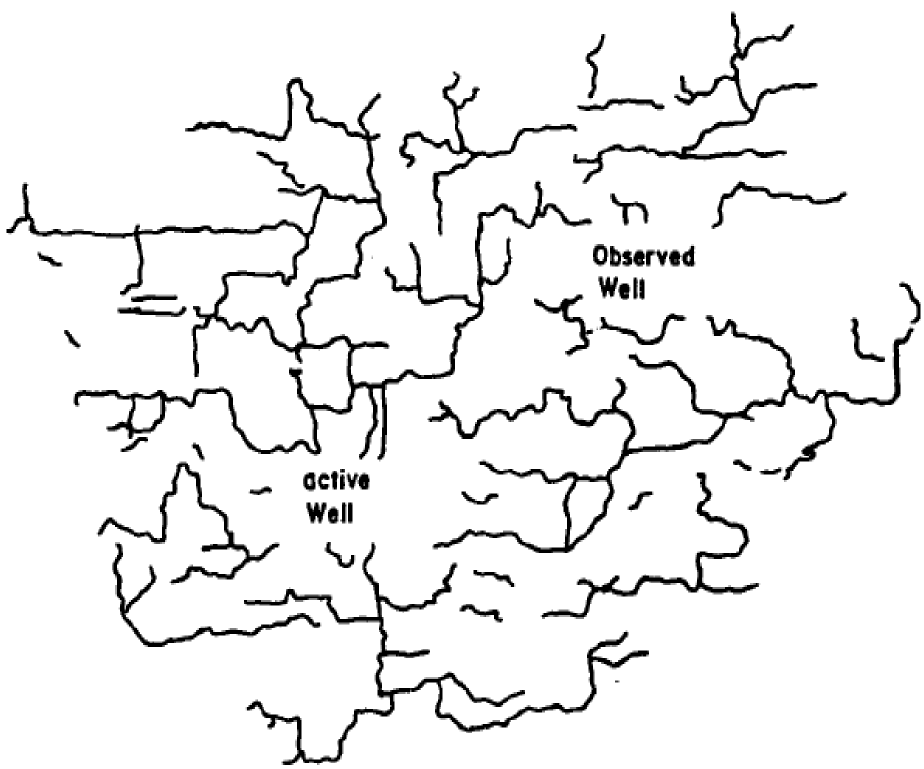

Figure 4.17 Schematic of Interference test in Kamojang Geothermal Field (Aprilian et al., 1993).

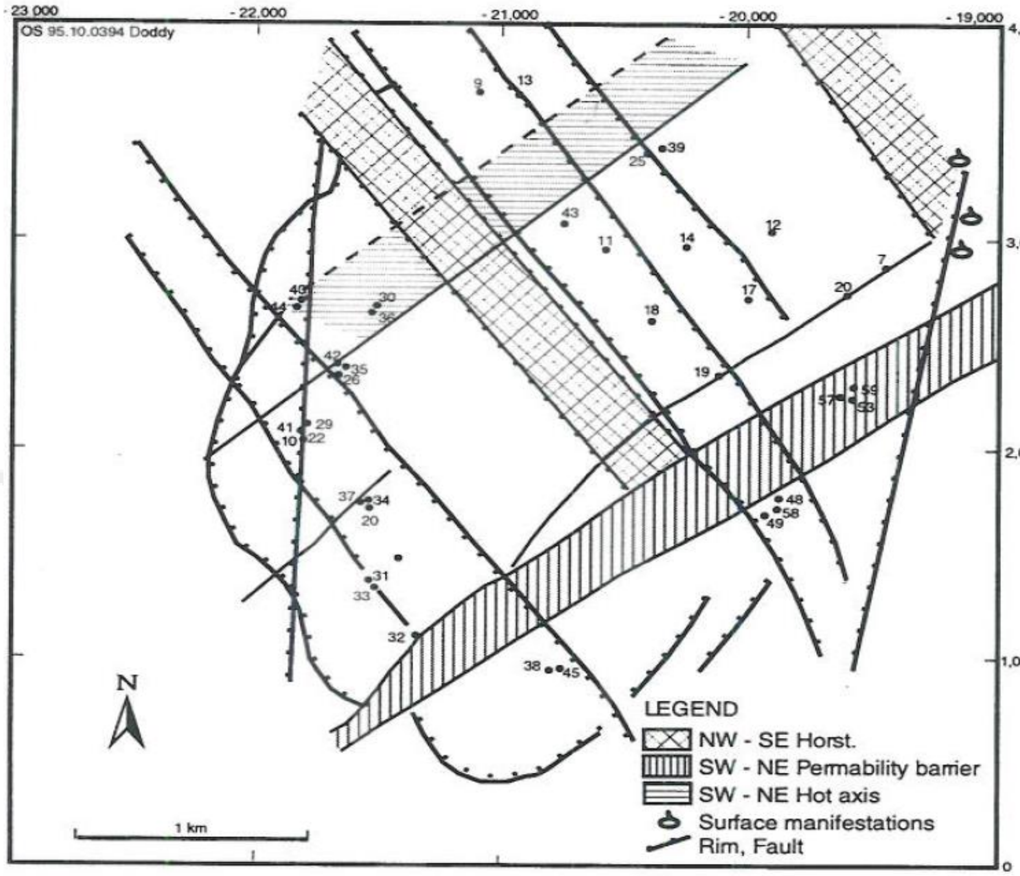

Figure 4.18 A structural map of Kamojang geothermal field (Irhas, 1996).

The duration of the interference test was 864 hours. A maximum temperature of this well was recorded up to 235 °C. KMJ – 46 well was produced at the constant rate of 41 t/h. The required well, reservoir and fluid property data are given the following table.

Table 4.6 KMJ – 46 and KMJ – 40 well, reservoir, and fluid property data for the interference test.

Parameter	***Value***
Flow rate (qB)	41 t/h
Reservoir thickness (h)	100 m
Fluid Viscosity (μ)	1.7x10^{-5} Pa s
Wellbore radius (r_w)	0.164 m
Bottomhole Temperature (T)	235 °C
Distance between wells (r_b)	360 m

The required data for ES – MDA is used as for both case 1 (*θ=0.50* and *d_f=1.6)* and case 2 (*θ=0.25* and *d_f=1.575).*

Table 4.7 ES – MDA input for KMJ – 40 well.

Input	***Value***
N_m	2
N_a	8
N_d	36
N_e	100

The pressure response in the observation well (KMJ – 40) is given in the following figure and table,

Table 4.8 Pressure change for the interference test in KMJ – 40 well.

Time (hours)	***Pressure Changes (kPa)***	***Time (hours)***	***Pressure Changes (kPa)***
24	0	456	1.999
48	0	480	2.199
72	0	504	2.496
96	0.097	528	2.537
120	0.296	552	2.599
144	0.296	576	2.682
168	0.400	600	2.799
192	0.400	624	2.999
216	0.800	648	2.999
240	0.800	672	2.896
264	1.000	696	3.096
288	1.096	720	3.296
312	1.296	744	3.496
336	1.400	768	3.696
360	1.400	792	3.399
384	1.496	816	3.799
408	1.496	840	3.799
432	1.600	864	3.999

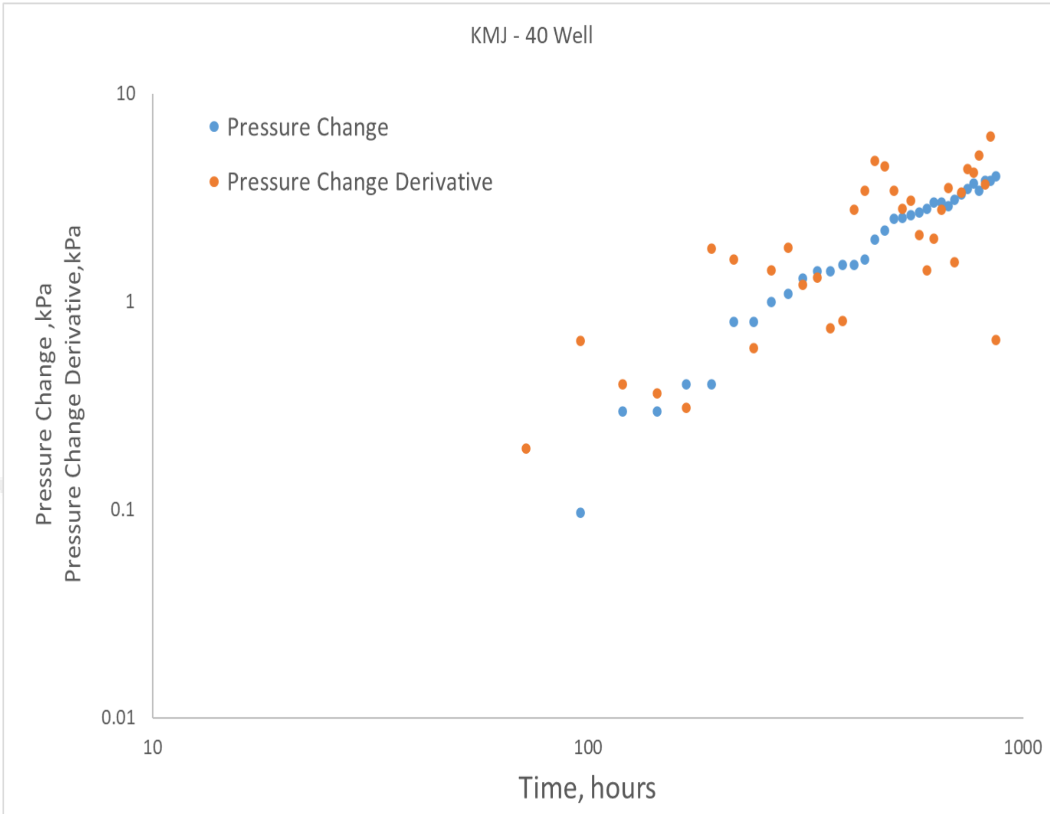

Figure 4.19 Pressure Change and Pressure Change Derivative with time for KMJ – 40 interference test.

4.3.1 Kamojang Geothermal Field Nonlinear Regression for θ=0.50 and d_f=1.6

In this section, kh and $\phi c_t h$ are determined by using nonlinear regression ES – MDA method. θ and d_f are assumed 0.50 and 1.6, respectively. Camacho et al. (2011) studied with these assumption for Metzler anomalous model. After all required information is inputted into ES – MDA, RMS, kh and $\phi c_t h$ are found. n is 2 for Raghavan anomalous model. The outcomes for kh and $\phi c_t h$ are shown in the following table. Then, the prior and assimilated results are demonstrated in the following figures.

Table 4.9 Nonlinear Regression Result for Θ=0.50 and d_f=1.6.

	Fractal Model	***Metzler Anomalous Model***	***Raghavan Anomalous Model***
kh, m³	5.65×10^{-12} ($4 \times 10^{-12} - 7 \times 10^{-12}$)	6.76×10^{-13} ($5 \times 10^{-13} - 8 \times 10^{-13}$)	5.36×10^{-11} * ($3 \times 10^{-11} - 7 \times 10^{-11}$)
$\phi c_t h$, m/Pa	7.47×10^{-6} ($6 \times 10^{-6} - 9 \times 10^{-6}$)	2.88×10^{-7} ($1 \times 10^{-7} - 4 \times 10^{-7}$)	7.91×10^{-6} ($6 \times 10^{-6} - 9 \times 10^{-6}$)
RMS, kPa	0.155	0.351	0.126

* The unit is $L^3 T^{1-\alpha}$.

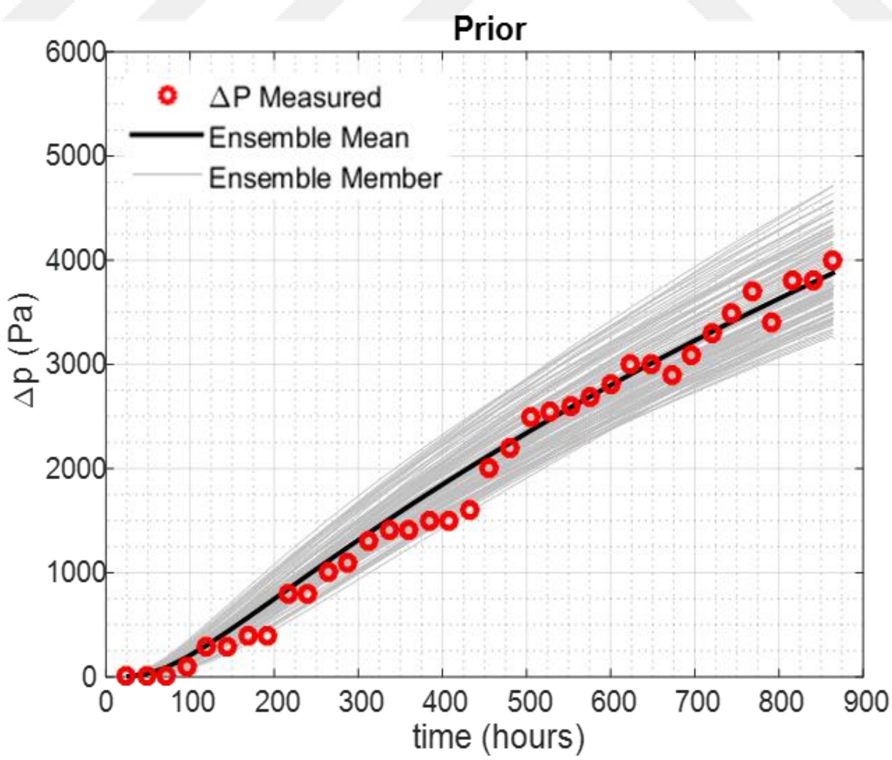

Figure 4.20 Fractal Model for Prior Results.

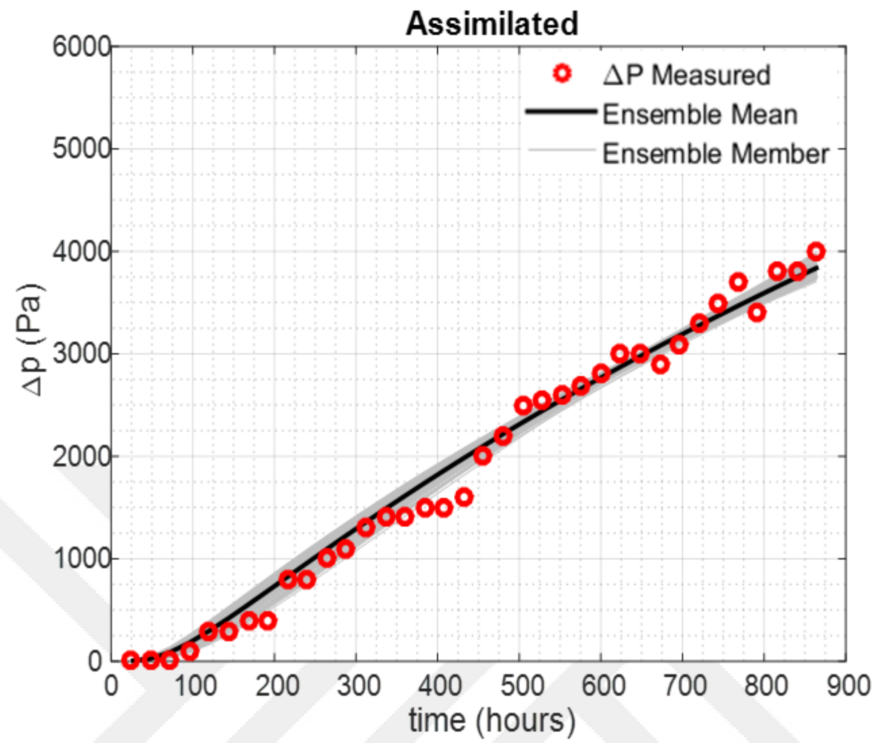

Figure 4.21 Fractal Model for Assimilated Results.

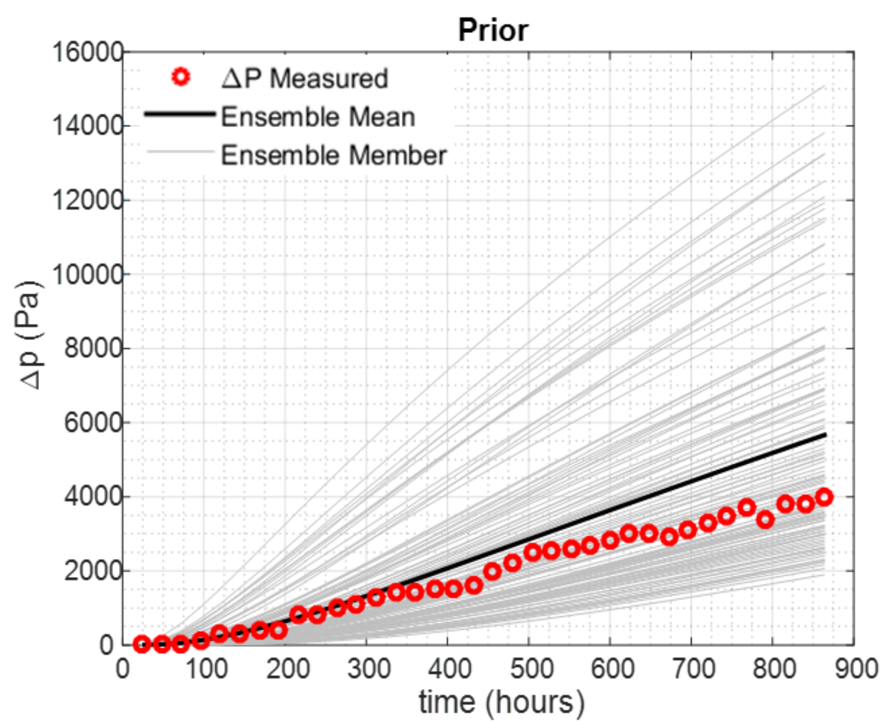

Figure 4.22 Metzler Anomalous Model for Prior Results.

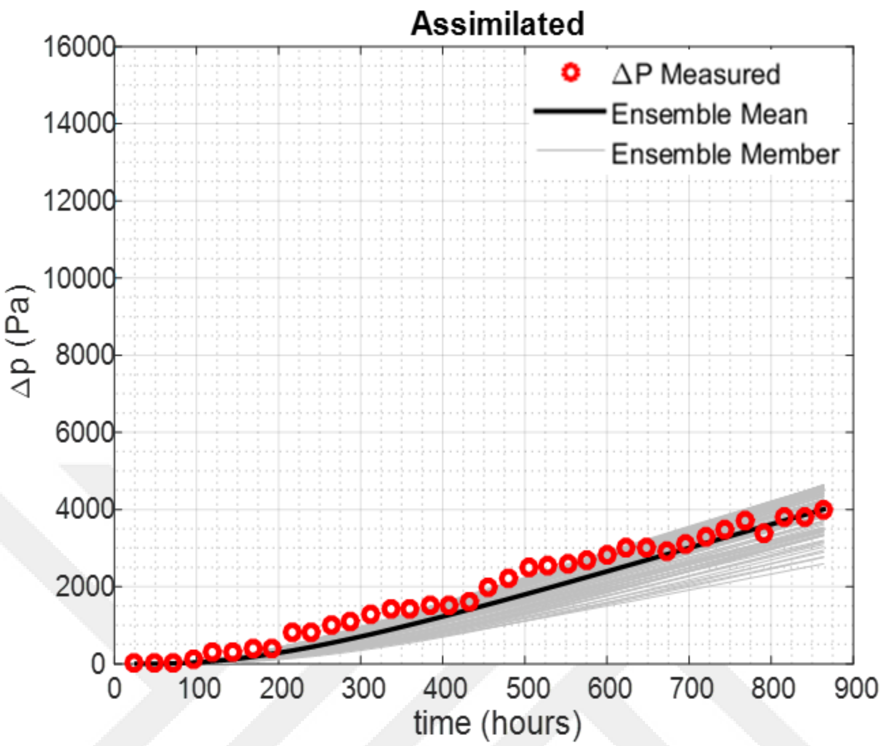

Figure 4.23 Metzler Anomalous Model for Assimilated Results.

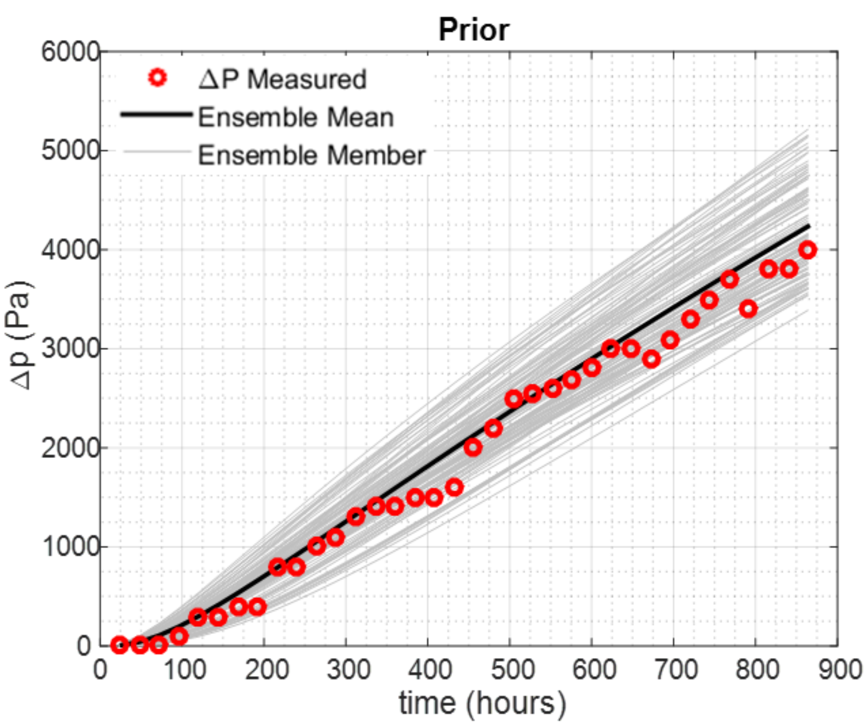

Figure 4.24 Raghavan Anomalous Model for Prior Results.

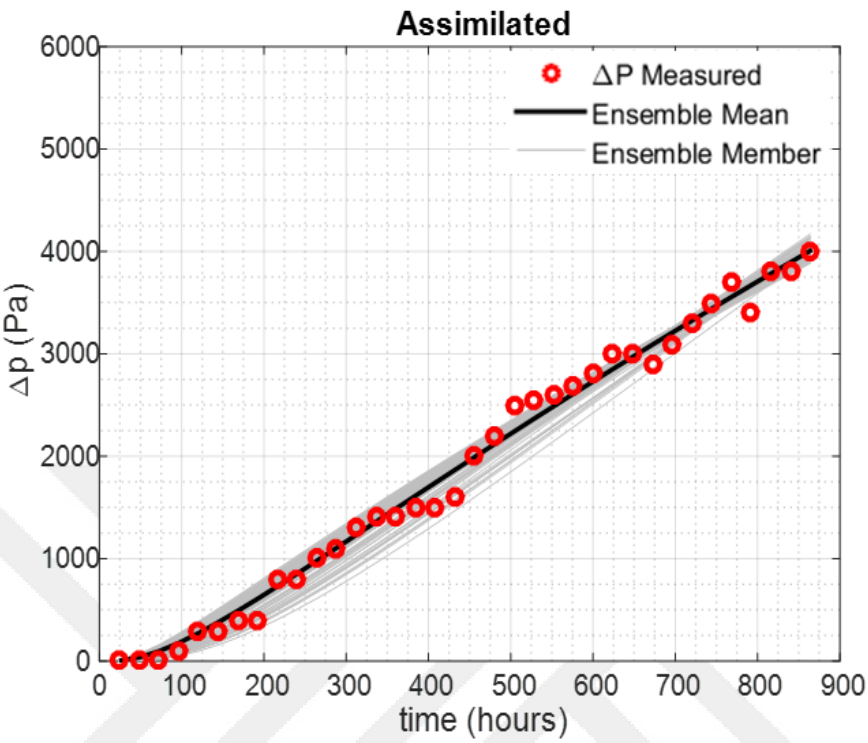

Figure 4.25 Raghavan Anomalous Model for Assimilated Results.

According to Table 4.9 and figures above, it is undeniable that each model performs very well. Although Raghavan anomalous model gets the lowest RMS, the fractal model achieves good match. In addition to that, even though Metzler anomalous model obtains good match both at the early time and late time, it underestimates at the middle time. Fractal model and Raghavan anomalous model behaves similar both early and late time outcomes. Moreover, Raghavan anomalous model and fractal model obtain nearly the same $\phi c_t h$ outcomes. If we compare fractal model and Metzler anomalous model, it is seen that Metzler anomalous model obtains roughly 10 times less than for kh and 25 times less than for $\phi c_t h$ fractal model. Raghavan anomalous model cannot compare with other models for kh because of the definition of kh. To conclude, every model works pretty well in this case. Raghavan anomalous model obtains the best match and the results should be compared with field outcrops.

4.3.2 Kamojang Geothermal Field Nonlinear Regression for θ=0.25 and d_f=1.575

In this part, Kamojang Geothermal Field is analyzed using another fractal dimension and topology of the network. The assumed values are taken from Aprilian et al. (1993). Aprilian et al. studied with these assumption for fractal model. Nevertheless, we consider all methods for these assumptions. n is 2 for Raghavan anomalous model. The main purpose is to find kh and $\phi c_t h$ by using nonlinear regression ES – MDA. Table 4.10 and the following figures show prior and assimilated outcomes.

Table 4.10 Nonlinear Regression Result for θ=0.25 and d_f=1.575.

	Fractal Model	***Metzler Anomalous Model***	***Raghavan Anomalous Model***
kh, m³	5.70×10^{-12} ($4 \times 10^{-12} – 7 \times 10^{-12}$)	2.68×10^{-12} ($1 \times 10^{-12} – 4 \times 10^{-12}$)	2.04×10^{-11} * ($1 \times 10^{-11} – 3 \times 10^{-11}$)
$\phi c_t h$, m/Pa	7.43×10^{-6} ($6 \times 10^{-6} – 9 \times 10^{-6}$)	1.45×10^{-6} ($9 \times 10^{-7} – 2 \times 10^{-6}$)	8.00×10^{-6} ($6 \times 10^{-6} – 9 \times 10^{-6}$)
RMS, kPa	0.155	0.176	0.173

* The unit is $L^3 T^{1-\alpha}$.

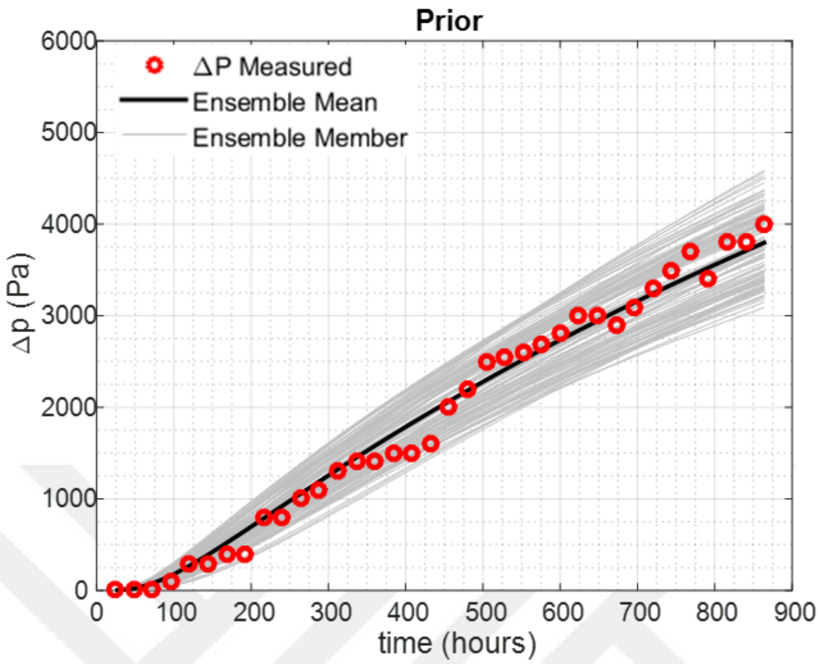

Figure 4.26 Fractal Model for Prior Results.

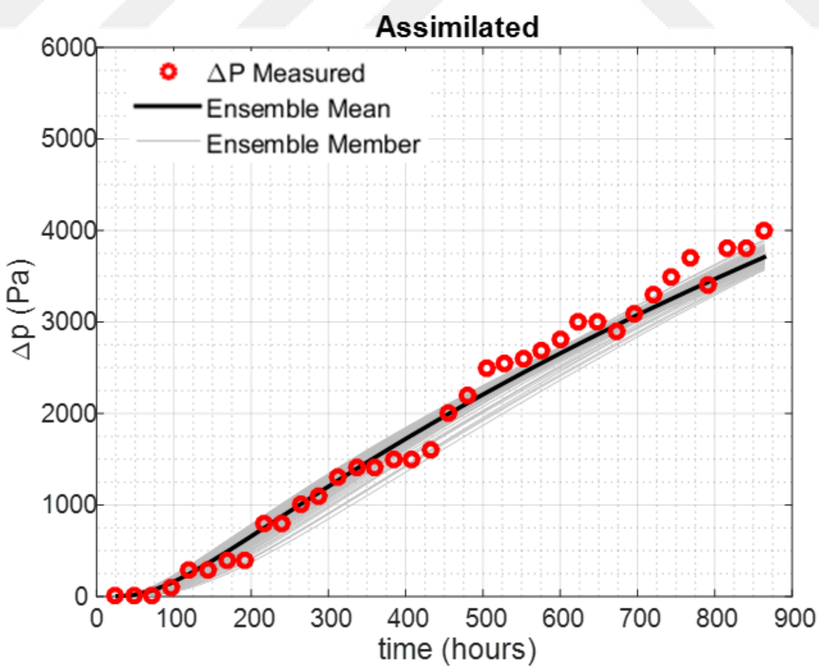

Figure 4.27 Fractal Model for Assimilated Results.

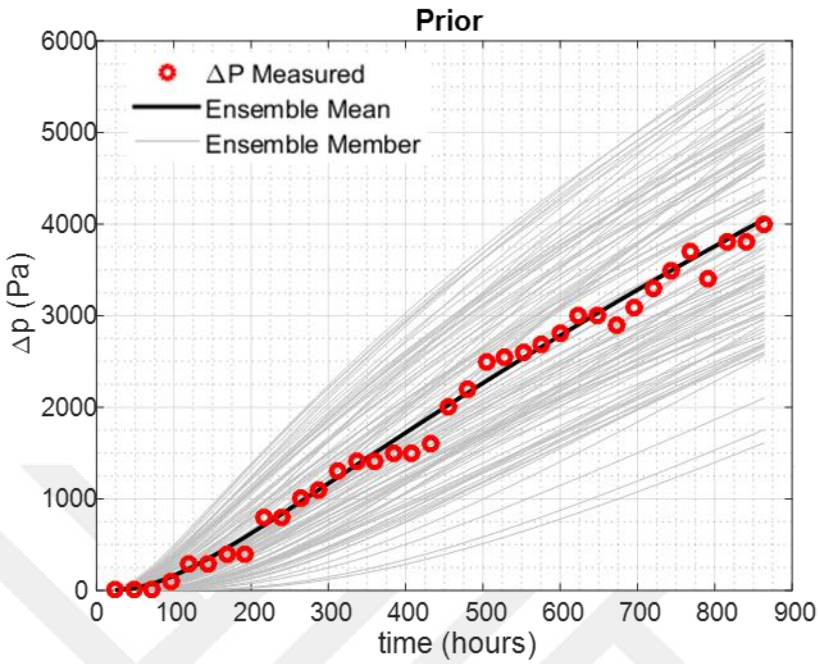

Figure 4.28 Metzler Anomalous Model for Prior Results.

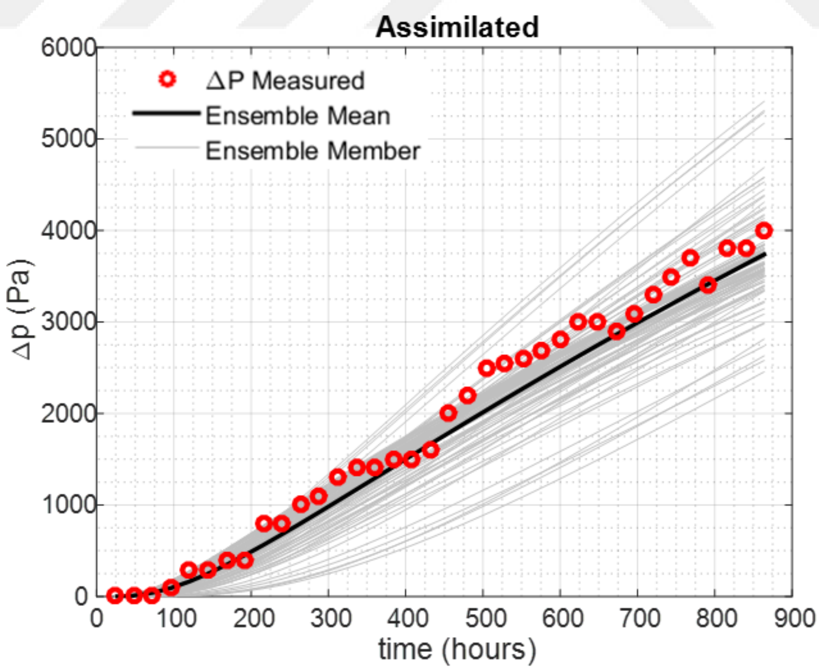

Figure 4.29 Metzler Anomalous Model for Assimilated Results.

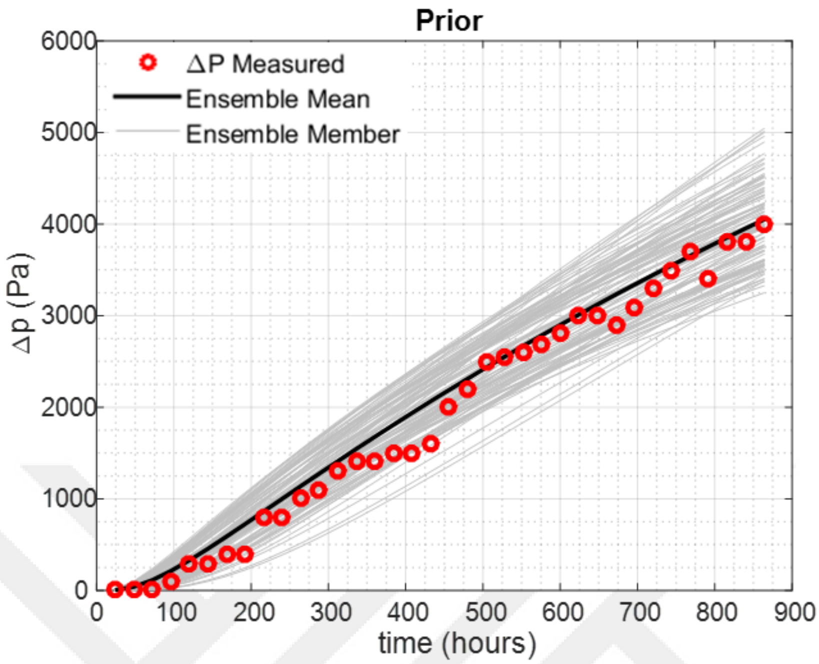

Figure 4.30 Raghavan Anomalous Model for Prior Results.

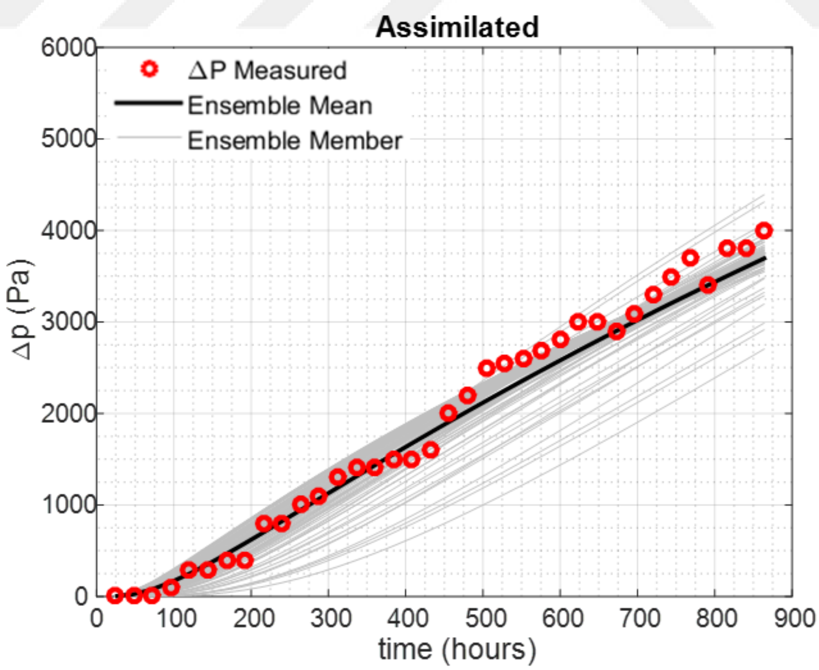

Figure 4.31 Raghavan Anomalous Model for Assimilated Results.

According to Table 4.10 and figures from Figure 4.26 to Figure 4.31, it is seen that all methods works very well. If we compare Case 1 and Case 2 for Kamojang geothermal field, fractal model behaves almost the same. In addition, Raghavan anomalous model gets the similar results. However, the range and outcome are changed for Metzler anomalous model. Perhaps, the reason is that Metzler anomalous model affected far more by θ and d_f. To put it another way, fractal model does not have time fractional derivative. Therefore, topology of the network may not affect more. Moreover, Raghavan anomalous model does not use fractal dimension. Hence, n is used as 2. Consequently, the results are quite similar for fractal model and Raghavan anomalous model because the assumed θ and d_f are so close when we compare Case 1 and Case 2. Although the smallest RMS is obtained by fractal model, anomalous models' performance should not be ignored. There is a good match at the early time for fractal model. Nonetheless, as test times get larger, the fractal model generates lower than measured value. Furthermore, Metzler anomalous model is the most dispersed model for the prior result. Thus, this model cannot gather the assimilated ensemble member easily. If some of the ensemble members are ignored, the smallest RMS may be obtained by Metzler anomalous model. In addition, Raghavan anomalous model acquires pretty good results at the early time. However, the outcomes are underestimated after time is 450 hours. Maybe, ignoring some of the ensemble members supplies better match for Raghavan anomalous model.

CHAPTER 5

SUMMARY, CONCLUSIONS, AND RECOMMENDATIONS

5.1 Summary and Conclusions

In this study, analytical solutions of fractal model and anomalous models were presented for different cases. Naturally fractured reservoirs such as geothermal and unconventional reservoirs can be modeled by using these models. Each model was examined for constant rate, constant bottomhole pressure and variable rate/variable pressure condition. Firstly, the solutions were obtained for dimensionless pressure in the Laplace domain for fractal model and Metzler anomalous model. Then, pressure change in the Laplace space was calculated by using scaling property for those models. In other words, dimensionless pressure in the Laplace space was converted to pressure change in the Laplace domain. In addition, Raghavan anomalous model was solved for constant rate and constant bottomhole pressure conditions separately for pressure change in the Laplace domain. After, dimensionless pressure solution for constant rate and dimensionless flow rate solution for constant bottomhole pressure conditions were presented individually. Furthermore, variable rate/variable bottomhole pressure was derived by utilizing constant rate and constant bottomhole pressure solutions because of unit rate pressure change and unit pressure change solution. Next, all models were applied to both liquid-dominated, and vapor-dominated geothermal reservoirs. Fractal reservoirs were analyzed by using nonlinear regression for every models. Note that the interference test was run in the constant rate for both Kizildere and Kamojang geothermal field. Nonlinear regression ES – MDA was used to determine reservoir characteristics (kh and $\phi c_t h$). The Stehfest algorithm was used to invert each solution to real time space. Each field is implemented for two different topologies of the network values and fractal dimension values. The main purpose is to show effects of fractal parameters on nonlinear regression.

The following conclusions are obtained from this thesis study, and can be stated,

- The flow regimes exhibited by the well-test data can be identified by plotting pressure response and derivative response vs time on a log – log plot.
- The analytical solutions of fractal model and Metzler anomalous model for constant rate, constant bottomhole pressure and variable rate/variable bottomhole pressure condition are quite similar. The only difference is that the Laplace variable s in Metzler anomalous model has an exponent θ. The reason is that Metzler and Chang and Yortsos derived the diffusivity equation using the same continuity equation and flux term. However, Metzler considered the history of the diffusion process.
- Raghavan used the convolved form of the continuity equation. However, he did not use conventional Darcy law. Thus, he modified the flux term by applying fractional derivative. He preferred Caputo fractional operator instead of Riemann – Liouville fractional operator because Riemann – Liouville does not let to use physically interpretable initial conditions.
- It is shown that the fractal model is the special case of the Metzler anomalous model because when $\theta = 0$, both models behaves the same for dimensionless pressure response and dimensionless pressure derivative response without depending on the location.
- Although the fractal and Metzler anomalous models describe the permeability and porosity as a function of location r, the Raghavan anomalous model only introduces the permeability depending upon the location. In addition to that, the basic dimension of permeability for the fractal model and Metzler anomalous model is L^2, while the basic

dimension of “permeability” for the Raghavan anomalous model is $L^{2+\theta}T^{1-\alpha}$ for k_α and $L^2T^{1-\alpha}$ for $k(r)$.

- Fractal dimension d_f can affect fractal model and Metzler anomalous model behaviors. Raghavan anomalous model does not consider fractal dimension and uses n which is integer. To put it another way, n is 1,2 and 3 for linear, radial, and spherical flow, respectively. Fractal model generates higher dimensionless pressure response than Metzler anomalous model for the same d_f. As the fractal dimension decreases, the pressure response difference between models goes up. In addition, if the topology of the network is double, the dimensionless pressure difference between models rises much more for the same fractal dimension.
- Effect of the topology of the network is undeniable for all methods. As the higher topology of the network exists, the Raghavan anomalous model produces far higher dimensionless pressure response. It is worth to note that effect of the topology of the network can be seen clearly after early times.
- Dimensionless pressure response in the reservoir varies according to models. Raghavan anomalous model generates higher dimensionless response than others. Moreover, Metzler anomalous model always produces the less dimensionless pressure response for different dimensionless radius and topology of the network.
- According to the field studies, fractal model performs very well for liquid-dominated field, Kizildere. On the other hand, every method acquires good match for the vapor-dominated field, Kamojang.
- For Kizildere geothermal field, even though the fractal model obtains the lowest RMS, Raghavan anomalous model assimilates the ensemble member better. Perhaps, a better

match can be achieved by Raghavan anomalous model if the minimum and maximum assumed values for kh and $\phi c_t h$ are changed.

- It is observed that if the assumed minimum and maximum value range for kh and $\phi c_t h$ are high, the dispersion of the ensemble member in the prior is extended. As a result, models cannot assimilate the ensemble member successfully.
- For both Kizildere and Kamojang geothermal field, it is proved that fractal dimension and the topology of the network influence the performance of nonlinear regression ES – MDA. This means that the box-counting method is crucially important.

5.2 Recommendations for a Future Study

To interpret the naturally fractured reservoirs, the following suggestions may help for future work.

- Analytical solutions given in this study for single-well active well-test could be applied to real field active well-test data.
- Analytical solutions of every model can be extended considering skin and wellbore storage effect for both active and observation well.
- Sensitivity analysis of skin and wellbore storage effect for every method can be examined.
- New field study can be worked for the highly conductive and well – connected path geothermal field. Consequently, superdiffusion can be inferred better for both active and observation well.

NOMENCLATURE

A = area, $[L^2]$

B = formation volume factor, $[L^3/L^3]$

c_t = compressibility, $[L\,T^2/M]$

d = Euclidean dimension

d_f = fractal dimension

d_w= Fickian value

h = thickness of the reservoir, $[L]$

k = permeability, $[L^2]$

m = fracture network parameter, $[L^{\theta+2}]$

n = dimension, 1, 2 or 3

p = pressure, $[M/L/T^2]$

p_D = dimensionless pressure

p_i = initial pressure, $[M/L/T^2]$

p_{wf} = flowing bottomhole pressure, $[M/L/T^2]$

q = flow rate, $[L^3/T]$

q_D = dimensionless flow rate

r = radial distance, $[L]$

r_D = dimensionless radius

r_w = wellbore radius, $[L]$

r_0 = reference radius, $[L]$

s = Laplace transform variable

t = time, $[T]$

t_D = dimensionless time

α = 1. Anomalous diffusion exponent, 2. Time fractional exponent

β = 1. Constant, 2. Space fractional exponent

γ = diffusion exponent

Δp = pressure change, $[M/L/T^2]$

η = diffusivity, $[L^2/T]$

Θ = anomalous diffusion coefficient

θ = topology of the network

λ = mobility, $[L\,T/M]$

μ = viscosity, $[M/L/T]$

ϕ = porosity

ϕ_0 = reference porosity

BIBLIOGRAPHY

Acuna, J. A., Ershaghi, I., and Yortsos, Y. C., 1995. Practical Application of Fractal Pressure-transient Analysis in Naturally Fractured Reservoirs, *SPE Formation Evaluation* 10(3): 173-179. Doi:10.2118/24705-PA.

Acuna, J. A., Yortsos, Y. C., 1995. Application of fractal geometry to the study of networks of fractures and their pressure transient. Water Resources Research 31(3), 527-540.

Aprilian, S., Abdassah, D., Mucharam, L., & Sumantri, R. (1993, January 1). Application of Fractal Reservoir Model for Interference Test Analysis in Kamojang Geothermal Field (Indonesia). Society of Petroleum Engineers. doi:10.2118/26465-MS

Babadagli, T., Coskun, T., Serpen, U., Karamanderesi, I.H., 1997. Evaluation of outcrop and thin section patterns of geothermal fields in Denizli-Aydin. Proceedings of 7th Energy Congress of Turkey, Istanbul, Turkey.

Beier, R.A., 1990. Pressure Transient Field Data Showing Fractal Reservoir Structure. paper 90‑04 presented at the Annual Technical Meeting. Petroleum Society of Canada, Calgary, Alberta. doi:10.2118/90-04.

Beier, R.A., 1994. Pressure-transient model for a vertically fractured well in a fractal reservoir. SPE Form. Eval. 9 (2), 122–128, http://dx.doi.org/10.2118/ 20582-PA.

BP. (2020, September 25). *Renewable energy*. Retrieved from bp.com: https://www.bp.com/en/global/corporate/energy-economics/statistical-review-of-world-energy/renewable-energy.html

Camacho-Velázquez, R., Fuentes-Cruz, G., Vásquez-Cruz, M., 2008. Decline-Curve Analysis of Fractured Reservoirs with Fractal Geometry. SPE Reserv. Eval. Eng. 11 (3), 606‑619.

Camacho-Velazquez, R., de Swaan-Oliva, A., Vasquez-Cruz, M., 2011. Interference Tests Analysis in Fractured Formations with a Time Fractional Equation. SPE 153615.

Caputo, M., 1967. Linear Models of Dissipation whose Q is almost Frequency Independent-II. Geophys. J. Roy. Astron. Soc. 13 (5), 529‑539.

Chang, J., Yortsos, Y.C., 1990. Pressure-transient analysis of fractal reservoirs. SPE Form. Eval. 5 (1), 31‑39.

Chen, C. and Raghavan, R. 2015. Transient Flow in a Linear Reservoir for Space-Time Fractional Diffusion, *J Pet Sci & Eng* **128**: 194-202

Cloot, A., Botha, J.F., 2006.A generalized groundwater flow equation using the concept of non-integer order derivatives. Water SA32 (1), 1–7 ⟨www.wrc.org.za⟩.

Duffield W.A., & Sass J. H., 2003. Geothermal Energy – Clean Power from the Earth’s Heat

Emerick, A. A. and Reynolds, A. C. (2013). Ensemble smoother with multiple data assimilations, *Computational Geosciences* 55:3-15

Falcone, G., De Witt, G. J., & Teodoriu, C. (2011). Worldwide Classification and Reporting Requirements for Geothermal Resources. *Society of Petroleum Engineers*.

Flamenco-Lopez. F. and Camacho-Velazquez, R. 2001. Fractal Transient Pressure Behavior of Naturally Fractured Reservoirs. Paper presented at the Annual Technical Conference and Exhibition, SPE, New Orleans, Louisiana, USA.

Flamenco-Lopez. F. and Camacho-Velazquez, R. 2003. Determination of Fractal Parameters of Fracture Networks Using Pressure Transient Data. *SPE Reservoir Evaluation & Engineering* **6** (1). SPE 82607-PA.

Gefen, Y., Aharony, A., Alexander, S., 1983. Anomalous Diffusion on Percolating Clusters. Phys. Rev. Lett. 50 (1). doi:10.1103/PhysRevLett.50.77.

Geology. (2020, September 27). *Plate tectonics map – plate boundary map*. Retrieved from geology.com: https://geology.com/plate-tectonics.shtml

Geothermal Basics. (2020, September 25). Retrieved from energy.gov: https://www.energy.gov/eere/geothermal/geothermal-basics

Geothermal Energy throughout the Ages. (2020 September). Retrieved from Alberta culture and tourism:http://history.alberta.ca/energyheritage/energy/alternative-energy/geothermal-energy/geothermal-energy-throughout-the-ages.aspx#:~:text=In%201904%2C%20Italian%20scientist%20Piero,first%20commercial%20geothermal%20power%20plant.

Hardy, H. H. and Beier, R. A. 1994. *Fractals in Reservoir Engineering*. World Scientific Publishing Co., River Edge, N. J.

History of geothermal energy. (2020 September). Retrieved from conserve energy future: https://www.conserve-energy-future.com/geothermalenergyhistory.php

Huttrer, G.W. Geothermal Power Generation in the World 2015-2020 Update Report. In World Geothermal Congress; International Geothermal Association: Reykjavik, Iceland, 2020

IEA (2019). *Geothermal power plants*. Retrieved from eia.gov: https://www.eia.gov/energyexplained/geothermal/geothermal-power-plants.php

IEA, Geothermal power generation in the Sustainable Development Scenario, 2000-2030, IEA, Paris. Retrieved from eia.gov: https://www.iea.org/data-and-statistics/charts/geothermal-power-generation-in-the-sustainable-development-scenario-2000-2030

IEA (2020 September). *Other renewables*. Retrieved from IEA: https://www.iea.org/fuels-and-technologies/other-renewables

Irhas, M., (1996), "Permeability from Pressure Build-Up Test in The Se-Kamojang Field, West Java, Indonesia", Geothermal Training Program, Iceland.

Liang, S., Wu R., and Chen, L., 2015. Laplace Transform of Fractional Order Differential Equations, Electronic Journal of Differential Equations, No. 139, pp. 1-15.

Lund, J.W.; Toth, A.N. Direct Utilization of Geothermal Energy 2020 Worldwide Review. In World Geothermal Congress; International Geothermal Association: Reykjavik, Iceland, 2020

Lynch, D. K. (2006). *The San Andreas Fault*. Retrieved from geology.com: https://geology.com/articles/san-andreas-fault.shtml

Metzler, R., Glöckle, W.G., and Nonnenmacher, T.F. 1994. Fractional Model Equation for Anomalous Diffusion. *Physica* **A** (211): 13–24. doi: 10.1016/0378-4371(94)90064-7.

Onur, M., Zeybek, A.D., Serpen, U., Gok, I.M., 2003. Application of modern well test analysis techniques to pressure transient tests in Kizildere geothermal field, Turkey. Geothermics 32, 147-170, doi:10.1016/S0375-6505(02)00068-8.

O'Shaughnessy, B., Procaccia, I., 1985a. Analytical solutions for diffusion on fractal objects. Phys. Rev. Lett. 54 (5), 455-458.

O'Shaughnessy, B., Procaccia, I., 1985b. Diffusion on fractals. Phys. Rev. A 32 (5), 3073-3083.

Park, H.W., Choe, J., Kang, J.M., 2000. Pressure Behavior of Transport in Fractal Porous Media Using a Fractional Calculus Approach, Energy Sources, Part A. Recovery, Utilization, and Environmental Effects 22 (10), 881‑890

Rafiee, J., Reynolds, A.C., 2017. "Theoretical and efficient practical procedures for the generation of inflation factors for ES-MDA. Inverse Probl. 33, 115003.

Raghavan, R. 2011. Fractional derivatives: Application to transient flow, *Journal of Petroleum Science and Engineering*, 80, 7-13.

Raghavan, R., 2012. Fractional diffusion: performance of fractured wells. J. Pet. Sci. Eng., 92–93, 167–173, http://dx.doi.org/10.1016/j.petrol.2012.06.003.

Raghavan, R. and Chen, C. 2013a. Fractional diffusion in rocks produced by horizontal wells with multiple, transverse hydraulic fractures of finite conductivity, *Journal of Petroleum Science and Engineering*, 109, 133-143.

Raghavan, R. and Chen, C. 2013b. Fractured-Well Performance under Anomalous Diffusion, *SPE Res Eval & Eng*, **16** (3), 237-245.

Redner S. (1989) Superdiffusive Transport Due to Random Velocity Fields, Physica D: Nonlinear Phenomena 38, 1-3, 287-290.

Serpen, U., 2000. Technical and Economical Evaluation of Kizildere Geothermal Field. PhD dissertation (September), Istanbul Technical University (in Turkish).

Shortall, R. & Davidsdottir, B. & Axelsson, G., 2015. Geothermal energy for sustainable development: A review of sustainability impacts and assessment frameworks. Renewable and Sustainable Energy Reviews, Elsevier, vol. 44(C), pages 391-406.

Sönnichsen, N. (2020, April 7). *Statista*. Retrieved from statista.com: https://www.statista.com/statistics/476281/global-capacity-of-geothermal-energy/#statisticContainer

Stehfest, H. (1970). Algorithm 368: Numerical inversion of Laplace transforms [D5]. Communications of the ACM, 13(1), 47-49.

Warren, J. E., & Root, P. J. (1963, September 1). The Behavior of Naturally Fractured Reservoirs. Society of Petroleum Engineers. doi:10.2118/426-PA

Zeybek D. A., 2000. Application of Fractals to Reservoir Characterization. PhD dissertation (September), Istanbul Technical University.

APPENDIX A

ANALYTICAL SOLUTION OF FRACTAL DIFFUSION MODEL AT CONSTANT RATE

In this appendix, we present the analytical solution of fractal diffusion model for constant rate condition. The initial boundary value problem for the fractal model is defined as follows:

$$\frac{\partial p_D}{\partial t_D} = \frac{1}{r_D^{d_f-1}} \frac{\partial}{\partial r_D}\left(r_D^{\beta} \frac{\partial p_D}{\partial r_D}\right), \tag{A.1}$$

where $\beta = d_f - \Theta - 1$. The initial condition is

$$p_D(r_D, t_D = 0) = 0. \tag{A.2}$$

The inner boundary condition for a finite wellbore is

$$\left(r_D^{\beta} \frac{\partial p_D}{\partial r_D}\right)_{r_D=1} = -1. \tag{A.3}$$

The outer boundary condition is described as

$$\lim_{r_D \to \infty} p_D(r_D, t_D) = 0. \tag{A.4}$$

To begin with, taking the Laplace transform of PDE with respect to t_D,

$$s\overline{p_D}(r_D, s) - p_D(r_D, t_D = 0) = \frac{1}{r_D^{d_f-1}} \frac{d}{dr_D}\left(r_D^{\beta} \frac{d\overline{p_D}}{dr_D}\right). \tag{A.5}$$

Applying the initial condition into the above equation,

$$s\overline{p_D}(r_D, s) = \frac{1}{r_D^{d_f-1}} \frac{d}{dr_D}\left(r_D^{\beta} \frac{d\overline{p_D}}{dr_D}\right) \tag{A.6}$$

or

$$s\overline{p_D}(r_D,s) = \frac{1}{r_D^{\beta+\theta}}\frac{d}{dr_D}\left(r_D^{\beta}\frac{d\overline{p_D}}{dr_D}\right). \tag{A.7}$$

Then, Eq. A.7 can be expanded by applying derivation to find a general solution,

$$s\overline{p_D}(r_D,s) = \frac{1}{r_D^{\beta+\theta}}\left(\beta r_D^{\beta-1}\frac{d\overline{p_D}}{dr_D} + r_D^{\beta}\frac{d^2\overline{p_D}}{dr_D^2}\right), \tag{A.8}$$

$$s\overline{p_D}(r_D,s) = \frac{\beta}{r_D^{\theta+1}}\frac{d\overline{p_D}}{dr_D} + \frac{1}{r_D^{\theta}}\frac{d^2\overline{p_D}}{dr_D^2}. \tag{A.9}$$

Let us rearrange the Eq. A.9

$$\frac{1}{r_D^{\theta}}\frac{d^2\overline{p_D}}{dr_D^2} + \frac{\beta}{r_D^{\theta+1}}\frac{d\overline{p_D}}{dr_D} - s\overline{p_D}(r_D,s) = 0. \tag{A.10}$$

Multiply with $r_D^{\theta+2}$,

$$r_D^{\theta+2}\frac{1}{r_D^{\theta}}\frac{d^2\overline{p_D}}{dr_D^2} + r_D^{\theta+2}\frac{\beta}{r_D^{\theta+1}}\frac{d\overline{p_D}}{dr_D} - r_D^{\theta+2}s\overline{p_D}(r_D,s) = 0. \tag{A.11}$$

So,

$$r_D^2\frac{d^2\overline{p_D}}{dr_D^2} + \beta r_D\frac{d\overline{p_D}}{dr_D} - r_D^{\theta+2}s\overline{p_D}(r_D,s) = 0. \tag{A.12}$$

Eq. A.12 has a general solution of

$$\overline{p_D}(r_D,s) = r_D^{\frac{\theta+2}{2}\nu}\left\{AI_\nu\left[\frac{2\sqrt{s}}{\theta+2}r_D^{\frac{\theta+2}{2}}\right] + BK_\nu\left[\frac{2\sqrt{s}}{\theta+2}r_D^{\frac{\theta+2}{2}}\right]\right\}, \tag{A.13}$$

where $\nu = \frac{1-\beta}{\theta+2}$. Before applying the inner and outer boundary conditions, we need to take the Laplace transform of them. The Laplace transform of the inner and outer boundary conditions are found respectively,

$$\left(r_D^{\beta}\frac{\partial\overline{p_D}}{\partial r_D}\right)_{r_D=1} = -\frac{1}{s} \tag{A.14}$$

and

$$\lim_{r_D\to\infty} \overline{p_D}(r_D, s) = 0. \tag{A.15}$$

Next, apply the outer boundary condition to Eq. A.13

$$\lim_{r_D\to\infty} \overline{p_D}(r_D, s) = \lim_{r_D\to\infty} r_D^{\frac{\theta+2}{2}\nu} \lim_{r_D\to\infty} \left\{ AI_\nu \left[\frac{2\sqrt{s}}{\theta+2} r_D^{\frac{\theta+2}{2}}\right] + BK_\nu \left[\frac{2\sqrt{s}}{\theta+2} r_D^{\frac{\theta+2}{2}}\right] \right\} = 0. \tag{A.16}$$

When r_D goes to infinity, Bessel I function approaches to infinity, and Bessel K function goes to zero. Hence, *A* must be zero, but *B* cannot be zero. As a result, Eq. A.16 reduces to

$$\overline{p_D}(r_D, s) = r_D^{\frac{\theta+2}{2}\nu} BK_\nu \left[\frac{2\sqrt{s}}{\theta+2} r_D^{\frac{\theta+2}{2}}\right]. \tag{A.17}$$

Let us say $\varepsilon = \frac{\theta+2}{2}$ and $\gamma = \frac{2\sqrt{s}}{\theta+2}$. Then, we apply inner boundary condition. Firstly, taking derivative of Eq. A.17 with respect to r_D,

$$\frac{d\overline{p_D}}{dr_D} = B(\varepsilon\nu) r_D^{\varepsilon\nu-1} K_\nu[\gamma r_D^\varepsilon] + B r_D^{\varepsilon\nu} \frac{dK_\nu[\gamma r_D^\varepsilon]}{d\mathrm{r_D}}. \tag{A.18}$$

To apply a chain rule,

$$\frac{dK_\nu}{dr_D} = \frac{dK_\nu}{dz}\frac{dz}{dr_D}, \tag{A.19}$$

where

$$z = \gamma r_D^\varepsilon \tag{A.20}$$

and

$$\frac{dz}{dr_D} = \gamma\varepsilon r_D^{\varepsilon-1}. \tag{A.21}$$

So, Eq. A.18 can be rewritten as

$$\frac{d\overline{p_D}}{dr_D} = B(\varepsilon\nu) r_D^{\varepsilon\nu-1} K_\nu[\gamma r_D^\varepsilon] + B r_D^{\varepsilon\nu} \frac{dK_\nu[z]}{d\mathrm{z}} (\gamma\varepsilon r_D^{\varepsilon-1}) \tag{A.22}$$

or

$$\frac{d\overline{p_D}}{dr_D} = B(\varepsilon\nu)r_D^{\varepsilon\nu-1}K_\nu[\gamma r_D^\varepsilon] + Br_D^{\varepsilon\nu}\,\frac{dK_\nu[\gamma r_D^\varepsilon]}{d(\gamma r_D^\varepsilon)}(\gamma\varepsilon r_D^{\varepsilon-1}) \tag{A.23}$$

or

$$\frac{d\overline{p_D}}{dr_D} = (\varepsilon\nu)r_D^{\varepsilon\nu-1}K_\nu[\gamma r_D^\varepsilon] + Br_D^{\varepsilon\nu+\varepsilon-1}\,\gamma\varepsilon\frac{dK_\nu[\gamma r_D^\varepsilon]}{d(\gamma r_D^\varepsilon)}, \tag{A.24}$$

where $\frac{dK_\nu[\gamma r_D^\varepsilon]}{d(\gamma r_D^\varepsilon)} = -K_{\nu-1}[\gamma r_D^\varepsilon] - \frac{\nu}{\gamma r_D^\varepsilon}K_\nu[\gamma r_D^\varepsilon]$. As a result, Eq. A.24 is equal to

$$\frac{d\overline{p_D}}{dr_D} = B(\varepsilon\nu)r_D^{\varepsilon\nu-1}K_\nu[\gamma r_D^\varepsilon] + B\gamma\varepsilon r_D^{\varepsilon\nu+\varepsilon-1}\left\{-K_{\nu-1}[\gamma r_D^\varepsilon] - \frac{\nu}{\gamma r_D^\varepsilon}K_\nu[\gamma r_D^\varepsilon]\right\} \tag{A.25}$$

or

$$\frac{d\overline{p_D}}{dr_D} = B(\varepsilon\nu)r_D^{\varepsilon\nu-1}K_\nu[\gamma r_D^\varepsilon] - B\gamma\varepsilon r_D^{\varepsilon\nu+\varepsilon-1}\,K_{\nu-1}[\gamma r_D^\varepsilon] - B\gamma\varepsilon r_D^{\varepsilon\nu+\varepsilon-1}\,\frac{\nu}{\gamma r_D^\varepsilon}K_\nu[\gamma r_D^\varepsilon]. \tag{A.26}$$

So, Eq. A.26 is equal to

$$\frac{d\overline{p_D}}{dr_D} = B(\varepsilon\nu)r_D^{\varepsilon\nu-1}K_\nu[\gamma r_D^\varepsilon] - B\gamma\varepsilon\, r_D^{\varepsilon\nu+\varepsilon-1}\,K_{\nu-1}[\gamma r_D^\varepsilon] - B(\varepsilon\nu)\, r_D^{\varepsilon\nu-1}\;K_\nu[\gamma r_D^\varepsilon]. \tag{A.27}$$

Then, multiply Eq. A.27 with r_D^β,

$$\begin{aligned} r_D^\beta\,\frac{d\overline{p_D}}{dr_D} &= \cancel{B(\varepsilon\nu)r_D^{\varepsilon\nu+\beta-1}}K_\nu[\gamma r_D^\varepsilon] - B\gamma\varepsilon\, r_D^{\varepsilon\nu+\varepsilon-1+\beta}K_{\nu-1}[\gamma r_D^\varepsilon] \\ &\quad \cancel{-B(\varepsilon\nu)\, r_D^{\varepsilon\nu+\beta-1}}\;K_\nu[\gamma r_D^\varepsilon] \end{aligned} \tag{A.28}$$

or

$$r_D^\beta\,\frac{d\overline{p_D}}{dr_D} = -B\gamma\varepsilon\, r_D^{\varepsilon\nu+\varepsilon-1+\beta}K_{\nu-1}[\gamma r_D^\varepsilon]. \tag{A.29}$$

So, at $r_D = 1$,

$$\left(r_D^\beta\,\frac{d\overline{p_D}}{dr_D}\right)_{r_D=1} = -B\gamma\varepsilon\, K_{\nu-1}[\gamma] = -\frac{1}{s}. \tag{A.30}$$

Consequently,

$$B = \frac{1}{s\gamma\varepsilon K_{\nu-1}[\gamma]}. \qquad \text{(A.31)}$$

Finally, Eq. A.17 is equal to

$$\overline{p_D}(r_D, s) = r_D^{\frac{\theta+2}{2}\nu} \left(\frac{K_\nu\left[\frac{2\sqrt{s}}{\theta+2} r_D^{\frac{\theta+2}{2}}\right]}{s\gamma\varepsilon K_{\nu-1}[\gamma]} \right). \qquad \text{(A.32)}$$

Let us change ε and γ,

$$\overline{p_D}(r_D, s) = r_D^{\frac{\theta+2}{2}\nu} \left(\frac{K_\nu\left[\frac{2\sqrt{s}}{\theta+2} r_D^{\frac{\theta+2}{2}}\right]}{s \cancel{\frac{2\sqrt{s}}{\theta+2}} \cancel{\frac{\theta+2}{2}} K_{\nu-1}\left[\frac{2\sqrt{s}}{\theta+2}\right]} \right). \qquad \text{(A.33)}$$

To conclude, the result is

$$\overline{p_D}(r_D, s) = r_D^{\frac{\theta+2}{2}\nu} \left(\frac{K_\nu\left[\frac{2\sqrt{s}}{\theta+2} r_D^{\frac{\theta+2}{2}}\right]}{s\sqrt{s}\ K_{\nu-1}\left[\frac{2\sqrt{s}}{\theta+2}\right]} \right) \qquad \text{(A.34)}$$

or

$$\overline{p_D}(r_D, s) = r_D^{\frac{1-\beta}{2}} \left(\frac{K_\nu\left[\frac{2\sqrt{s}}{\theta+2} r_D^{\frac{\theta+2}{2}}\right]}{s\sqrt{s}\ K_{\nu-1}\left[\frac{2\sqrt{s}}{\theta+2}\right]} \right). \qquad \text{(A.35)}$$

APPENDIX B

FRACTAL DIFFUSION MODEL AT A CONSTANT RATE CONVERSION FROM DIMENSIONLESS TO DIMENSIONAL

In this appendix, we convert the analytical solution of fractal model at a constant rate from dimensionless to dimensional coordinate in the SI unit by using scaling property. The dimensionless pressure and time are given by,

$$p_D = \frac{kh}{2\pi q B \mu} \Delta p(t) \tag{B.1}$$

and

$$t_D = \frac{k(r_w)t}{\phi(r_w)c_t\mu\, r_w^2}. \tag{B.2}$$

Dimensionless time can be expressed as

$$t_D = \eta^* t, \tag{B.3}$$

where

$$\eta^* = \frac{k(r_w)}{\phi(r_w)c_t\mu r_w^2}. \tag{B.4}$$

Taking the Laplace transform of Eq. B.1,

$$\overline{\overline{p_D}}(s) = \frac{kh}{2\pi q B \mu} \overline{\overline{\Delta p}}(r,s), \tag{B.5}$$

where $\overline{\overline{p_D}}(s)$ is the Laplace transform of $p_D(t_D)$ with respect to time t, and $\overline{\overline{\Delta p}}(r,s)$ represents the Laplace transform of $\Delta p(t)$ with respect to t. Furthermore, the solution of fractal diffusion model for finite wellbore and constant rate is

$$\overline{p_D}(r_D, s) = r_D^{\frac{\theta+2}{2}\nu} \frac{K_\nu \left[\frac{2\sqrt{s}}{\theta+2} r_D^{\frac{\theta+2}{2}}\right]}{s\sqrt{s}\ K_{\nu-1}\left[\frac{2\sqrt{s}}{\theta+2}\right]}, \tag{B.6}$$

where $\overline{p_D}(r_D, s)$ represents the Laplace transform of $p_D(t_D)$ with respect to t_D. Then, by applying scaling property, $\overline{\overline{p_D}}(s)$ can be represented as:

$$\overline{\overline{p_D}}(s) = \mathcal{L}_t[p_D(\eta^* t)] = \frac{1}{\eta^*}\overline{p_D}\left(\frac{s}{\eta^*}\right). \tag{B.7}$$

So,

$$\overline{\overline{p_D}}(s) = \mathcal{L}_t[p_D(\eta^* t)] = \frac{1}{\cancel{\eta^*}} r_D^{\frac{\theta+2}{2}\nu} \left(\frac{K_\nu \left[\frac{2\sqrt{\frac{s}{\eta^*}}}{\theta+2} r_D^{\frac{\theta+2}{2}}\right]}{\frac{s}{\cancel{\eta^*}}\sqrt{\frac{s}{\eta^*}}\ \ K_{\nu-1}\left[\frac{2\sqrt{\frac{s}{\eta^*}}}{\theta+2}\right]} \right) \tag{B.8}$$

or

$$\overline{\overline{p_D}}(s) = \mathcal{L}_t[p_D(\eta^* t)] = r_D^{\frac{\theta+2}{2}\nu} \left(\frac{K_\nu \left[\frac{2\sqrt{\frac{s}{\eta^*}}}{\theta+2} r_D^{\frac{\theta+2}{2}}\right]}{s\sqrt{\frac{s}{\eta^*}}\ \ K_{\nu-1}\left[\frac{2\sqrt{\frac{s}{\eta^*}}}{\theta+2}\right]} \right). \tag{B.9}$$

Equalizing Eq. B.5 and B.9 provides:

$$\frac{kh}{2\pi qB\mu}\overline{\overline{\Delta p}}(r,s) = r_D^{\frac{\theta+2}{2}\nu}\left(\frac{K_\nu\left[\frac{2\sqrt{\frac{s}{\eta^*}}}{\theta+2}r_D^{\frac{\theta+2}{2}}\right]}{s\sqrt{\frac{s}{\eta^*}}\;\;K_{\nu-1}\left[\frac{2\sqrt{\frac{s}{\eta^*}}}{\theta+2}\right]}\right). \tag{B.10}$$

Consequently, $\overline{\overline{\Delta p}}(r,s)$ is equal to

$$\overline{\overline{\Delta p}}(r,s) = \frac{2\pi qB\mu}{kh}r_D^{\frac{\theta+2}{2}\nu}\left(\frac{K_\nu\left[\frac{2\sqrt{\frac{s}{\eta^*}}}{\theta+2}r_D^{\frac{\theta+2}{2}}\right]}{s\sqrt{\frac{s}{\eta^*}}\;\;K_{\nu-1}\left[\frac{2\sqrt{\frac{s}{\eta^*}}}{\theta+2}\right]}\right), \tag{B.11}$$

where $r_D = \frac{r}{r_w}$.

APPENDIX C

ANALYTICAL SOLUTION OF FRACTAL MODEL AT CONSTANT BOTTOMHOLE PRESSURE

In this appendix, we present the analytical solution of fractal diffusion model for constant bottomhole pressure condition. The initial boundary value problem for the fractal model is defined as follows:

$$\frac{\partial p_D}{\partial t_D} = \frac{1}{r_D^{d_f - 1}} \frac{\partial}{\partial r_D}\left(r_D^{\beta} \frac{\partial p_D}{\partial r_D}\right), \tag{C.1}$$

where $\beta = d_f - \theta - 1$. The initial condition is

$$p_D(r_D, t_D = 0) = 0. \tag{C.2}$$

The inner boundary condition for a finite wellbore is

$$p_D(r_D = 1, t_D) = 1. \tag{C.3}$$

The outer boundary condition is described as

$$\lim_{r_D \to \infty} p_D(r_D, t_D) = 0. \tag{C.4}$$

To begin with, taking the Laplace transform of PDE with respect to t_D,

$$s\overline{p_D}(r_D, s) - p_D(r_D, t_D = 0) = \frac{1}{r_D^{d_f - 1}} \frac{d}{dr_D}\left(r_D^{\beta} \frac{d\overline{p_D}}{dr_D}\right). \tag{C.5}$$

Using the initial condition into the above equation,

$$s\overline{p_D}(r_D, s) = \frac{1}{r_D^{d_f - 1}} \frac{d}{dr_D}\left(r_D^{\beta} \frac{d\overline{p_D}}{dr_D}\right) \tag{C.6}$$

or

$$s\overline{p_D}(r_D,s) = \frac{1}{r_D^{\beta+\theta}}\frac{d}{dr_D}\left(r_D^{\beta}\frac{d\overline{p_D}}{dr_D}\right). \tag{C.7}$$

Next, the Laplace transform of the inner and outer boundaries are, respectively

$$\overline{p_D}(r_D = 1, s) = \frac{1}{s} \tag{C.8}$$

and

$$\lim_{r_D\to\infty}\overline{p_D}(r_D,s) = 0. \tag{C.9}$$

Then, Eq. C.7 can be written as,

$$s\overline{p_D}(r_D,s) = \frac{1}{r_D^{\beta+\theta}}\left(\beta r_D^{\beta-1}\frac{d\overline{p_D}}{dr_D} + r_D^{\beta}\frac{d^2\overline{p_D}}{dr_D^2}\right), \tag{C.10}$$

$$s\overline{p_D}(r_D,s) = \frac{\beta}{r_D^{\theta+1}}\frac{d\overline{p_D}}{dr_D} + \frac{1}{r_D^{\theta}}\frac{d^2\overline{p_D}}{dr_D^2}. \tag{C.11}$$

Let us rearrange the Eq. C.11 to find a general solution,

$$\frac{1}{r_D^{\theta}}\frac{d^2\overline{p_D}}{dr_D^2} + \frac{\beta}{r_D^{\theta+1}}\frac{d\overline{p_D}}{dr_D} - s\overline{p_D}(r_D,s) = 0. \tag{C.12}$$

Multiply with $r_D^{\theta+2}$,

$$r_D^{\theta+2}\frac{1}{r_D^{\theta}}\frac{d^2\overline{p_D}}{dr_D^2} + r_D^{\theta+2}\frac{\beta}{r_D^{\theta+1}}\frac{d\overline{p_D}}{dr_D} - r_D^{\theta+2}s\overline{p_D}(r_D,s) = 0. \tag{C.13}$$

So,

$$r_D^2\frac{d^2\overline{p_D}}{dr_D^2} + \beta r_D\frac{d\overline{p_D}}{dr_D} - r_D^{\theta+2}s\overline{p_D}(r_D,s) = 0. \tag{C.14}$$

The general solution of Eq. C.14 is

$$\overline{p_D}(r_D,s) = r_D^{\frac{\theta+2}{2}\nu}\left\{AI_\nu\left[\frac{2\sqrt{s}}{\theta+2}r_D^{\frac{\theta+2}{2}}\right] + BK_\nu\left[\frac{2\sqrt{s}}{\theta+2}r_D^{\frac{\theta+2}{2}}\right]\right\}, \tag{C.15}$$

where $\nu = \frac{1-\beta}{\theta+2}$. Next, apply the outer boundary condition in the Laplace space to the general solution

$$\lim_{r_D\to\infty} \overline{p_D}(r_D,s) = \lim_{r_D\to\infty} r_D^{\frac{\theta+2}{2}\nu} \lim_{r_D\to\infty}\left\{AI_\nu\left[\frac{2\sqrt{s}}{\theta+2}r_D^{\frac{\theta+2}{2}}\right] + BK_\nu\left[\frac{2\sqrt{s}}{\theta+2}r_D^{\frac{\theta+2}{2}}\right]\right\} = 0. \quad \text{(C.16)}$$

When r_D goes to infinity, Bessel I function approaches to infinity, and Bessel K function goes to zero. Hence, *A* must be zero, but *B* cannot be zero. Consequently, Eq. C.16 reduces to

$$\overline{p_D}(r_D,s) = r_D^{\frac{\theta+2}{2}\nu} BK_\nu\left[\frac{2\sqrt{s}}{\theta+2}r_D^{\frac{\theta+2}{2}}\right]. \quad \text{(C.17)}$$

Next, apply the inner boundary condition ($r_D = 1$),

$$\overline{p_D}(r_D = 1,s) = BK_\nu\left[\frac{2\sqrt{s}}{\theta+2}\right] = \frac{1}{s}. \quad \text{(C.18)}$$

So,

$$B = \frac{1}{sK_\nu\left[\frac{2\sqrt{s}}{\theta+2}\right]}. \quad \text{(C.19)}$$

In conclusion, dimensionless pressure is equal to

$$\overline{p_D}(r_D,s) = r_D^{\frac{\theta+2}{2}\nu} \frac{K_\nu\left[\frac{2\sqrt{s}}{\theta+2}r_D^{\frac{\theta+2}{2}}\right]}{sK_\nu\left[\frac{2\sqrt{s}}{\theta+2}\right]} \quad \text{(C.20)}$$

or

$$\overline{p_D}(r_D,s) = r_D^{\frac{1-\beta}{2}} \frac{K_\nu\left[\frac{2\sqrt{s}}{\theta+2}r_D^{\frac{\theta+2}{2}}\right]}{sK_\nu\left[\frac{2\sqrt{s}}{\theta+2}\right]}. \quad \text{(C.21)}$$

APPENDIX D

FRACTAL DIFFUSION MODEL AT A CONSTANT BOTTOMHOLE PRESSURE CONVERSION FROM DIMENSIONLESS TO DIMENSIONAL

In this appendix, we convert the analytical solution of fractal model at a constant bottomhole pressure from dimensionless to dimensional coordinate in the SI unit by using scaling property. The dimensionless pressure and time are

$$p_D = \frac{p_i - p}{p_i - p_{wf}} = \frac{\Delta p(r,t)}{\Delta p_{wf}} \tag{D.1}$$

and

$$t_D = \frac{k(r_w)t}{\phi(r_w)c_t\mu\, r_w^2}. \tag{D.2}$$

Dimensionless time can be expressed as

$$t_D = \eta^* t, \tag{D.3}$$

where

$$\eta^* = \frac{k(r_w)}{\phi(r_w)c_t\mu r_w^2}. \tag{D.4}$$

Taking the Laplace transform of Eq. D.1,

$$\overline{\overline{p_D}}(s) = \frac{1}{\Delta p_{wf}}\overline{\overline{\Delta p}}(r,s), \tag{D.5}$$

where $\overline{\overline{p_D}}(s)$ is the Laplace transform of $p_D(t_D)$ with respect to time t, and $\overline{\overline{\Delta p}}(r,s)$ represents the Laplace transform of $\Delta p(r,t)$ with respect to t. In addition, the solution of fractal model for finite wellbore and constant bottomhole pressure is

$$\overline{p_D}(r_D, s) = r_D^{\frac{\theta+2}{2}\nu} \frac{K_\nu\left[\frac{2\sqrt{s}}{\theta+2} r_D^{\frac{\theta+2}{2}}\right]}{sK_\nu\left[\frac{2\sqrt{s}}{\theta+2}\right]}, \tag{D.6}$$

where $\overline{p_D}(r_D, s)$ represents the Laplace transform of $p_D(t_D)$ with respect to t_D. Then, by applying scaling property, $\overline{\overline{p_D}}(s)$ can be represented as:

$$\overline{\overline{p_D}}(s) = \mathcal{L}_t[p_D(\eta^* t)] = \frac{1}{\eta^*}\overline{p_D}\left(\frac{s}{\eta^*}\right). \tag{D.7}$$

So,

$$\overline{\overline{p_D}}(s) = \mathcal{L}_t[p_D(\eta^* t)] = \frac{1}{\cancel{\eta^*}} r_D^{\frac{\theta+2}{2}\nu} \left(\frac{K_\nu\left[\frac{2\sqrt{\frac{s}{\eta^*}}}{\theta+2} r_D^{\frac{\theta+2}{2}}\right]}{\frac{s}{\cancel{\eta^*}} K_\nu\left[\frac{2\sqrt{\frac{s}{\eta^*}}}{\theta+2}\right]} \right) \tag{D.8}$$

or

$$\overline{\overline{p_D}}(s) = \mathcal{L}_t[p_D(\eta^* t)] = r_D^{\frac{\theta+2}{2}\nu} \left(\frac{K_\nu\left[\frac{2\sqrt{\frac{s}{\eta^*}}}{\theta+2} r_D^{\frac{\theta+2}{2}}\right]}{sK_\nu\left[\frac{2\sqrt{\frac{s}{\eta^*}}}{\theta+2}\right]} \right). \tag{D.9}$$

Equalizing Eq. D.5 and D.9 give us:

$$\frac{1}{\Delta p_{wf}}\overline{\overline{\Delta p}}(r,s) = r_D^{\frac{\theta+2}{2}\nu}\left(\frac{K_\nu\left[\frac{2\sqrt{\frac{s}{\eta^*}}}{\theta+2}r_D^{\frac{\theta+2}{2}}\right]}{sK_\nu\left[\frac{2\sqrt{\frac{s}{\eta^*}}}{\theta+2}\right]}\right). \tag{D.10}$$

As a result, $\overline{\overline{\Delta p}}(s)$ is defined as:

$$\overline{\overline{\Delta p}}(r,s) = \frac{\Delta p_{wf}}{s}r_D^{\frac{\theta+2}{2}\nu}\left(\frac{K_\nu\left[\frac{2\sqrt{\frac{s}{\eta^*}}}{\theta+2}r_D^{\frac{\theta+2}{2}}\right]}{K_\nu\left[\frac{2\sqrt{\frac{s}{\eta^*}}}{\theta+2}\right]}\right), \tag{D.11}$$

where $r_D = \frac{r}{r_w}$.

APPENDIX E

ANALYTICAL SOLUTION OF METZLER ANOMALOUS DIFFUSION MODEL AT CONSTANT RATE

In this appendix, we present the analytical solution of Metzler anomalous model for constant rate condition. The PDE of Metzler anomalous model is given as:

$$\frac{\partial^\alpha p_D}{\partial t_D^\alpha} = \frac{1}{r_D^{d_f-1}}\frac{\partial}{\partial r_D}\left(r_D^\beta \frac{\partial p_D}{\partial r_D}\right), \tag{E.1}$$

where $\beta = d_f - \Theta - 1$ and $\alpha = \frac{2}{\Theta+2}$. The initial condition is

$$p_D(r_D, t_D = 0) = 0. \tag{E.2}$$

The inner boundary condition for a finite wellbore is

$$\left(r_D^\beta \frac{\partial p_D}{\partial r_D}\right)_{r_D=1} = -1. \tag{E.3}$$

The outer boundary condition is described as

$$\lim_{r_D\to\infty} p_D(r_D, t_D) = 0. \tag{E.4}$$

To begin with, the Laplace transform of Eq. E.1 with respect to t_D,

$$s^\alpha \overline{p_D}(r_D, s) - s^{\alpha-1} p_D(r_D, t_D = 0) = \frac{1}{r_D^{d_f-1}}\frac{d}{dr_D}\left(r_D^\beta \frac{d\overline{p_D}}{dr_D}\right). \tag{E.5}$$

Because of the initial condition, Eq. E.5 is rewritten as:

$$s^\alpha \overline{p_D}(r_D, s) = \frac{1}{r_D^{d_f-1}}\frac{d}{dr_D}\left(r_D^\beta \frac{d\overline{p_D}}{dr_D}\right) \tag{E.6}$$

or

$$s^{\alpha}\overline{p_D}(r_D,s) = \frac{1}{r_D^{\beta+\theta}}\frac{d}{dr_D}\left(r_D^{\beta}\frac{d\overline{p_D}}{dr_D}\right). \tag{E.7}$$

Next, applying derivation to inside the parentheses, Eq. E.7 is equal to

$$s^{\alpha}\overline{p_D}(r_D,s) = \frac{1}{r_D^{\beta+\theta}}\left(\beta r_D^{\beta-1}\frac{d\overline{p_D}}{dr_D} + r_D^{\beta}\frac{d^2\overline{p_D}}{dr_D^2}\right), \tag{E.8}$$

$$s^{\alpha}\overline{p_D}(r_D,s) = \frac{\beta}{r_D^{\theta+1}}\frac{d\overline{p_D}}{dr_D} + \frac{1}{r_D^{\theta}}\frac{d^2\overline{p_D}}{dr_D^2}. \tag{E.9}$$

Let us rewrite the Eq. E.9

$$\frac{1}{r_D^{\theta}}\frac{d^2\overline{p_D}}{dr_D^2} + \frac{\beta}{r_D^{\theta+1}}\frac{d\overline{p_D}}{dr_D} - s^{\alpha}\overline{p_D}(r_D,s) = 0. \tag{E.10}$$

Multiply with $r_D^{\theta+2}$,

$$r_D^{\theta+2}\frac{1}{r_D^{\theta}}\frac{d^2\overline{p_D}}{dr_D^2} + r_D^{\theta+2}\frac{\beta}{r_D^{\theta+1}}\frac{d\overline{p_D}}{dr_D} - r_D^{\theta+2}s^{\alpha}\overline{p_D}(r_D,s) = 0. \tag{E.11}$$

So,

$$r_D^2\frac{d^2\overline{p_D}}{dr_D^2} + \beta r_D\frac{d\overline{p_D}}{dr_D} - r_D^{\theta+2}s^{\alpha}\overline{p_D}(r_D,s) = 0. \tag{E.12}$$

Eq. E.12 has the general solution of

$$\overline{p_D}(r_D,s) = r_D^{\frac{\theta+2}{2}\nu}\left\{AI_{\nu}\left[\frac{2\sqrt{s^{\alpha}}}{\theta+2}r_D^{\frac{\theta+2}{2}}\right] + BK_{\nu}\left[\frac{2\sqrt{s^{\alpha}}}{\theta+2}r_D^{\frac{\theta+2}{2}}\right]\right\}, \tag{E.13}$$

where $\nu = \frac{1-\beta}{\theta+2}$. Then, take the Laplace transform of the inner boundary condition,

$$\left(r_D^{\beta}\frac{\partial\overline{p_D}}{\partial r_D}\right)_{r_D=1} = -\frac{1}{s}. \tag{E.14}$$

Next, the outer boundary condition in the Laplace space can be written as

$$\lim_{r_D\to\infty}\overline{p_D}(r_D,s) = 0. \tag{E.15}$$

The outer boundary condition is used to find the general solution coefficients.

$$\lim_{r_D\to\infty}\overline{p_D}(r_D,s)=\lim_{r_D\to\infty} r_D^{\frac{\theta+2}{2}\nu}\ \lim_{r_D\to\infty}\left\{AI_\nu\left[\frac{2\sqrt{s^\alpha}}{\theta+2}r_D^{\frac{\theta+2}{2}}\right]+BK_\nu\left[\frac{2\sqrt{s^\alpha}}{\theta+2}r_D^{\frac{\theta+2}{2}}\right]\right\}=0. \quad \text{(E.16)}$$

As r_D goes to infinity, Bessel I function approaches to infinity, and Bessel K function goes to zero. Thus, *A* must be zero, but *B* cannot be zero. As a consequence, Eq. E.13 is equal to

$$\overline{p_D}(r_D,s)=r_D^{\frac{\theta+2}{2}\nu}BK_\nu\left[\frac{2\sqrt{s^\alpha}}{\theta+2}r_D^{\frac{\theta+2}{2}}\right]. \quad \text{(E.17)}$$

Before applying inner boundary condition, let us introduce new variables to do operation easily.

$$\overline{p_D}(r_D,s)=r_D^{\varepsilon\nu}BK_\nu[\gamma r_D^\varepsilon], \quad \text{(E.18)}$$

where $\varepsilon=\frac{\theta+2}{2}$ and $\gamma=\frac{2\sqrt{s^\alpha}}{\theta+2}$. Take the derivative of Eq. E.18 with respect to r_D,

$$\frac{d\overline{p_D}}{dr_D}=B(\varepsilon\nu)r_D^{\varepsilon\nu-1}K_\nu[\gamma r_D^\varepsilon]+Br_D^{\varepsilon\nu}\frac{dK_\nu[\gamma r_D^\varepsilon]}{d\mathrm{r_D}}. \quad \text{(E.19)}$$

Let us apply the chain rule,

$$\frac{dK_\nu}{dr_D}=\frac{dK_\nu}{dz}\frac{dz}{dr_D}, \quad \text{(E.20)}$$

where

$$z=\gamma r_D^\varepsilon \quad \text{(E.21)}$$

and

$$\frac{dz}{dr_D}=\gamma\varepsilon r_D^{\varepsilon-1}. \quad \text{(E.22)}$$

So, Eq. E.19 can be rewritten as

$$\frac{d\overline{p_D}}{dr_D}=B(\varepsilon\nu)r_D^{\varepsilon\nu-1}K_\nu[\gamma r_D^\varepsilon]+Br_D^{\varepsilon\nu}\frac{dK_\nu[z]}{dz}(\gamma\varepsilon r_D^{\varepsilon-1}) \quad \text{(E.23)}$$

or

$$\frac{d\overline{p_D}}{dr_D}=B(\varepsilon\nu)r_D^{\varepsilon\nu-1}K_\nu[\gamma r_D^\varepsilon]+Br_D^{\varepsilon\nu}\frac{dK_\nu[\gamma r_D^\varepsilon]}{d(\gamma r_D^\varepsilon)}(\gamma\varepsilon r_D^{\varepsilon-1}) \quad \text{(E.24)}$$

or

$$\frac{d\overline{p_D}}{dr_D} = (\varepsilon\nu)r_D^{\varepsilon\nu-1}K_\nu[\gamma r_D^\varepsilon] + Br_D^{\varepsilon\nu+\varepsilon-1}\gamma\varepsilon\frac{dK_\nu[\gamma r_D^\varepsilon]}{d(\gamma r_D^\varepsilon)}, \tag{E.25}$$

where $\frac{dK_\nu[\gamma r_D^\varepsilon]}{d(\gamma r_D^\varepsilon)} = -K_{\nu-1}[\gamma r_D^\varepsilon] - \frac{\nu}{\gamma r_D^\varepsilon}K_\nu[\gamma r_D^\varepsilon]$. Under the circumstances, Eq. E.25 is equal to

$$\frac{d\overline{p_D}}{dr_D} = B(\varepsilon\nu)r_D^{\varepsilon\nu-1}K_\nu[\gamma r_D^\varepsilon] + B\gamma\varepsilon r_D^{\varepsilon\nu+\varepsilon-1}\left\{-K_{\nu-1}[\gamma r_D^\varepsilon] - \frac{\nu}{\gamma r_D^\varepsilon}K_\nu[\gamma r_D^\varepsilon]\right\} \tag{E.26}$$

or

$$\frac{d\overline{p_D}}{dr_D} = B(\varepsilon\nu)r_D^{\varepsilon\nu-1}K_\nu[\gamma r_D^\varepsilon] - B\gamma\varepsilon r_D^{\varepsilon\nu+\varepsilon-1}K_{\nu-1}[\gamma r_D^\varepsilon] - B\gamma\varepsilon r_D^{\varepsilon\nu+\varepsilon-1}\frac{\nu}{\gamma r_D^\varepsilon}K_\nu[\gamma r_D^\varepsilon]. \tag{E.27}$$

So, Eq. E.27 is equal to

$$\frac{d\overline{p_D}}{dr_D} = B(\varepsilon\nu)r_D^{\varepsilon\nu-1}K_\nu[\gamma r_D^\varepsilon] - B\gamma\varepsilon\, r_D^{\varepsilon\nu+\varepsilon-1}K_{\nu-1}[\gamma r_D^\varepsilon] - B(\varepsilon\nu)\, r_D^{\varepsilon\nu-1}\, K_\nu[\gamma r_D^\varepsilon]. \tag{E.28}$$

Then, multiply Eq. E.28 with r_D^β,

$$\begin{aligned} r_D^\beta\frac{d\overline{p_D}}{dr_D} &= \cancel{B(\varepsilon\nu)r_D^{\varepsilon\nu+\beta-1}}K_\nu[\gamma r_D^\varepsilon] - B\gamma\varepsilon\, r_D^{\varepsilon\nu+\varepsilon-1+\beta}K_{\nu-1}[\gamma r_D^\varepsilon] \\ &\quad - \cancel{B(\varepsilon\nu)\, r_D^{\varepsilon\nu+\beta-1}}\, K_\nu[\gamma r_D^\varepsilon] \end{aligned} \tag{E.29}$$

or

$$r_D^\beta\frac{d\overline{p_D}}{dr_D} = -B\gamma\varepsilon\, r_D^{\varepsilon\nu+\varepsilon-1+\beta}K_{\nu-1}[\gamma r_D^\varepsilon]. \tag{E.30}$$

So, at $r_D = 1$,

$$\left(r_D^\beta\frac{d\overline{p_D}}{dr_D}\right)_{r_D=1} = -B\gamma\varepsilon\, K_{\nu-1}[\gamma] = -\frac{1}{s}. \tag{E.31}$$

As a consequence,

$$B = \frac{1}{s\gamma\varepsilon K_{\nu-1}[\gamma]}. \tag{E.32}$$

Finally, dimensionless pressure comes to

$$\overline{p_D}(r_D,s)=r_D^{\frac{\theta+2}{2}\nu}\left(\frac{K_\nu\left[\frac{2\sqrt{s^\alpha}}{\theta+2}r_D^{\frac{\theta+2}{2}}\right]}{s\gamma\varepsilon K_{\nu-1}[\gamma]}\right). \tag{E.33}$$

Let us change ε and γ,

$$\overline{p_D}(r_D,s)=r_D^{\frac{\theta+2}{2}\nu}\left(\frac{K_\nu\left[\frac{2\sqrt{s^\alpha}}{\theta+2}r_D^{\frac{\theta+2}{2}}\right]}{s\frac{\cancel{2}\sqrt{s^\alpha}}{\cancel{\theta+2}}\frac{\cancel{\theta+2}}{\cancel{2}}K_{\nu-1}\left[\frac{2\sqrt{s^\alpha}}{\theta+2}\right]}\right). \tag{E.34}$$

To conclude, the result is

$$\overline{p_D}(r_D,s)=r_D^{\frac{\theta+2}{2}\nu}\left(\frac{K_\nu\left[\frac{2\sqrt{s^\alpha}}{\theta+2}r_D^{\frac{\theta+2}{2}}\right]}{s\sqrt{s^\alpha}\;K_{\nu-1}\left[\frac{2\sqrt{s^\alpha}}{\theta+2}\right]}\right) \tag{E.35}$$

or

$$\overline{p_D}(r_D,s)=r_D^{\frac{1-\beta}{2}}\left(\frac{K_\nu\left[\frac{2\sqrt{s^\alpha}}{\theta+2}r_D^{\frac{\theta+2}{2}}\right]}{s\sqrt{s^\alpha}\;K_{\nu-1}\left[\frac{2\sqrt{s^\alpha}}{\theta+2}\right]}\right). \tag{E.36}$$

APPENDIX F

METZLER ANOMALOUS DIFFUSION MODEL AT A CONSTANT RATE CONVERSION FROM DIMENSIONLESS TO DIMENSIONAL

In this appendix, we convert the analytical solution of Metzler anomalous model at a constant rate condition from dimensionless to dimensional coordinate in the SI unit by using scaling property. The dimensionless pressure and time are given by

$$p_D = \frac{kh}{2\pi q B \mu} \Delta p(t) \tag{F.1}$$

and

$$t_D = \frac{k(r_w)t}{\phi(r_w) c_t \mu\, r_w^2}. \tag{F.2}$$

Dimensionless time can be written as

$$t_D = \eta^* t, \tag{F.3}$$

where

$$\eta^* = \frac{k(r_w)}{\phi(r_w) c_t \mu r_w^2}. \tag{F.4}$$

Taking the Laplace transform of Eq. F.1,

$$\overline{\overline{p_D}}(s) = \frac{kh}{2\pi q B \mu} \overline{\overline{\Delta p}}(s), \tag{F.5}$$

where $\overline{\overline{p_D}}(s)$ is the Laplace transform of $p_D(t_D)$ with respect to time t, and $\overline{\overline{\Delta p}}(s)$ represents the Laplace transform of $\Delta p(t)$ with respect to t. In addition, the solution of Metzler Anomalous diffusion model for finite wellbore and constant rate is

$$\overline{p_D}(r_D, s) = r_D^{\frac{\theta+2}{2}\nu} \frac{K_\nu\left[\frac{2\sqrt{s^\alpha}}{\theta + 2} r_D^{\frac{\theta+2}{2}}\right]}{s\sqrt{s^\alpha}\, K_{\nu-1}\left[\frac{2\sqrt{s^\alpha}}{\theta + 2}\right]}, \tag{F.6}$$

where $\overline{p_D}(r_D, s)$ represents the Laplace transform of $p_D(t_D)$ with respect to t_D. After, by applying scaling property, $\overline{\overline{p_D}}(s)$ can be represented as:

$$\overline{\overline{p_D}}(s) = \mathcal{L}_t[p_D(\eta^* t)] = \frac{1}{\eta^*}\overline{p_D}\left(\frac{s}{\eta^*}\right). \tag{F.7}$$

So,

$$\overline{\overline{p_D}}(s) = \mathcal{L}_t[p_D(\eta^* t)] = \frac{1}{\cancel{\eta^*}} r_D^{\frac{\theta+2}{2}\nu} \left(\frac{K_\nu\left[\frac{2\sqrt{\frac{s^\alpha}{\eta^*}}}{\theta + 2} r_D^{\frac{\theta+2}{2}}\right]}{\frac{s}{\cancel{\eta^*}}\sqrt{\frac{s^\alpha}{\eta^*}}\;\; K_{\nu-1}\left[\frac{2\sqrt{\frac{s^\alpha}{\eta^*}}}{\theta + 2}\right]} \right) \tag{F.8}$$

or

$$\overline{\overline{p_D}}(s) = \mathcal{L}_t[p_D(\eta^* t)] = r_D^{\frac{\theta+2}{2}\nu} \left(\frac{K_\nu\left[\frac{2\sqrt{\frac{s^\alpha}{\eta^*}}}{\theta + 2} r_D^{\frac{\theta+2}{2}}\right]}{s\sqrt{\frac{s^\alpha}{\eta^*}}\;\; K_{\nu-1}\left[\frac{2\sqrt{\frac{s^\alpha}{\eta^*}}}{\theta + 2}\right]} \right). \tag{F.9}$$

Make equal to Eq. F.5 and F.9 supplies:

$$\frac{kh}{2\pi qB\mu}\overline{\overline{\Delta p}}(s) = r_D^{\frac{\theta+2}{2}\nu}\left(\frac{K_\nu\left[\frac{2\sqrt{\frac{s^\alpha}{\eta^*}}}{\theta+2}r_D^{\frac{\theta+2}{2}}\right]}{s\sqrt{\frac{s^\alpha}{\eta^*}}\;\;K_{\nu-1}\left[\frac{2\sqrt{\frac{s^\alpha}{\eta^*}}}{\theta+2}\right]}\right). \tag{F.10}$$

Consequently, $\overline{\overline{\Delta p}}(s)$ is equal to

$$\overline{\overline{\Delta p}}(s) = \frac{2\pi qB\mu}{kh}r_D^{\frac{\theta+2}{2}\nu}\left(\frac{K_\nu\left[\frac{2\sqrt{\frac{s^\alpha}{\eta^*}}}{\theta+2}r_D^{\frac{\theta+2}{2}}\right]}{s\sqrt{\frac{s^\alpha}{\eta^*}}\;\;K_{\nu-1}\left[\frac{2\sqrt{\frac{s^\alpha}{\eta^*}}}{\theta+2}\right]}\right), \tag{F.11}$$

where $r_D = \frac{r}{r_w}$.

APPENDIX G

ANALYTICAL SOLUTION OF METZLER ANOMALOUS MODEL AT CONSTANT BOTTOMHOLE PRESSURE

In this appendix, the analytical solution of Metzler anomalous diffusion model is presented for constant bottomhole pressure condition. The initial boundary value problem for the fractal model is defined as follows:

$$\frac{\partial^\alpha p_D}{\partial t_D^\alpha} = \frac{1}{r_D^{d_f-1}} \frac{\partial}{\partial r_D}\left(r_D^\beta \frac{\partial p_D}{\partial r_D}\right), \tag{G.1}$$

where $\beta = d_f - \Theta - 1$ and $\alpha = \frac{2}{\theta+2}$. Initial condition is given as

$$p_D(r_D, t_D = 0) = 0. \tag{G.2}$$

The inner boundary condition for a finite wellbore is described as

$$p_D(r_D = 1, t_D) = 1. \tag{G.3}$$

The outer boundary condition is described as

$$\lim_{r_D \to \infty} p_D(r_D, t_D) = 0. \tag{G.4}$$

To begin with, taking the Laplace transform of PDE with respect to t_D,

$$s^\alpha \overline{p_D}(r_D, s) - s^{\alpha-1} p_D(r_D, t_D = 0) = \frac{1}{r_D^{d_f-1}} \frac{d}{dr_D}\left(r_D^\beta \frac{d\overline{p_D}}{dr_D}\right). \tag{G.5}$$

Applying the initial condition into the above equation,

$$s^\alpha \overline{p_D}(r_D, s) = \frac{1}{r_D^{d_f-1}} \frac{d}{dr_D}\left(r_D^\beta \frac{d\overline{p_D}}{dr_D}\right) \tag{G.6}$$

or

$$s^{\alpha}\overline{p_D}(r_D,s) = \frac{1}{r_D^{\beta+\theta}}\frac{d}{dr_D}\left(r_D^{\beta}\frac{d\overline{p_D}}{dr_D}\right). \tag{G.7}$$

Next, Laplace transform of inner and outer boundaries are, respectively

$$\overline{p_D}(r_D = 1, s) = \frac{1}{s} \tag{G.8}$$

and

$$\lim_{r_D \to \infty} \overline{p_D}(r_D, s) = 0. \tag{G.9}$$

Then, Eq. G.7 develops into,

$$s^{\alpha}\overline{p_D}(r_D,s) = \frac{1}{r_D^{\beta+\theta}}\left(\beta r_D^{\beta-1}\frac{d\overline{p_D}}{dr_D} + r_D^{\beta}\frac{d^2\overline{p_D}}{dr_D^2}\right), \tag{G.10}$$

$$s^{\alpha}\overline{p_D}(r_D,s) = \frac{\beta}{r_D^{\theta+1}}\frac{d\overline{p_D}}{dr_D} + \frac{1}{r_D^{\theta}}\frac{d^2\overline{p_D}}{dr_D^2}. \tag{G.11}$$

Let us rearrange the Eq. G.11 to find a general solution,

$$\frac{1}{r_D^{\theta}}\frac{d^2\overline{p_D}}{dr_D^2} + \frac{\beta}{r_D^{\theta+1}}\frac{d\overline{p_D}}{dr_D} - s^{\alpha}\overline{p_D}(r_D,s) = 0. \tag{G.12}$$

Multiply with $r_D^{\theta+2}$,

$$r_D^{\theta+2}\frac{1}{r_D^{\theta}}\frac{d^2\overline{p_D}}{dr_D^2} + r_D^{\theta+2}\frac{\beta}{r_D^{\theta+1}}\frac{d\overline{p_D}}{dr_D} - r_D^{\theta+2}s^{\alpha}\overline{p_D}(r_D,s) = 0. \tag{G.13}$$

So,

$$r_D^2\frac{d^2\overline{p_D}}{dr_D^2} + \beta r_D\frac{d\overline{p_D}}{dr_D} - r_D^{\theta+2}s^{\alpha}\overline{p_D}(r_D,s) = 0. \tag{G.14}$$

The general solution of Eq. G.14 is

$$\overline{p_D}(r_D,s) = r_D^{\frac{\theta+2}{2}\nu}\left\{AI_{\nu}\left[\frac{2\sqrt{s^{\alpha}}}{\theta+2}r_D^{\frac{\theta+2}{2}}\right] + BK_{\nu}\left[\frac{2\sqrt{s^{\alpha}}}{\theta+2}r_D^{\frac{\theta+2}{2}}\right]\right\}, \tag{G.15}$$

where $\nu = \frac{1-\beta}{\theta+2}$. Next, apply the outer boundary condition in Laplace space to the general solution

$$\lim_{r_D\to\infty}\overline{p_D}(r_D,s)=\lim_{r_D\to\infty}r_D^{\frac{\theta+2}{2}\nu}\lim_{r_D\to\infty}\left\{AI_\nu\left[\frac{2\sqrt{s^\alpha}}{\theta+2}r_D^{\frac{\theta+2}{2}}\right]+BK_\nu\left[\frac{2\sqrt{s^\alpha}}{\theta+2}r_D^{\frac{\theta+2}{2}}\right]\right\}=0. \quad \text{(G.16)}$$

When r_D goes to infinity, Bessel I function approaches to infinity, and Bessel K function goes to zero. Hence, *A* must be zero, but *B* cannot be zero. Consequently, Eq. G.16 reduces to

$$\overline{p_D}(r_D,s)=r_D^{\frac{\theta+2}{2}\nu}BK_\nu\left[\frac{2\sqrt{s^\alpha}}{\theta+2}r_D^{\frac{\theta+2}{2}}\right]. \quad \text{(G.17)}$$

Next, apply the inner boundary condition ($r_D=1$),

$$\overline{p_D}(r_D=1,s)=BK_\nu\left[\frac{2\sqrt{s^\alpha}}{\theta+2}\right]=\frac{1}{s}. \quad \text{(G.18)}$$

So,

$$B=\frac{1}{sK_\nu\left[\frac{2\sqrt{s^\alpha}}{\theta+2}\right]}. \quad \text{(G.19)}$$

To sum up, dimensionless pressure is equal to

$$\overline{p_D}(r_D,s)=r_D^{\frac{\theta+2}{2}\nu}\frac{K_\nu\left[\frac{2\sqrt{s^\alpha}}{\theta+2}r_D^{\frac{\theta+2}{2}}\right]}{sK_\nu\left[\frac{2\sqrt{s^\alpha}}{\theta+2}\right]} \quad \text{(G.20)}$$

or

$$\overline{p_D}(r_D,s)=r_D^{\frac{1-\beta}{2}}\frac{K_\nu\left[\frac{2\sqrt{s^\alpha}}{\theta+2}r_D^{\frac{\theta+2}{2}}\right]}{sK_\nu\left[\frac{2\sqrt{s^\alpha}}{\theta+2}\right]}. \quad \text{(G.21)}$$

APPENDIX H

METZLER ANOMALOUS DIFFUSION MODEL AT A CONSTANT BOTTOMHOLE PRESSURE CONVERSION FROM DIMENSIONLESS TO DIMENSIONAL

In this appendix, the analytical solution of Metzler anomalous model at a constant bottomhole pressure is converted from dimensionless to dimensional coordinate in the SI unit by using scaling property. The dimensionless pressure and time are given by,

$$p_D = \frac{p_i - p}{p_i - p_{wf}} = \frac{\Delta p(r,t)}{\Delta p_{wf}} \tag{H.1}$$

and

$$t_D = \frac{k(r_w)t}{\phi(r_w)c_t \mu\, r_w^2}. \tag{H.2}$$

Dimensionless time can be written as

$$t_D = \eta^* t, \tag{H.3}$$

where

$$\eta^* = \frac{k(r_w)}{\phi(r_w)c_t \mu r_w^2}. \tag{H.4}$$

Laplace transform of Eq. H.1 is equal to

$$\overline{\overline{p_D}}(s) = \frac{1}{\Delta p_{wf}} \overline{\overline{\Delta p}}(r,s), \tag{H.5}$$

where $\overline{\overline{p_D}}(s)$ is the Laplace transform of $p_D(t_D)$ with respect to time t, and $\overline{\overline{\Delta p}}(s)$ represents the Laplace transform of $\Delta p(t)$ with respect to t. Moreover, the solution of Metzler anomalous diffusion model for finite wellbore and constant bottomhole pressure is

$$\overline{p_D}(r_D, s) = r_D^{\frac{\theta+2}{2}\nu} \frac{K_\nu\left[\frac{2\sqrt{s^\alpha}}{\theta+2} r_D^{\frac{\theta+2}{2}}\right]}{sK_\nu\left[\frac{2\sqrt{s^\alpha}}{\theta+2}\right]}, \qquad \text{(H.6)}$$

where $\overline{p_D}(r_D, s)$ represents the Laplace transform of $p_D(t_D)$ with respect to t_D. After, by applying scaling property, $\overline{\overline{p_D}}(s)$ can be represented as:

$$\overline{\overline{p_D}}(s) = \mathcal{L}_t[p_D(\eta^* t)] = \frac{1}{\eta^*}\overline{p_D}\left(\frac{s}{\eta^*}\right). \qquad \text{(H.7)}$$

So,

$$\overline{\overline{p_D}}(s) = \mathcal{L}_t[p_D(\eta^* t)] = \frac{1}{\cancel{\eta^*}} r_D^{\frac{\theta+2}{2}\nu} \left(\frac{K_\nu\left[\frac{2\sqrt{\frac{s^\alpha}{\eta^*}}}{\theta+2} r_D^{\frac{\theta+2}{2}}\right]}{\frac{s}{\cancel{\eta^*}}\, K_\nu\left[\frac{2\sqrt{\frac{s^\alpha}{\eta^*}}}{\theta+2}\right]} \right) \qquad \text{(H.8)}$$

or

$$\overline{\overline{p_D}}(s) = \mathcal{L}_t[p_D(\eta^* t)] = r_D^{\frac{\theta+2}{2}\nu} \left(\frac{K_\nu\left[\frac{2\sqrt{\frac{s^\alpha}{\eta^*}}}{\theta+2} r_D^{\frac{\theta+2}{2}}\right]}{sK_\nu\left[\frac{2\sqrt{\frac{s^\alpha}{\eta^*}}}{\theta+2}\right]} \right). \qquad \text{(H.9)}$$

Make equal to Eq. H.5 and H.9 supplies:

$$\frac{1}{\Delta p_{wf}}\overline{\overline{\Delta p}}(r_D,s)=r_D^{\frac{\theta+2}{2}\nu}\left(\frac{K_\nu\left[\frac{2\sqrt{\frac{s^\alpha}{\eta^*}}}{\theta+2}r_D^{\frac{\theta+2}{2}}\right]}{sK_\nu\left[\frac{2\sqrt{\frac{s^\alpha}{\eta^*}}}{\theta+2}\right]}\right). \tag{H.10}$$

Consequently, $\overline{\overline{\Delta p}}(s)$ is equal to:

$$\overline{\overline{\Delta p}}(r_D,s)=\frac{\Delta p_{wf}}{s}r_D^{\frac{\theta+2}{2}\nu}\left(\frac{K_\nu\left[\frac{2\sqrt{\frac{s^\alpha}{\eta^*}}}{\theta+2}r_D^{\frac{\theta+2}{2}}\right]}{K_\nu\left[\frac{2\sqrt{\frac{s^\alpha}{\eta^*}}}{\theta+2}\right]}\right), \tag{H.11}$$

where $r_D=\frac{r}{r_w}$.

APPENDIX I

ANALYTICAL SOLUTION OF RAGHAVAN ANOMALOUS DIFFUSION MODEL AT CONSTANT RATE

In this appendix, we present the analytical solution of Raghavan anomalous diffusion model for constant rate condition. The diffusivity equation of this model is

$$\frac{1}{r^{n-1}}\frac{\partial}{\partial r}\left(r^{n-1-\theta}\lambda_\alpha \frac{\partial \Delta p}{\partial r}\right) = \phi c_t \frac{\partial^\alpha \Delta p(r,t)}{\partial t^\alpha}, \tag{I.1}$$

where $\alpha = \frac{2}{2+\theta}$ and $\lambda_\alpha = \frac{k_\alpha}{\mu}$. The initial condition is

$$\Delta p(r, t=0) = 0. \tag{I.2}$$

The inner boundary condition for finite wellbore is

$$\lim_{r\to r_w}\left(r^{n-1-\theta}\frac{\partial^{1-\alpha}}{\partial t^{1-\alpha}}\frac{\partial \Delta p}{\partial r}\right) = -\frac{q_{sc}B}{\alpha_n \lambda_\alpha h}, \tag{I.3}$$

where $\alpha_n = \frac{2\pi^{\frac{n}{2}}}{\Gamma\left(\frac{n}{2}\right)}$, and $n = 2$. The outer boundary condition is defined as,

$$\lim_{r\to\infty} \Delta p(r,t) = 0. \tag{I.4}$$

Taking Laplace transform of PDE with respect to t gives

$$\frac{1}{r^{n-1}}\frac{\partial}{\partial r}\left(r^{n-1-\theta}\lambda_\alpha \frac{\partial \overline{\Delta p}}{\partial r}\right) = \phi c_t\{s^\alpha \overline{\Delta p}(r,s) - s^{\alpha-1}\Delta p(r, t=0)\}. \tag{I.5}$$

Apply the initial condition into the above equation,

$$\frac{1}{r^{n-1}}\frac{\partial}{\partial r}\left(r^{n-1-\theta}\frac{\partial \overline{\Delta p}}{\partial r}\right) = \frac{\phi c_t}{\lambda_\alpha} s^\alpha \overline{\Delta p}(r,s). \tag{I.6}$$

Let us rearrange the Eq. I.6

$$\beta = n - 1 - \theta \tag{I.7}$$

and

$$\eta_i = \frac{\lambda_\alpha}{\phi c_t}, \tag{I.8}$$

so, the PDE can be rewritten as,

$$\frac{1}{r^{\beta+\theta}} \frac{d}{dr}\left(r^\beta \frac{d\overline{\Delta p}}{dr} \right) = \frac{1}{\eta_i} s^\alpha \overline{\Delta p}(r, s). \tag{I.9}$$

Left hand side of Eq. I.9 can be expanded as,

$$\frac{1}{r^{\beta+\theta}}\left(\beta r^{\beta-1} \frac{d\overline{\Delta p}}{dr} + r^\beta \frac{d^2\overline{\Delta p}}{dr^2} \right) = \frac{1}{\eta_i} s^\alpha \overline{\Delta p}(r, s) \tag{I.10}$$

or

$$\beta \frac{r^{\beta-1}}{r^{\beta+\theta}} \frac{d\overline{\Delta p}}{dr} + \frac{r^\beta}{r^{\beta+\theta}} \frac{d^2\overline{\Delta p}}{dr^2} = \frac{1}{\eta_i} s^\alpha \overline{\Delta p}(r, s) \tag{I.11}$$

or

$$\frac{\beta}{r^{\theta+1}} \frac{d\overline{\Delta p}}{dr} + \frac{1}{r^\theta} \frac{d^2\overline{\Delta p}}{dr^2} = \frac{1}{\eta_i} s^\alpha \overline{\Delta p}(r, s). \tag{I.12}$$

Multiply Eq. I.12 with $r^{\theta+2}$, and rearrange it

$$r^2 \frac{d^2\overline{\Delta p}}{dr^2} + \beta r \frac{d\overline{\Delta p}}{dr} - r^{\theta+2} \frac{s^\alpha}{\eta_i} \overline{\Delta p}(r, s) = 0. \tag{I.13}$$

The general solution of Eq. I.13 is equal to

$$\overline{\Delta p}(r, s) = r^{-\frac{\theta+2}{2}\nu\prime} \left\{ C I_{\nu'} \left[\frac{2\sqrt{\frac{s^\alpha}{\eta_i}}}{\theta + 2} r^{\frac{\theta+2}{2}} \right] + D K_{\nu'} \left[\frac{2\sqrt{\frac{s^\alpha}{\eta_i}}}{\theta + 2} r^{\frac{\theta+2}{2}} \right] \right\}, \tag{I.14}$$

where *C* and *D* are the arbitrary constants, and these constants can be determined from the outer and inner boundary conditions. The order of the above equation,

$$\nu' = \frac{n}{d_w} - 1 = \frac{\beta - 1}{\theta + 2}, \tag{I.15}$$

where

$$\mathrm{d_w} = \theta + 2\,. \tag{I.16}$$

First, take the Laplace transform of the outer boundary, and then apply into the Eq. I.14,

$$\lim_{r\to\infty} \overline{\Delta p}(r,s) = 0. \tag{I.17}$$

Applying outer boundary gives result that *C* must be zero because $I_{\nu'}$ is unbounded as the argument r goes to infinity for any ν'. Therefore, Eq. I.14 reduces to:

$$\overline{\Delta p}(r,s) = Dr^{-\frac{\theta+2}{2}\nu'} K_{\nu'}\left[\frac{2\sqrt{\frac{s^\alpha}{\eta_i}}}{\theta+2} r^{\frac{\theta+2}{2}}\right] \tag{I.18}$$

or

$$\overline{\Delta p}(r,s) = Dr^{-\frac{d_w}{2}\nu'} K_{\nu'}\left[2s^{\frac{\alpha}{2}}\left(\frac{r^{d_w}}{\eta_i d_w^2}\right)^{\frac{1}{2}}\right]. \tag{I.19}$$

To determine the constant *D*, we use the inner boundary condition given by Eq. I.3. Initially, we take the Laplace transform of Eq. I.3,

$$\lim_{r\to r_w}\left[r^{n-1-\theta}\mathcal{L}_t\left(\frac{\partial^{1-\alpha}}{\partial t^{1-\alpha}}\frac{\partial \Delta p}{\partial r}\right)\right] = -\frac{q_{sc}B}{\alpha_n\lambda_\alpha hs}, \tag{I.20}$$

where

$$\mathcal{L}_t\left(\frac{\partial^{1-\alpha}}{\partial t^{1-\alpha}}\frac{\partial \Delta p}{\partial r}\right) = s^{1-\alpha}\frac{d\overline{\Delta p}(r,s)}{dr}. \tag{I.21}$$

So,

$$\lim_{r\to r_w}\left[r^{n-1-\theta}s^{1-\alpha}\frac{d\overline{\Delta p}(r,s)}{dr}\right] = -\frac{q_{sc}B}{\alpha_n\lambda_\alpha hs} \tag{I.22}$$

or

$$\lim_{r \to r_w} \left[r^{n-1-\theta} \frac{d\overline{\Delta p}(r,s)}{dr} \right] = -\frac{q_{sc}B}{\alpha_n \lambda_\alpha h s^{2-\alpha}}. \tag{I.23}$$

To apply inner boundary condition, firstly take the derivative of Eq. I.19

$$\frac{d\overline{\Delta p}(r,s)}{dr} = -D\frac{d_w}{2}\nu' r^{-\frac{d_w}{2}\nu'-1} K_{\nu'}\left[2s^{\frac{\alpha}{2}}\left(\frac{r^{d_w}}{\eta_i d_w^2}\right)^{\frac{1}{2}}\right] + Dr^{-\frac{d_w}{2}\nu'} \frac{dK_{\nu'}\left[2s^{\frac{\alpha}{2}}\left(\frac{r^{d_w}}{\eta_i d_w^2}\right)^{\frac{1}{2}}\right]}{dr}. \tag{I.24}$$

The derivative of Bessel K function is equal to

$$\frac{dK_\nu(z)}{dr} = \frac{\nu}{z}K_\nu(z) - K_{\nu+1}(z) \tag{I.25}$$

and the chain rule is

$$\frac{dK_\nu(z)}{dr} = \frac{dK_\nu(z)}{dz}\frac{dz}{dr}. \tag{I.26}$$

Therefore,

$$\frac{dK_{\nu'}\left[2s^{\frac{\alpha}{2}}\left(\frac{r^{d_w}}{\eta_i d_w^2}\right)^{\frac{1}{2}}\right]}{dr} = \left\{\left(\frac{\nu'}{2s^{\frac{\gamma}{2}}\left(\frac{r^{d_w}}{\eta_i d_w^2}\right)^{\frac{1}{2}}}\right) K_{\nu'}\left[2s^{\frac{\alpha}{2}}\left(\frac{r^{d_w}}{\eta_i d_w^2}\right)^{\frac{1}{2}}\right] - K_{\nu'+1}\left[2s^{\frac{\alpha}{2}}\left(\frac{r^{d_w}}{\eta_i d_w^2}\right)^{\frac{1}{2}}\right]\right\}\left(2s^{\frac{\alpha}{2}}\left(\frac{1}{2}\right)\left(\frac{r^{d_w}}{\eta_i d_w^2}\right)^{-\frac{1}{2}}\right)\left(d_w\frac{r^{d_w-1}}{\eta_i d_w^2}\right) \tag{I.27}$$

or

$$\frac{dK_{\nu\prime}\left(2s^{\frac{\alpha}{2}}\left(\frac{r^{d_w}}{\eta_i d_w^2}\right)^{\frac{1}{2}}\right)}{dr} = \left(\frac{\nu'}{2s^{\frac{\alpha}{2}}\left(\frac{r^{d_w}}{\eta_i d_w^2}\right)^{\frac{1}{2}}}\right)\left(s^{\frac{\alpha}{2}}\left(\frac{r^{d_w}}{\eta_i d_w^2}\right)^{-\frac{1}{2}}\right)\left(\frac{r^{d_w-1}}{\eta_i d_w}\right)K_{\nu\prime}\left[2s^{\frac{\alpha}{2}}\left(\frac{r^{d_w}}{\eta_i d_w^2}\right)^{1/2}\right] - \left(s^{\frac{\alpha}{2}}\left(\frac{r^{d_w}}{\eta_i d_w^2}\right)^{-\frac{1}{2}}\right)\left(\frac{r^{d_w-1}}{\eta_i d_w}\right)K_{\nu'+1}\left[2s^{\frac{\alpha}{2}}\left(\frac{r^{d_w}}{\eta_i d_w^2}\right)^{\frac{1}{2}}\right] \quad \text{(I.28)}$$

or

$$\frac{dK_{\nu\prime}\left(2s^{\frac{\alpha}{2}}\left(\frac{r^{d_w}}{\eta_i d_w^2}\right)^{\frac{1}{2}}\right)}{dr} = \left(\frac{\nu' d_w}{2r}\right)K_{\nu\prime}\left[2s^{\frac{\alpha}{2}}\left(\frac{r^{d_w}}{\eta_i d_w^2}\right)^{1/2}\right] - \left(s^{\frac{\alpha}{2}}\ \frac{r^{\frac{d_w}{2}-1}}{\eta_i^{\frac{1}{2}}}\right)K_{\nu'+1}\left[2s^{\frac{\alpha}{2}}\left(\frac{r^{d_w}}{\eta_i d_w^2}\right)^{\frac{1}{2}}\right]. \quad \text{(I.29)}$$

Hence, Eq. I.24 develops into

$$\frac{d\overline{\Delta p}(r,s)}{dr} = -D\,\frac{d_w}{2}\,\nu' r^{-\frac{d_w}{2}\nu'-1}\,K_{\nu\prime}\left[2s^{\frac{\alpha}{2}}\left(\frac{r^{d_w}}{\eta_i d_w^2}\right)^{\frac{1}{2}}\right] + Dr^{-\frac{d_w}{2}\nu\prime}\left\{\left(\frac{\nu' d_w}{2r}\right)K_{\nu'}\left[2s^{\frac{\alpha}{2}}\left(\frac{r^{d_w}}{\eta_i d_w^2}\right)^{\frac{1}{2}}\right] - \left(s^{\frac{\alpha}{2}}\ \frac{r^{\frac{d_w}{2}-1}}{\eta_i^{\frac{1}{2}}}\right)K_{\nu'+1}\left[2s^{\frac{\alpha}{2}}\left(\frac{r^{d_w}}{\eta_i d_w^2}\right)^{\frac{1}{2}}\right]\right\} \quad \text{(I.30)}$$

or

$$\frac{d\overline{\Delta p}(r,s)}{dr} = \cancel{-D\frac{d_w}{2}\nu' r^{-\frac{d_w}{2}\nu'-1} K_{\nu'}\left[2s^{\frac{\alpha}{2}}\left(\frac{r^{d_w}}{\eta_i d_w^2}\right)^{\frac{1}{2}}\right]}$$

$$\cancel{+\,Dr^{-\frac{d_w}{2}\nu'}\left(\frac{\nu' d_w}{2r}\right)K_{\nu'}\left[2s^{\frac{\alpha}{2}}\left(\frac{r^{d_w}}{\eta_i d_w^2}\right)^{\frac{1}{2}}\right]} \tag{I.31}$$

$$-\,Dr^{-\frac{d_w}{2}\nu'}\left(s^{\frac{\alpha}{2}}\,\frac{r^{\frac{d_w}{2}-1}}{\eta_i^{\frac{1}{2}}}\right)K_{\nu'+1}\left[2s^{\frac{\alpha}{2}}\left(\frac{r^{d_w}}{\eta_i d_w^2}\right)^{\frac{1}{2}}\right].$$

As a result of simplifying gives,

$$\frac{d\overline{\Delta p}(r,s)}{dr} = -Dr^{-\frac{d_w}{2}\nu'}\left(s^{\frac{\alpha}{2}}\,\frac{r^{\frac{d_w}{2}-1}}{\eta_i^{\frac{1}{2}}}\right)K_{\nu'+1}\left[2s^{\frac{\alpha}{2}}\left(\frac{r^{d_w}}{\eta_i d_w^2}\right)^{\frac{1}{2}}\right]. \tag{I.32}$$

Multiply both sides of Eq. I.32 by

$$-r^{n-1-\theta} = r^{d_w\nu+1}. \tag{I.33}$$

Hence, Eq. I.32 comes into

$$r^{d_w\nu+1}\frac{d\overline{\Delta p}(r,s)}{dr} = -Dr^{\frac{d_w}{2}(\nu'+1)}\left(\frac{s^{\frac{\alpha}{2}}}{\eta_i^{1/2}}\right)K_{\nu'+1}\left[2s^{\frac{\alpha}{2}}\left(\frac{r^{d_w}}{\eta_i d_w^2}\right)^{\frac{1}{2}}\right]. \tag{I.34}$$

Take the limit as r goes to r_w provides,

$$\lim_{r\to r_w} r^{d_w\nu+1}\frac{d\overline{\Delta p}(r,s)}{dr} = -D\frac{s^{\frac{\alpha}{2}}}{\sqrt{\eta_i}}\lim_{r\to r_w} r^{\frac{d_w}{2}(\nu'+1)}K_{\nu'+1}\left[2s^{\frac{\alpha}{2}}\left(\frac{r^{d_w}}{\eta_i d_w^2}\right)^{\frac{1}{2}}\right] \tag{I.35}$$

or

$$\lim_{r\to r_w} r^{n-1-\theta}\frac{d\overline{\Delta p}(r,s)}{dr} = -D\frac{s^{\frac{\alpha}{2}}}{\sqrt{\eta_i}}r_w^{\frac{d_w}{2}(\nu'+1)}K_{\nu'+1}\left[2s^{\frac{\alpha}{2}}\left(\frac{r_w^{d_w}}{\eta_i d_w^2}\right)^{\frac{1}{2}}\right]. \tag{I.36}$$

Equalizing Eq. I.23 and I.36,

$$-D\frac{s^{\frac{\alpha}{2}}}{\sqrt{\eta_i}}r_w^{\frac{d_w}{2}(\nu'+1)}K_{\nu'+1}\left[2s^{\frac{\alpha}{2}}\left(\frac{r_w^{d_w}}{\eta_i d_w^2}\right)^{\frac{1}{2}}\right]=-\frac{q_{sc}B}{\alpha_n\lambda_\alpha h s^{2-\alpha}}. \tag{I.37}$$

As a consequence, D is equal to

$$D=\frac{q_{sc}B}{\alpha_n\lambda_\alpha h s^{2-\alpha}}\frac{\sqrt{\eta_i}}{s^{\frac{\alpha}{2}}r_w^{\frac{d_w}{2}(\nu'+1)}K_{\nu'+1}\left[2s^{\frac{\alpha}{2}}\left(\frac{r_w^{d_w}}{\eta_i d_w^2}\right)^{\frac{1}{2}}\right]} \tag{I.38}$$

or

$$D=\frac{q_{sc}B}{\alpha_n\lambda_\alpha h s^{2-\frac{\alpha}{2}}}\frac{\sqrt{\eta_i}}{r_w^{\frac{d_w}{2}(\nu'+1)}K_{\nu'+1}\left[2s^{\frac{\alpha}{2}}\left(\frac{r_w^{d_w}}{\eta_i d_w^2}\right)^{\frac{1}{2}}\right]}. \tag{I.39}$$

Finally, pressure change in the Laplace space is found as

$$\overline{\Delta p}(r,s)=\frac{q_{sc}B}{\alpha_n\lambda_\alpha h s^{2-\frac{\alpha}{2}}}\frac{\sqrt{\eta_i}}{r_w^{\frac{d_w}{2}(\nu'+1)}K_{\nu'+1}\left[2s^{\frac{\alpha}{2}}\left(\frac{r_w^{d_w}}{\eta_i d_w^2}\right)^{\frac{1}{2}}\right]}r^{-\frac{d_w}{2}\nu'}K_{\nu'}\left[2s^{\frac{\alpha}{2}}\left(\frac{r^{d_w}}{\eta_i d_w^2}\right)^{\frac{1}{2}}\right]. \tag{I.40}$$

APPENDIX J

ANALYTICAL SOLUTION OF RAGHAVAN ANOMALOUS DIFFUSION MODEL AT CONSTANT BOTTOMHOLE PRESSURE

In this appendix, the analytical solution of Raghavan anomalous model at the constant bottomhole pressure is showed. The diffusivity equation is

$$\frac{1}{r^{n-1}}\frac{\partial}{\partial r}\left(r^{n-1-\theta}\lambda_\alpha \frac{\partial \Delta p}{\partial r}\right) = \phi c_t \frac{\partial^\alpha \Delta p(r,t)}{\partial t^\alpha}, \tag{J.1}$$

where $\alpha = \frac{2}{2+\theta}$ and $\lambda_\alpha = \frac{k_\alpha}{\mu}$. The initial condition is given by

$$\Delta p(r, t = 0) = 0. \tag{J.2}$$

The inner boundary condition for finite wellbore case

$$\Delta p(r = r_w, t) = \Delta p_w = constant. \tag{J.3}$$

The outer boundary condition is defined as

$$\lim_{r\to\infty} \Delta p(r,t) = 0. \tag{J.4}$$

Taking the Laplace transform of PDE is equal to

$$\frac{1}{r^{n-1}}\frac{\partial}{\partial r}\left(r^{n-1-\theta}\lambda_\alpha \frac{\partial \overline{\Delta p}}{\partial r}\right) = \phi c_t \{s^\alpha \overline{\Delta p}(r,s) - s^{\alpha-1}\Delta p(r, t = 0)\}. \tag{J.5}$$

Use the initial condition and rearrange the above equation develop into

$$\frac{1}{r^{n-1}}\frac{d}{dr}\left(r^{n-1-\theta} \frac{d\overline{\Delta p}}{dr}\right) = \frac{\phi c_t}{\lambda_\alpha} s^\alpha \overline{\Delta p}(r,s). \tag{J.6}$$

Eq. J.6 can be written as

$$\frac{1}{r^{\beta+\theta}}\frac{d}{dr}\left(r^{\beta} \frac{d\overline{\Delta p}}{dr}\right) = \frac{1}{\eta_i} s^\alpha \overline{\Delta p}(r,s), \tag{J.7}$$

where $\beta = n - 1 - \theta$ and $\eta_i = \frac{\lambda_\alpha}{\phi c_t}$. Then, left hand side of Eq. J.7 can be rewritten as,

$$\frac{1}{r^{\beta+\theta}}\left(\beta r^{\beta-1}\frac{d\overline{\Delta p}}{dr} + r^{\beta}\frac{d^2\overline{\Delta p}}{dr^2}\right) = \frac{1}{\eta_i}s^{\alpha}\overline{\Delta p}(r,s) \tag{J.8}$$

or

$$\frac{\beta}{r^{\theta+1}}\frac{d\overline{\Delta p}}{dr} + \frac{1}{r^{\theta}}\frac{d^2\overline{\Delta p}}{dr^2} = \frac{1}{\eta_i}s^{\alpha}\overline{\Delta p}(r,s). \tag{J.9}$$

Expand Eq. J.9 with $r^{\theta+2}$, and rewrite it

$$r^2\frac{d^2\overline{\Delta p}}{dr^2} + \beta r\frac{d\overline{\Delta p}}{dr} - r^{\theta+2}\frac{s^{\alpha}}{\eta_i}\overline{\Delta p}(r,s) = 0. \tag{J.10}$$

The solution of Eq. J.10 is equal to

$$\overline{\Delta p}(r,s) = r^{-\frac{\theta+2}{2}\nu'}\left\{CI_{\nu'}\left[\frac{2\sqrt{\frac{s^{\alpha}}{\eta_i}}}{\theta+2}r^{\frac{\theta+2}{2}}\right] + DK_{\nu'}\left[\frac{2\sqrt{\frac{s^{\alpha}}{\eta_i}}}{\theta+2}r^{\frac{\theta+2}{2}}\right]\right\}, \tag{J.11}$$

where *C* and *D* are the arbitrary constants, and these constants can be determined from the outer and inner boundary conditions. The order of the Bessel functions,

$$\nu' = \frac{n}{d_w} - 1 = \frac{\beta - 1}{\theta + 2}, \tag{J.12}$$

where

$$\mathrm{d_w} = \theta + 2\,. \tag{J.13}$$

Next, the Laplace transform of outer boundary condition is found to determine *C* and *D* constants.

$$\lim_{r\to\infty}\overline{\Delta p}(r,s) = 0\,. \tag{J.14}$$

Applying the outer boundary condition into Eq. J.11 results in *C* must be zero because $I_{\nu'}$ is unbounded when r goes to infinity. As a consequence, Eq. J.11 is equal to

$$\overline{\Delta p}(r,s) = r^{-\frac{\theta+2}{2}\nu} D K_{\nu'}\left[\frac{2\sqrt{\frac{s^{\alpha}}{\eta_i}}}{\theta+2} r^{\frac{\theta+2}{2}}\right] \tag{J.15}$$

or

$$\overline{\Delta p}(r,s) = D r^{-\frac{d_w}{2}\nu'} K_{\nu'}\left[2 s^{\frac{\alpha}{2}} \left(\frac{r^{d_w}}{\eta_i d_w^2}\right)^{\frac{1}{2}}\right]. \tag{J.16}$$

To find the constant *D*, the inner boundary condition in the Laplace space is used

$$\overline{\Delta p}(r = r_w, s) = \frac{\Delta p_w}{s}. \tag{J.17}$$

Using Eq. J.17 in Eq. J.16 gives

$$\overline{\Delta p}(r = r_w, s) = \frac{\Delta p_w}{s} = D r_w^{-\frac{d_w}{2}\nu'} K_{\nu'}\left[2 s^{\frac{\alpha}{2}} \left(\frac{r_w^{d_w}}{\eta_i d_w^2}\right)^{\frac{1}{2}}\right]. \tag{J.18}$$

So, the constant *D* is equal to

$$\mathrm{D} = \frac{\Delta p_w}{s} \frac{1}{r_w^{-\frac{d_w}{2}\nu'} K_{\nu'}\left[2 s^{\frac{\alpha}{2}} \left(\frac{r_w^{d_w}}{\eta_i d_w^2}\right)^{\frac{1}{2}}\right]}. \tag{J.19}$$

Finally, pressure change is expressed as

$$\overline{\Delta p}(r,s) = \frac{\Delta p_w}{s} \frac{r^{-\frac{d_w}{2}\nu'}}{r_w^{-\frac{d_w}{2}\nu'}} \frac{K_{\nu'}\left[2 s^{\frac{\alpha}{2}} \left(\frac{r^{d_w}}{\eta_i d_w^2}\right)^{\frac{1}{2}}\right]}{K_{\nu'}\left[2 s^{\frac{\alpha}{2}} \left(\frac{r_w^{d_w}}{\eta_i d_w^2}\right)^{\frac{1}{2}}\right]}. \tag{J.20}$$

APPENDIX K

ANALYTICAL SOLUTION OF DIMENSIONLESS RATE FOR RAGHAVAN ANOMALOUS DIFFUSION MODEL AT CONSTANT BOTTOMHOLE PRESSURE

In this appendix, the analytical solution of dimensionless rate is presented by using Raghavan anomalous model at the constant bottomhole pressure. Dimensionless rate is found by using the following equation.

$$r^{n-1-\theta}\,\frac{\partial^{1-\alpha}}{\partial t^{1-\alpha}}\frac{\partial \Delta p}{\partial r} = -\frac{q_{sc}(r,t)B}{\alpha_n \lambda_\alpha h}. \tag{K.1}$$

where Δp is constant and $q_{sc}(r,t)$ changes with time and location. Taking the Laplace transform of Eq. K.1 develops into

$$r^{n-1-\theta}\,\mathcal{L}_t\left(\frac{\partial^{1-\alpha}}{\partial t^{1-\alpha}}\frac{\partial \Delta p}{\partial r}\right) = -\mathcal{L}_t\left(\frac{q_{sc}(r,t)B}{\alpha_n \lambda_\alpha h}\right) \tag{K.2}$$

or

$$r^{n-1-\theta}\,\mathcal{L}_t\left(\frac{\partial^{1-\alpha}}{\partial t^{1-\alpha}}\frac{\partial \Delta p}{\partial r}\right) = -\frac{B}{\alpha_n \lambda_\alpha h}\mathcal{L}_t(q_{sc}(r,t)) \tag{K.3}$$

or

$$\left\{r^{n-1-\theta} s^{1-\alpha}\,\frac{\mathrm{d}\overline{\Delta p}}{dr}\right\} = -\frac{B}{\alpha_n \lambda_\alpha h}\overline{q_{sc}}(r,s), \tag{K.4}$$

where

$$\overline{\Delta p}(r,s)=\frac{\Delta p_w}{s}\frac{r^{-\frac{d_w}{2}\nu'}}{r_w^{-\frac{d_w}{2}\nu'}}\frac{K_{\nu'}\left[2s^{\frac{\alpha}{2}}\left(\frac{r^{d_w}}{\eta_i d_w^2}\right)^{\frac{1}{2}}\right]}{K_{\nu'}\left[2s^{\frac{\alpha}{2}}\left(\frac{r_w^{d_w}}{\eta_i d_w^2}\right)^{\frac{1}{2}}\right]}, \tag{K.5}$$

where $\eta_i=\frac{\phi c}{\lambda}=\frac{\phi c \mu}{k}$,and Δp_w is the well pressure, and $\overline{\Delta p}(r,s)$ is the Laplace transform of $\Delta p(r,t)$ with respect to t. Next, taking the derivative of Eq. K.5 with respect to r comes into

$$\frac{d\overline{\Delta p}(r,s)}{dr}=\frac{d\left\{\frac{\Delta p_w}{s}\frac{r^{-\frac{d_w}{2}\nu'}}{r_w^{-\frac{d_w}{2}\nu'}}\frac{K_{\nu'}\left[2s^{\frac{\alpha}{2}}\left(\frac{r^{d_w}}{\eta_i d_w^2}\right)^{\frac{1}{2}}\right]}{K_{\nu'}\left[2s^{\frac{\alpha}{2}}\left(\frac{r_w^{d_w}}{\eta_i d_w^2}\right)^{\frac{1}{2}}\right]}\right\}}{dr} \tag{K.6}$$

or

$$\frac{d\overline{\Delta p}(r,s)}{dr}=\frac{\Delta p_w}{s r_w^{-\frac{d_w}{2}\nu'}K_{\nu'}\left[2s^{\frac{\alpha}{2}}\left(\frac{r_w^{d_w}}{\eta_i d_w^2}\right)^{\frac{1}{2}}\right]}\frac{d\left\{r^{-\frac{d_w}{2}\nu'}K_{\nu'}\left[2s^{\frac{\alpha}{2}}\left(\frac{r^{d_w}}{\eta_i d_w^2}\right)^{\frac{1}{2}}\right]\right\}}{dr}\ . \tag{K.7}$$

Let us focus on the second term of Eq. K.7

$$\frac{d\left\{r^{-\frac{d_w}{2}\nu'}K_{\nu'}\left[2s^{\frac{\alpha}{2}}\left(\frac{r^{d_w}}{\eta_i d_w^2}\right)^{\frac{1}{2}}\right]\right\}}{dr}=\left(-\frac{d_w}{2}\nu' r^{-\frac{d_w}{2}\nu'-1}K_{\nu'}\left[2s^{\frac{\alpha}{2}}\left(\frac{r^{d_w}}{\eta_i d_w^2}\right)^{\frac{1}{2}}\right]\right)$$
$$+\,r^{-\frac{d_w}{2}\nu'}\frac{dK_{\nu'}\left[2s^{\frac{\alpha}{2}}\left(\frac{r^{d_w}}{\eta_i d_w^2}\right)^{\frac{1}{2}}\right]}{dr}. \tag{K.8}$$

Let us assume

$$z = 2s^{\frac{\alpha}{2}}\left(\frac{r^{d_w}}{\eta_i d_w^2}\right)^{\frac{1}{2}}. \tag{K.9}$$

The chain rule is applied for derivative of Bessel K function,

$$\frac{dK_{\nu'}(z)}{dr} = \frac{dK_{\nu'}(z)}{dz}\frac{dz}{dr}. \tag{K.10}$$

Derivative of Eq. K.9 with respect to r

$$\frac{dz}{dr} = \left\{s^{\frac{\alpha}{2}}\left(\frac{r^{d_w}}{\eta_i d_w^2}\right)^{-\frac{1}{2}}\right\}\left\{d_w\frac{r^{d_w-1}}{\eta_i d_w^2}\right\}. \tag{K.11}$$

Then, derivative of Bessel K function is equal to

$$\frac{dK_{\nu}(z)}{dz} = \frac{\nu'}{z}K_{\nu'}(z) - K_{\nu'+1}(z). \tag{K.12}$$

So, Eq. K.12 can be written as

$$\frac{dK_{\nu}(z)}{dz} = \frac{\nu'}{2s^{\frac{\alpha}{2}}\left(\frac{r^{d_w}}{\eta_i d_w^2}\right)^{\frac{1}{2}}}K_{\nu'}\left[2s^{\frac{\alpha}{2}}\left(\frac{r^{d_w}}{\eta_i d_w^2}\right)^{\frac{1}{2}}\right] - K_{\nu'+1}\left[2s^{\frac{\alpha}{2}}\left(\frac{r^{d_w}}{\eta_i d_w^2}\right)^{\frac{1}{2}}\right]. \tag{K.13}$$

As a result, Eq. K.10 develops into

$$\begin{aligned}\frac{dK_{\nu'}(z)}{dr} = &\left\{\frac{\nu'}{2s^{\frac{\alpha}{2}}\left(\frac{r^{d_w}}{\eta_i d_w^2}\right)^{\frac{1}{2}}}K_{\nu'}\left[2s^{\frac{\alpha}{2}}\left(\frac{r^{d_w}}{\eta_i d_w^2}\right)^{\frac{1}{2}}\right]\right. \\ &\left. - K_{\nu'+1}\left[2s^{\frac{\alpha}{2}}\left(\frac{r^{d_w}}{\eta_i d_w^2}\right)^{\frac{1}{2}}\right]\right\}\left\{s^{\frac{\alpha}{2}}\left(\frac{r^{d_w}}{\eta_i d_w^2}\right)^{-\frac{1}{2}}d_w\frac{r^{d_w-1}}{\eta_i d_w^2}\right\}\end{aligned} \tag{K.14}$$

or

$$\frac{dK_{\nu'}(z)}{dr}=\left\{\frac{\nu' d_w}{2r}K_{\nu'}\left[2s^{\frac{\alpha}{2}}\left(\frac{r^{d_w}}{\eta_i d_w^2}\right)^{\frac{1}{2}}\right]-s^{\frac{\alpha}{2}}\left(\frac{r^{d_w}}{\eta_i d_w^2}\right)^{\frac{1}{2}}\left(\frac{d_w}{r}\right)K_{\nu'+1}\left[2s^{\frac{\alpha}{2}}\left(\frac{r^{d_w}}{\eta_i d_w^2}\right)^{\frac{1}{2}}\right]\right\}. \quad \text{(K.15)}$$

Apply Eq. K.15 into Eq. K.8,

$$\frac{d\left\{r^{-\frac{d_w}{2}\nu'}K_{\nu'}\left[2s^{\frac{\alpha}{2}}\left(\frac{r^{d_w}}{\eta_i d_w^2}\right)^{\frac{1}{2}}\right]\right\}}{dr}=\left(-\frac{d_w}{2}\nu' r^{-\frac{d_w}{2}\nu'-1}K_{\nu'}\left[2s^{\frac{\alpha}{2}}\left(\frac{r^{d_w}}{\eta_i d_w^2}\right)^{\frac{1}{2}}\right]\right)$$

$$+r^{-\frac{d_w}{2}\nu'}\left\{\frac{\nu' d_w}{2r}K_{\nu'}\left[2s^{\frac{\alpha}{2}}\left(\frac{r^{d_w}}{\eta_i d_w^2}\right)^{\frac{1}{2}}\right]\right. \quad \text{(K.16)}$$

$$\left.-s^{\frac{\alpha}{2}}\left(\frac{r^{d_w}}{\eta_i d_w^2}\right)^{\frac{1}{2}}\left(\frac{d_w}{r}\right)K_{\nu'+1}\left[2s^{\frac{\alpha}{2}}\left(\frac{r^{d_w}}{\eta_i d_w^2}\right)^{\frac{1}{2}}\right]\right\}$$

or

$$\frac{d\left\{r^{-\frac{d_w}{2}\nu'}K_{\nu'}\left[2s^{\frac{\alpha}{2}}\left(\frac{r^{d_w}}{\eta_i d_w^2}\right)^{\frac{1}{2}}\right]\right\}}{dr}$$

$$=\cancel{-\frac{d_w}{2}\nu' r^{-\frac{d_w}{2}\nu'-1}K_{\nu'}\left[2s^{\frac{\alpha}{2}}\left(\frac{r^{d_w}}{\eta_i d_w^2}\right)^{\frac{1}{2}}\right]}$$

$$\cancel{+\frac{d_w}{2}\nu' r^{-\frac{d_w}{2}\nu'-1}K_{\nu'}\left[2s^{\frac{\alpha}{2}}\left(\frac{r^{d_w}}{\eta_i d_w^2}\right)^{\frac{1}{2}}\right]} \quad \text{(K.17)}$$

$$-r^{-\frac{d_w}{2}\nu'}\left(\frac{d_w}{r}\right)s^{\frac{\alpha}{2}}\left(\frac{r^{d_w}}{\eta_i d_w^2}\right)^{\frac{1}{2}}K_{\nu'+1}\left[2s^{\frac{\alpha}{2}}\left(\frac{r^{d_w}}{\eta_i d_w^2}\right)^{\frac{1}{2}}\right].$$

So, Eq. K.17 is equal to

$$\frac{d\left\{r^{-\frac{d_w}{2}\nu'}K_{\nu'}\left[2s^{\frac{\alpha}{2}}\left(\frac{r^{d_w}}{\eta_i d_w^2}\right)^{\frac{1}{2}}\right]\right\}}{dr} = \tag{K.18}$$
$$-r^{-\frac{d_w}{2}\nu'}\left(\frac{d_w}{r}\right)s^{\frac{\alpha}{2}}\left(\frac{r^{d_w}}{\eta_i d_w^2}\right)^{\frac{1}{2}} K_{\nu'+1}\left[2s^{\frac{\alpha}{2}}\left(\frac{r^{d_w}}{\eta_i d_w^2}\right)^{\frac{1}{2}}\right].$$

As a consequence, Eq. K.7 develops into

$$\frac{d\overline{\Delta p}(r,s)}{dr}$$
$$= -\frac{\Delta p_w}{s r_w^{-\frac{d_w}{2}\nu'} K_{\nu'}\left[2s^{\frac{\alpha}{2}}\left(\frac{r_w^{d_w}}{\eta_i d_w^2}\right)^{\frac{1}{2}}\right]}\left\{r^{-\frac{d_w}{2}\nu'}\left(\frac{d_w}{r}\right)s^{\frac{\alpha}{2}}\left(\frac{r^{d_w}}{\eta_i d_w^2}\right)^{\frac{1}{2}} K_{\nu'+1}\left[2s^{\frac{\alpha}{2}}\left(\frac{r^{d_w}}{\eta_i d_w^2}\right)^{\frac{1}{2}}\right]\right\} \tag{K.19}$$

or

$$\frac{d\overline{\Delta p}(r,s)}{dr} = -\frac{\Delta p_w}{s^{1-\frac{\alpha}{2}}}\frac{r^{-\frac{d_w}{2}\nu'}}{r_w^{-\frac{d_w}{2}\nu'}}\left(\frac{r^{d_w}}{\eta_i d_w^2}\right)^{\frac{1}{2}}\frac{d_w}{r}\frac{K_{\nu'+1}\left[2s^{\frac{\alpha}{2}}\left(\frac{r^{d_w}}{\eta_i d_w^2}\right)^{\frac{1}{2}}\right]}{K_{\nu'}\left[2s^{\frac{\alpha}{2}}\left(\frac{r_w^{d_w}}{\eta_i d_w^2}\right)^{\frac{1}{2}}\right]}. \tag{K.20}$$

Use Eq. K. 20 into Eq. K.4

$$-\left\{r^{n-1-\theta}s^{1-\alpha}\frac{\Delta p_w}{s^{1-\frac{\alpha}{2}}}\frac{r^{-\frac{d_w}{2}\nu'}}{r_w^{-\frac{d_w}{2}\nu'}}\left(\frac{r^{d_w}}{\eta_i d_w^2}\right)^{\frac{1}{2}}\frac{d_w}{r}\frac{K_{\nu'+1}\left[2s^{\frac{\alpha}{2}}\left(\frac{r^{d_w}}{\eta_i d_w^2}\right)^{\frac{1}{2}}\right]}{K_{\nu'}\left[2s^{\frac{\alpha}{2}}\left(\frac{r_w^{d_w}}{\eta_i d_w^2}\right)^{\frac{1}{2}}\right]}\right\} \tag{K.21}$$
$$= -\frac{B}{\alpha_n \lambda_\alpha h}\overline{q_{sc}}(r,s)$$

or

$$-\left\{r^{n-1-\theta}\frac{\Delta p_w}{s^{\frac{\alpha}{2}}}\frac{r^{-\frac{d_w}{2}\nu'}}{r_w^{-\frac{d_w}{2}\nu'}}\left(\frac{r^{d_w}}{\eta_i d_w^2}\right)^{\frac{1}{2}}\frac{d_w}{r}\frac{K_{\nu'+1}\left[2s^{\frac{\alpha}{2}}\left(\frac{r^{d_w}}{\eta_i d_w^2}\right)^{\frac{1}{2}}\right]}{K_{\nu'}\left[2s^{\frac{\alpha}{2}}\left(\frac{r_w^{d_w}}{\eta_i d_w^2}\right)^{\frac{1}{2}}\right]}\right\}=-\frac{B}{\alpha_n\lambda_\alpha h}\overline{q_{sc}}(r,s). \quad (K.22)$$

Note that, dimensionless rate is described as

$$q_D(r_D,t_D)=\frac{\alpha_p B}{\alpha_n\lambda_\alpha h\Delta p_w}q_{sc}(r,t), \quad (K.23)$$

where dimensionless time

$$t_D=\frac{\eta_i}{r^{d_w}}t^\alpha \quad (K.24)$$

and

$$\alpha_n=\frac{2\pi^{\frac{n}{2}}}{\Gamma\left(\frac{n}{2}\right)} \quad (K.25)$$

and

$$\alpha_p=\left(\frac{1}{\eta_i d_w^2}\right)^{\frac{1}{\gamma}-1}r_w^{d_w\left(\frac{1}{\gamma}-\xi\right)}, \quad (K.26)$$

where $\xi=\frac{n}{d_w}$ and $n=2$. Taking the Laplace transform of Eq. K.23 with respect to t

$$\overline{q_D}(r_D,s)=\frac{\alpha_p B}{\alpha_n\lambda_\alpha h\Delta p_w}\overline{q_{sc}}(r,s) \quad (K.27)$$

or

$$\overline{q_{sc}}(r,s)=\frac{\alpha_n\lambda_\alpha h\Delta p_w}{\alpha_p B}\overline{q_D}(r_D,s). \quad (K.28)$$

Consequently, Eq. K.22 can be rewritten as

$$\frac{\alpha_n \lambda_\alpha h}{B}\left\{r^{n-1-\theta}\frac{\Delta p_w}{s^{\frac{\alpha}{2}}}\frac{r^{-\frac{d_w}{2}\mathrm{v}'}}{r_w^{-\frac{d_w}{2}\mathrm{v}'}}\left(\frac{r^{d_w}}{\eta_i d_w^2}\right)^{\frac{1}{2}}\frac{d_w}{r}\frac{K_{\mathrm{v}'+1}\left[2s^{\frac{\alpha}{2}}\left(\frac{r^{d_w}}{\eta_i d_w^2}\right)^{\frac{1}{2}}\right]}{K_{\mathrm{v}'}\left[2s^{\frac{\alpha}{2}}\left(\frac{r_w^{d_w}}{\eta_i d_w^2}\right)^{\frac{1}{2}}\right]}\right\} \tag{K.29}$$

$$= \frac{\alpha_n \lambda_\alpha h \Delta p_w}{\alpha_p B}\overline{q_D}(r_D, s).$$

Simplifying Eq. K.29 comes into

$$\left\{r^{n-1-\theta}\frac{1}{s^{\frac{\alpha}{2}}}\frac{r^{-\frac{d_w}{2}\mathrm{v}'}}{r_w^{-\frac{d_w}{2}\mathrm{v}'}}\left(\frac{r^{d_w}}{\eta_i d_w^2}\right)^{\frac{1}{2}}\frac{d_w}{r}\frac{K_{\mathrm{v}'+1}\left[2s^{\frac{\alpha}{2}}\left(\frac{r^{d_w}}{\eta_i d_w^2}\right)^{\frac{1}{2}}\right]}{K_{\mathrm{v}'}\left[2s^{\frac{\alpha}{2}}\left(\frac{r_w^{d_w}}{\eta_i d_w^2}\right)^{\frac{1}{2}}\right]}\right\} = \frac{1}{\alpha_p}\overline{q_D}(r_D, s). \tag{K.30}$$

Applying the α_p and ξ into the above equation comes up to

$$\left(\frac{1}{\eta_i d_w^2}\right)^{\frac{1}{\alpha}-1} r_w^{d_w\left(\frac{1}{\alpha}-\frac{n}{d_w}\right)}\left\{r^{n-1-\theta}\frac{1}{s^{\frac{\alpha}{2}}}\frac{r^{-\frac{d_w}{2}\mathrm{v}'}}{r_w^{-\frac{d_w}{2}\mathrm{v}'}}\left(\frac{r^{d_w}}{\eta_i d_w^2}\right)^{\frac{1}{2}}\frac{d_w}{r}\frac{K_{\mathrm{v}'+1}\left[2s^{\frac{\alpha}{2}}\left(\frac{r^{d_w}}{\eta_i d_w^2}\right)^{\frac{1}{2}}\right]}{K_{\mathrm{v}'}\left[2s^{\frac{\alpha}{2}}\left(\frac{r_w^{d_w}}{\eta_i d_w^2}\right)^{\frac{1}{2}}\right]}\right\} \tag{K.31}$$

$$= \overline{q_D}(r_D, s),$$

where $n-1-\theta = d_w\mathrm{v}' + 1$ and $\alpha = \frac{2}{d_w}$. As a result, the dimensionless rate is equal to

$$\overline{q_D}(r_D, s) = d_w r_D^{-d_w\left(\frac{1}{\alpha}-\frac{1+\xi}{2}\right)} \left(\frac{r^{d_w}}{\eta_i d_w^2}\right)^{\frac{1}{\alpha}-\frac{1}{2}} s^{-\frac{\alpha}{2}} \frac{K_{\nu'+1}\left[2s^{\frac{\alpha}{2}}\left(\frac{r^{d_w}}{\eta_i d_w^2}\right)^{\frac{1}{2}}\right]}{K_{\nu'}\left[2s^{\frac{\alpha}{2}}\left(\frac{r_w^{d_w}}{\eta_i d_w^2}\right)^{\frac{1}{2}}\right]}, \tag{K.31}$$

where $r_D = \frac{r}{r_w}$. At the wellbore $(r_D = 1)$. The well response is

$$\overline{q_D}(r_D, s) = d_w \left(\frac{r_w^{d_w}}{\eta_i d_w^2}\right)^{\frac{1}{\alpha}-\frac{1}{2}} s^{-\frac{\alpha}{2}} \frac{K_{\nu'+1}\left[2s^{\frac{\alpha}{2}}\left(\frac{r_w^{d_w}}{\eta_i d_w^2}\right)^{\frac{1}{2}}\right]}{K_{\nu'}\left[2s^{\frac{\alpha}{2}}\left(\frac{r_w^{d_w}}{\eta_i d_w^2}\right)^{\frac{1}{2}}\right]}. \tag{K.32}$$